

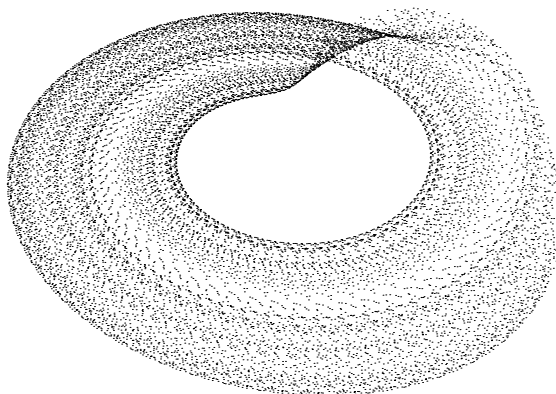


# GUIDING CHAOTIC ORBITS

**Research Report : 3 January 1997**

by

Masayuki Otani and Antonia J. Jones



Department of Computing  
Imperial College of Science  
Technology and Medicine  
London SW7 2BX, England.

Department of Computer Science  
University of Wales, Cardiff  
PO Box 916  
Cardiff CF2 3XF, Wales.



## ABSTRACT

This report studies chaotic systems with particular emphasis on the recently developed method of E. Ott, C. Grebogi and J. A. Yorke [Ott 1990] (the OGY method) for controlling such systems.

Concepts useful in understanding chaos in general are introduced. We can conceptualise chaotic systems as arising from classes of differential equations having particularly intractable solutions sets. However, in many applications the underlying equations are unknown, one works from observations of measurable parameters of the system. The use of successive samples of a single variable (or few variables) to generate an embedding with a view to reconstructing the details of an attractor for a higher dimensional dynamic system was suggested in [Packard 1980] and a frequently quoted embedding theorem [Takens 1980] establishes the existence of such models for homogeneous systems: if the underlying state space of a system has  $d$ -dimensions then the embedding space needs to have at most  $(2d + 1)$  dimensions to capture the dynamics of the system completely. These results were later generalised and improved by [Levin 1993]. It is a remarkable fact that much of the dynamics of a high dimensional system can be recovered from a suitable embedding of a *single* variable, but in practice a critical factor in the accuracy of such reconstructions is the sampling delay.

In this report a number of existing techniques for deriving delay time, sampling delays, suitable for reconstruction are examined and improved methods for estimating jump time, the time between each embedding space vector, and embedding dimension are elaborated. Combining a new technique (the  $\Gamma$ -test) [Stefánsson 1995] with existing techniques leads to a new and effective automated framework for attractor reconstruction. Choice of the jump time is critical in extracting an infinite number of nearly periodic behaviours which exist within a reconstructed chaotic attractor. Study of techniques in choosing the jump time led us to discover the *creep phenomenon*, where successive embedding space vectors remain nearby and slowly cover the entire attractor in sections. Techniques which facilitate attractor reconstruction become critical when one seeks to apply the OGY method in cases where the mathematical equations which define the dynamic system are not available.

The original OGY method and a variation due to U. Dressler and G. Nitsche [Dressler 1992] are consolidated into a single formal framework and comparative results are presented. One major disadvantage of the OGY method is an inability to control complex system behaviour. The method is extended to control complex behaviours which exists within the system.

The ability to control chaotic systems may possibly help us to understand some aspects of biological brain function. It has been suggested by W. J. Freeman [Freeman 1991] that chaos is evident in the brain and may play an important role in cognitive processes. According to this model the brain at rest is in a chaotic

mode. Upon receiving a sensory input the response to the stimulus is more ordered, more nearly periodic during perception, than at rest. In the language of nonlinear dynamics this may be interpreted as a shift from a chaotic orbit to a periodic orbit. Thus there are possibilities that ideas based on the OGY method could be used to simulate this aspect of brain function.

# TABLE OF CONTENTS

ABSTRACT .....	I
CHAPTER I	
INTRODUCTION .....	1
1.1 Introduction .....	1
1.2 Chaos in biological systems .....	2
1.3 Control of chaos in biological systems .....	3
1.4 An overview of the report .....	3
Chapter references .....	5
CHAPTER II	
NONLINEAR DYNAMICS .....	7
2.1 Introduction .....	7
2.2 Nonlinear dynamics - basic terminology .....	8
2.3 Stability of limit sets .....	10
2.4 Chaos .....	12
2.5 Lyapunov exponent .....	14
2.6 The Poincaré map .....	16
2.7 Fractal dimension .....	19
2.7.1 Capacity dimension .....	19
2.7.2 Lyapunov dimension .....	19
2.7.3 Correlation dimension .....	20
2.8 Routes to chaos .....	21
2.9 Other key areas of chaos theory .....	23
2.10 Detecting chaos .....	24
2.10.1 Test 1: Time series .....	24
2.10.2 Test 2: Poincaré section .....	24
2.10.3 Test 3: Return and stroboscopic maps .....	25
2.10.4 Test 4: Fractal dimension .....	25
2.10.5 Test 5: Lyapunov exponents .....	25
2.10.6 Test 6: Power spectra .....	25
2.10.7 Test 7: Autocorrelation .....	26
2.10.8 Conclusion .....	27
2.11 Numerical integration .....	27
2.11.1 Types of integration algorithms .....	28
2.11.2 Integration error .....	28
2.11.2.1 Round-off error .....	28
2.11.2.2 Truncation error .....	29
2.11.3 Integration routines .....	29
2.11.4 Integration of chaotic systems .....	30
2.12 Chapter summary .....	31
2.13 Further reading .....	32
Chapter references .....	32

## CHAPTER III

CHAOTIC MODELS . . . . .	35
3.1 Introduction . . . . .	35
3.2 Hamiltonian systems . . . . .	35
3.3 Dissipative systems . . . . .	36
3.3.1 The Lorenz model . . . . .	36
3.3.2 The Hénon map: A two-dimensional Iterated Map . . . . .	39
3.3.3 The Rössler model . . . . .	40
3.3.4 The Duffing oscillator model . . . . .	42
3.4 Chapter summary . . . . .	43
Chapter references . . . . .	44

## CHAPTER IV

EMBEDDING TECHNIQUES . . . . .	45
4.1 Introduction . . . . .	45
4.2 Delay coordinates method . . . . .	46
4.3 Delay time . . . . .	47
4.3.1 Autocorrelation based methods . . . . .	49
4.3.2 Mutual information . . . . .	50
4.3.3 Average displacement . . . . .	50
4.3.4 Other methods . . . . .	52
4.3.5 Summary of methods for delay time . . . . .	52
4.4 Jump time . . . . .	53
4.5 Embedding dimension . . . . .	54
4.5.1 Correlation dimension . . . . .	55
4.5.2 Lyapunov dimension . . . . .	56
4.5.3 $\Gamma$ -test . . . . .	57
4.5.4 Conclusion . . . . .	62
4.6 Automated embedding method . . . . .	62
4.7 Unstable periodic orbits . . . . .	64
4.7.1 Extraction of unstable periodic points and orbits . . . . .	64
4.7.2 Stability of an unstable periodic point . . . . .	69
4.7.3 Choice of the jump time : The creep phenomenon . . . . .	69
4.8 Chapter summary . . . . .	72
Chapter references . . . . .	73

## CHAPTER V

CONTROL OF CHAOTIC SYSTEMS . . . . .	77
5.1 Introduction . . . . .	77
5.2 The OGY method . . . . .	78
5.3 The original OGY control law . . . . .	81
5.4 Variations and use of the OGY method . . . . .	83
5.5 The Dressler and Nitsche control law . . . . .	87
5.6 Derivation of the Dressler and Nitsche control law . . . . .	89
5.7 High period control strategy . . . . .	91
5.8 Chapter summary . . . . .	95
Chapter references . . . . .	96

## CHAPTER VI

CONTROL EXPERIMENTS . . . . .	99
6.1 Introduction . . . . .	99
6.2 Control experiment : A variation of the Hénon Map . . . . .	99
6.3 Control experiment : The Duffing's oscillator model . . . . .	110
6.4 Investigation : Periodic forcing to gain control . . . . .	112

6.5 Conclusion . . . . .	113
Chapter references . . . . .	114

CHAPTER VII

FUTURE RESEARCH . . . . .	117
7.1 Introduction . . . . .	117
7.2 Alternatives to OGY . . . . .	117
The Otani-Jones control law . . . . .	118
7.2 Future research . . . . .	120
Chapter references . . . . .	121
INDEX . . . . .	129

*Figures*

Figure 2.1 A limit cycle. . . . .	8
Figure 2.2 Stable attractor. . . . .	10
Figure 2.3 Types of fixed points. . . . .	10
Figure 2.4 A periodic time series. . . . .	12
Figure 2.5 A chaotic time series. . . . .	13
Figure 2.6 The butterfly effect. . . . .	13
Figure 2.7 A surface of section. . . . .	17
Figure 2.8 Bifurcation diagram - Logistic map. . . . .	22
Figure 2.9 A power spectrum for Sun spot data. . . . .	26
Figure 2.10 Autocorrelation of a chaotic system. . . . .	26
Figure 2.11 Trajectory Hopping. . . . .	31
Figure 3.1 Lorenz attractor : $x$ vs $y$ . . . . .	37
Figure 3.2 Lorenz attractor : $x$ vs $z$ . . . . .	37
Figure 3.3 Lorenz attractor : $y$ vs $z$ . . . . .	38
Figure 3.4 Chaotic Lorenz attractor . . . . .	38
Figure 3.5 The Hénon attractor. . . . .	40
Figure 3.6 Chaotic Rössler attractor. . . . .	41
Figure 3.7 Two dimensional chaotic Rössler attractors. . . . .	41
Figure 3.8 Autocorrelation of the Rössler model. . . . .	41
Figure 3.9 The Duffing oscillator time series displaying the secondary resonances. . . . .	42
Figure 3.10 Stroboscopic maps of the Duffing oscillator for different value of $f$ . . . . .	43
Figure 4.1 Irrelevance, $t_D = 0.82$ . . . . .	48
Figure 4.2 Redundance, $t_D = 0.05$ . . . . .	48
Figure 4.3 Reconstruction error. . . . .	51
Figure 4.4 Average displacement. . . . .	51
Figure 4.5 Reconstruction by average displacement, $t_D = 0.28$ . . . . .	52
Figure 4.6 Reconstruction by trial and error, $t_D = 0.15$ . . . . .	52
Figure 4.7 Natural logarithms of the correlation integral versus $R$ . . . . .	56
Figure 4.8 $\underline{C}$ correlation dimension versus $m$ . . . . .	56
Figure 4.9 $\underline{\Gamma}$ versus embedding dimension using the average displacement method. . . . .	59
Figure 4.10 $\underline{\Gamma}$ versus embedding dimension using the autocorrelation method. . . . .	60
Figure 4.11 $\underline{\Gamma}$ versus the dimension for the Rössler model. . . . .	60
Figure 4.12 The slope versus the dimension for the Rössler model. . . . .	61
Figure 4.13 Unstable periodic and periodic orbits. . . . .	66
Figure 4.14 Reconstructed Rössler attractor with a set of suitable embedding parameters. . . . .	70
Figure 4.15 Reconstructed Duffing attractor with a set of suitable embedding parameters. . . . .	70
Figure 5.1 OGY control. . . . .	79
Figure 5.2 Control using a surface of section. . . . .	80

Figure 5.3 Intervals for which the variables are defined. . . . .	81
Figure 5.4 Comparison of the sensitivity vectors $g$ and $u$ . . . . .	88
Figure 5.5 The combined effects of $J$ in combination with $\delta p_{i-1}$ and $\delta p_i$ . . . . .	90
Figure 5.6 A periodic orbit of period $k$ on the return map. . . . .	92
Figure 5.7 The transformation matrix and the sensitivity vector. . . . .	93
Figure 6.1 Uncontrolled time series . . . . .	99
Figure 6.2 The return map plot with the diagonal line. . . . .	100
Figure 6.3 Control of the map using $a$ as the control parameter (without noise). . . . .	101
Figure 6.4 Control of the map using $a$ as the control parameter (with noise for whole data). . . . .	102
Figure 6.5 Control of the map using $a$ as the control parameter (with noise for control data only). . . . .	102
Figure 6.6 Control of the map using $b$ as the control parameter (without noise). . . . .	103
Figure 6.7 Control of the map for period two and one orbits using $a$ as the control parameter. . . . .	103
Figure 6.8 Controlled time series of periods two and one. . . . .	104
Figure 6.9 Control of unstable orbit of period 50, orbit 1. . . . .	109
Figure 6.10 Control of unstable orbit of period 50, orbit 2. . . . .	109
Figure 6.11 Return map of the oscillator model. . . . .	110
Figure 6.12 The time series sampled at 0.1 second. . . . .	110
Figure 6.13 The time series sampled at $2\pi/\omega$ . . . . .	110
Figure 6.14 The controlled map. . . . .	110
Figure 6.15 Changes in the control parameter. . . . .	111
Figure 6.16 Difference between the controlled and uncontrolled time series sampled at $2\pi/\omega$ . . . . .	111
Figure 6.17 The controlled time series sampled at 0.1 second. . . . .	111
Figure 7.1 Proposed computer simulator model. . . . .	117

### *Algorithms*

Algorithm 4.1 The $\Gamma$ -test. . . . .	61
Algorithm 4.2 The automated embedding method. . . . .	63
Algorithm 4.3 Locate close returning points. . . . .	65
Algorithm 4.4 Distinguish and average the unstable periodic points. . . . .	67
Algorithm 4.5 Remove repeated unstable periodic orbits. . . . .	68
Algorithm 4.6 The jump time for close returns. . . . .	71
Algorithm 5.1 OGY chaos control method. . . . .	86

### *Tables*

Table 2.1 Conditions on the types of equilibrium points. . . . .	12
Table 2.2 Routes to chaos. . . . .	21
Table 3.1 The control parameter combinations for chaotic behaviours. . . . .	44
Table 4.1 The delay times estimated by the average displacement and the autocorrelation based methods for the three continuous time chaotic systems. . . . .	53
Table 4.2 The delay times and the embedding dimensions estimated for the three chaotic models. . . . .	64
Table 4.3 Distinct unstable periodic orbits of orders up to 10 extracted - the Rössler model. . . . .	72
Table 6.1 Number of unstable periodic orbits of orders up to 10 which were extracted. . . . .	105
Table 6.2 Control of unstable orbits of periods between 1 and 10. . . . .	106
Table 6.3 Control of unstable orbits of periods between 11 and 20. . . . .	107
Table 6.4 Control of unstable orbits of periods between 21 and 30. . . . .	107
Table 6.5 Control of unstable orbits of periods between 31 and 40. . . . .	108
Table 6.6 Control of unstable orbits of periods between 41 and 50. . . . .	108

# CHAPTER I

## INTRODUCTION

---

### 1.1 Introduction

About a century ago, Henri Poincaré observed that the motion of three bodies under gravity can be extremely complicated. His discovery was the first mathematical evidence of chaos. Since that time there have been many observations of chaos both in mathematical models and natural systems. For many years chaos observed through the study of nonlinear dynamic systems was avoided, due to its complexity. In practice such behaviour was often totally ignored being interpreted as either completely unpredictable or ascribed to statistical noise. The theory of nonlinear dynamics founded by Poincaré describes and classifies the behaviour of complex dynamical systems and the manner in which they evolve through time. Such systems were extraordinarily difficult to study. The situation changed dramatically with the invention of the modern computer. Scientists, especially mathematicians and physicists, who had previously encountered chaos could pursue a more systematic study of the phenomenon using the new tool.

The crucial importance of chaos is that it provides an alternative explanation for apparent randomness, one that depends on neither noise nor complexity. Chaotic behaviour shows up in systems that are essentially free from noise and are also relatively simple, often with only a few degrees of freedom.

In fact, many natural systems exhibit chaos. In the early years of the study, it was common to assume that such behaviour is unpredictable<sup>1</sup> and therefore uncontrollable. Since the late 1980's, a number of quite different techniques have been proposed for controlling chaotic systems [Ott 1990], [Dracopoulos 1994], [Ogorzalek 1993].

At about the same time, W. J. Freeman [Freeman 1991] observed that in the olfactory bulb of the rabbit recognition of scent seems to utilise a shift in chaotic mode. He has also proposed that chaos is present in other aspects of brain function such as visual perception. In the olfactory bulb chaotic behaviour is evident when at rest. The response of the system to sensory input is to undergo a change of chaotic mode, shifting into a still chaotic but more orderly state. Freeman believes that this new state corresponds to a

---

<sup>1</sup> Unpredictable in the sense that, although completely deterministic the computational 'cost' of an accurate prediction rapidly becomes prohibitive as the prediction interval increases - we shall return to this point in Chapter II.

recognition of the stimulus. The control of chaotic behaviour may thus play an important role in the recall of some types of memories. This offers the intriguing possibility that methods for controlling chaotic systems, such as the OGY method, might be used as a basis for a new type of simulation of cognitive perception. It is this thought which has motivated the present work.

Unfortunately, before one can seek to construct such neural simulations it is first necessary to systematise much of the extensive literature associated with chaotic systems and their control. It is to this end that the present report is written, the reader will find much on chaos and the OGY method and very little on chaotic neural simulations, such work being reserved for subsequent research.

This report will introduce some of the key theories which are helpful in understanding chaos. A number of techniques used to study chaotic systems are described with a strong emphasis on embedding techniques, which are used to reconstruct the high dimensional behaviour of a system from a single variable time series. Four of the well known chaotic models are then described. The main theme of this report is the study of the recently developed control technique, the OGY method [Ott 1990]. Validity of the OGY method is examined and the control law is proved. We also propose some extensions of the OGY method which may be more appropriate for high dimensional embeddings. Some classic chaotic models are then used to illustrate the embedding techniques and the OGY method.

## **1.2 Chaos in biological systems**

The modern picture of brain function, as described by Freeman [Freeman 1991], is that 'thought' (in particular perception, prediction and control) consists of the flow (in the high dimensional state space of vast assemblies of neurons) from one chaotic orbit to a periodic orbit. Freeman argues that chaos is evident in the tendency of neural assemblies to shift abruptly from one complex activity pattern to a more stable one in response to the smallest of inputs. This is a plausible model and if it stands the test of experiment and scrutiny then chaos is an intrinsic feature of brain function.

Phase portraits made from EEGs (electroencephalographs) generated by computer models reflect the overall activity of the olfactory bulb of a rabbit at rest and in response to a familiar scent (e.g. banana). The resemblance of these portraits to irregularly shaped, but still structured, coils of wire reveals that brain activity in both conditions is chaotic but that the response to the known stimulus is more ordered, more nearly periodic during perception, than at rest.

The heart also provides interesting examples of chaotic behaviour in biological systems. It is clear that the cardiac waveform is nonlinear. There is also evidence that the cardiac cycle can usefully be described

in terms of chaos. A. Babloyantz and A. Destexhe [Babloyantz 1988] examined the ECGs (electrocardiographs) of four normal human hearts, using qualitative and quantitative methods. With a variety of processing algorithms, such as power spectrum, autocorrelation function, phase portrait, Poincaré section, Lyapunov exponent etc, they demonstrated that the heart is not a perfect oscillator, but that cardiac activity stems from deterministic dynamics of a chaotic nature. Numerous in-vivo and in-vitro experiments have investigated cardiac oscillatory activity and found characteristic signatures of chaos [Choi 1983], [Chay 1985], [Geuvara 1981], [Goldberg 1984], [Keener 1981].

### **1.3 Control of chaos in biological systems**

The work in [Garfinkel 1992] shows that the OGY method has potential to control cardiac dynamics in a chaotic regime. In eight out of eleven studies, the authors successfully stabilised cardiac arrhythmias induced by the drug ouabain in rabbit ventricular by administering electrical stimuli to the heart, at irregular times determined by a variation of the OGY control law. This raises the possibility that to stabilise cardiac arrhythmias more effectively, sophisticated models and control techniques from neural computing or the OGY method might be used to, for example, improve pacemaker design.

[Schiff 1994] shows that a neural network prepared from a hippocampal slice of rat brain displays chaotic behaviour. The chaos was controlled using the OGY method, moreover, periodic behaviour in certain preparations were made to behave chaotically (anticontrol).

### **1.4 An overview of the report**

Following this introductory chapter this report is divided into six chapters as follows.

- II. Nonlinear dynamics
- III. Chaotic models
- IV. Embedding techniques
- V. Control of chaotic systems
- VI. Experimental results
- VII. Future research

It should be noted that this report only covers those aspects of chaos theory important in understanding the techniques used to control chaotic systems. Chaos is a large subject and a comprehensive survey would be a very ambitious undertaking.

In chapter II, key areas of nonlinear dynamics are briefly described with explanations of the basic terms often used. The theory of chaos attempts to study the order and universality that underlies the visible complexities. The key areas include *stability of limit sets*, *Lyapunov exponents*, *Poincaré maps*, *fractal dimension*, *routes to chaos*, i.e. the progression of a dynamical system from order to a chaotic mode of behaviour, and *detecting chaos*. Other areas of research and developments are introduced throughout the report as required. Use of numerical integration algorithms are an important issue especially in studying deterministic chaotic systems, and the simulation of chaotic systems utilising such algorithms are examined carefully. At the end of the chapter, further readings are suggested so that interested readers may refer to them for more detail.

In chapter III, conservative systems (referred to as Hamiltonian systems) are briefly described. This is followed by studies of four well known dissipative systems which exhibit chaos. The first model is a continuous time system known as the *Lorenz model* [Lorenz 1963]. The second system studied is a discrete time system called the *Hénon map* [Hénon 1976] which is based on the Lorenz model. The other two systems are also continuous time systems. They are the *Rössler model* [Rössler 1976] and the *Duffing oscillator* [Parlitz 1985] model.

In chapter IV, methods known as *embedding techniques* are described. The objective is to construct models of high dimensional dynamic systems from a single dynamic variable time series. These techniques play an important role in what follows and are described in detail. We have described a method of estimating the essential parameters of the embedding techniques. A chaotic system has an infinite number of unstable periodic orbits within itself. A method of locating such orbits by using the embedding techniques is described. This study has lead us to discover *creep phenomenon*. Also a method used to study the stability of unstable orbits is discussed.

In chapter V, a number of recently developed techniques to suppress or control chaos are briefly described. The developments in the control of chaotic systems proposed by E. Ott, C. Grebogi and J. A. Yorke in 1990, referred to as the *OGY method*, are discussed in detail. We have also included some variants of the OGY method including the *Dressler and Nitsche* and newly developed *high period control strategy*.

In chapter VI, results of a number of experiments to control chaotic systems are reported. Using computer simulations of three variations of the OGY method, two well known chaotic systems have been controlled successfully. These systems were a variation of the Hénon iterative map and the Duffing oscillator model. The chaotic iterative map was chosen as it is a low dimensional discrete time system and therefore forms a simple test bed to examine the efficiencies of the control methods. The control methods examined are the OGY, the Dressler and Nitsche and the high period control strategy. The oscillator model was chosen

## Chapter 1 - Introduction

as the OGY method could be tested by utilising a stroboscopic return map for a continuous time system.

In chapter VII, a proposal is made for further studies and the final goal of this research. An immediate goal is to implement a chaotic system modeled by an artificial neural network and control the system's behaviour by the high period control strategy. The final goal is to implement the whole system, both models to be controlled and the control system using a number of artificial neural networks.

### Chapter references

[Babloyantz 1988] A. Babloyantz and A. Destexhe. *Is the normal heart a periodic oscillator?* Biol. Cybern. 58, 203-211, 1988.

[Chay 1985] T. R. Chay and J. Rinzel. *Bursting, beating, and chaos in an excitable membrane model*, J. Biophysical Society, 47, 357-366, 1985.

[Choi 1983] M. Y. Choi and B. A. Huberman. *Dynamic behaviour of nonlinear networks*, The American Physical Society, 28, 1204-1206, 1983.

[Dracopoulos 1994] D. C. Dracopoulos and A. J. Jones. *Neuro-Genetic Adaptive Attitude Control*, Neural Computing & Applications, 2, 4, 183-204, 1994.

[Freeman 1991] W. J. Freeman. *The physiology of perception*, Scientific American, 34-41, February 1991.

[Garfinkel 1992] A. Garfinkel, M. L. Spano, W. L. Ditto and J. N. Weiss. *Controlling cardiac chaos*, Science 257, 1230-1235, August 1992.

[Geuvara 1981] M. R. Geuvara, L. Glass and A. Shrier. *Phase locking, period-doubling bifurcations, and irregular dynamics in periodically stimulated cardiac cells*, Science 214, 1350-1352, 1981.

[Goldberg 1984] A. L. Goldberger, L. J. Findley, M. R. Blackburn and A. J. Mandell. *Nonlinear dynamics in heart failure: Implications of long-wavelengths cardiopulmonary oscillations*, Amer. Heart J. 107, 612-615, 1984.

[Hénon 1976] M. Hénon. *A Two-dimensional Mapping with a Strange Attractor*, Communications in Mathematical Physics 50, 69-77, 1976.

[Keener 1981] J. P. Keener. *Chaotic cardiac dynamics*, Lectures in Applied Mathematics 19, 299-325, 1981.

[Lorenz 1963] E. N. Lorenz. *Deterministic Nonperiodic Flow*, J. Atmospheric Sciences 20, 130-141, 1963.

[Ogorzalek 1993] M. J. Ogorzalek. *Taming Chaos Part II: Control*, IEEE Transactions on circuits and systems - 1: Fundamental theory and Applications. Volume 40, 10, 700-706, October 1993.

[Ott 1990] E. Ott, Celso Grebogi and J. A. Yorke. *Controlling chaos*, Physical Review Letters 64, 11, 1196-1199, 1990.

[Parlitz 1985] U. Parlitz and W. Lauterborn. *Superstructure in the bifurcation set of the Duffing equation*,

Physics Letters A 107, 8, 351-355, 1985.

[Rössler 1976] O. E. Rössler. *An Equation for Continuous Chaos*, Physics Letters A 57, 397-398, 1976.

[Schiff 1994] S. J. Schiff, K. Jerger, D. H. Duong, T. Chang, M. L. Spano and W. L. Ditto, *Controlling chaos in the brain*, Nature, 370, 615-620, 1994.

## CHAPTER II

# NONLINEAR DYNAMICS

---

### 2.1 Introduction

It is interesting to observe from a modern standpoint that Newtonian physics already contained the seeds of its own destruction. Quite apart from the later quantum mechanical caveat of the Heisenberg Uncertainty Principle, the classicists overlooked the ‘computational cost’ of making deterministic predictions an indeterminate time into the future. The fact is that for many deterministic systems, the computational cost of making an accurate prediction a substantial time into the future becomes prohibitive. Thus the classical view that if a system is deterministic then its future behaviour could be predicted for all time contains a basic flaw. This flaw becomes particularly apparent when we consider chaotic systems.

*Chaos* is the word we use to describe deterministic behaviour for which nevertheless, in view of the computational cost, even if the initial conditions were known to an arbitrary degree of precision, the long term behaviour cannot be accurately predicted. This is certainly the case with many natural systems for which in any case we cannot know the initial conditions to an arbitrary degree of precision. A classic example, first considered by E. N. Lorenz, is the weather [Lorenz 1963].

Many mathematical models describing natural systems are just simplified cases of those systems and are developed in such a way to be deterministic and predictable in the long run. These systems are often used as rough approximations. In reality even the correct number of variables may be unknown and such models can at best form only a localised approximation to the true dynamics. Models which yield better results are often nonlinear and here even in what appears to be a very simple set of differential equations, chaos can be present. It is usually not possible to integrate such models symbolically and most frequently the best approach to modelling is to use multi-step adaptive numerical integration (refer to section 2.11 for detail). As we shall see, this fact plays an important role in studying systems with chaotic behaviour. Another key observation is the fact that in the real world, we can never specify initial conditions exactly.

In this chapter, we first introduce some of the terms often used in the study of nonlinear dynamical systems. This is followed by descriptions of a number of key ideas in chaos theory, which are important in understanding the concepts introduced in later chapters. We shall discuss why chaos occurs and how it can best be studied. Also a number of tests are suggested to detect chaos.

The chapter concludes with a discussion of the numerical integration techniques used to simulate chaotic systems.

## 2.2 Nonlinear dynamics - basic terminology.

Any nonlinear system which can be expressed by a set of mathematical equations includes two types of variables - *dynamic* and *static*. Dynamic variables are the quantities which change with time whereas the static variables, often referred to as the *control* or *system parameters*, remain constant until changed by an outside force. When studying a nonlinear system, the control parameters are often changed so as to learn how the behaviour of the system changes in response. The act of changing a control parameter to change the system behaviour is known as *perturbation*.

*State space*, or *phase space*, is the space of the dynamic variables and might in some cases include their derivatives.

A point in the state space represents a state of the system at a given time. As the system evolves with time, the state of the system moves from point to point in the state space, thus defining a *trajectory*. A trajectory therefore displays the history of the states of the system. A *limit set* is the set of points in state space that a trajectory repeatedly visits. It is defined only for discrete or continuous *autonomous systems*.

A *limit cycle* is a periodic solution of the system. A limit set is stable if all nearby trajectories remain nearby, it is

unstable if no nearby trajectories, except those lying on the limit set, remain nearby. In Figure 2.1, a stable limit cycle is illustrated. The model used to obtain the diagram was the Duffing oscillator for  $d = 0.15$ ,  $f = 0.3$  and  $\omega = 1.0$ . The Duffing oscillator is studied in detail in section 3.3.4. A collection of several trajectories with different initial conditions is called a *phase portrait* for the system, which is a graphical representation of the global behaviour of the system.

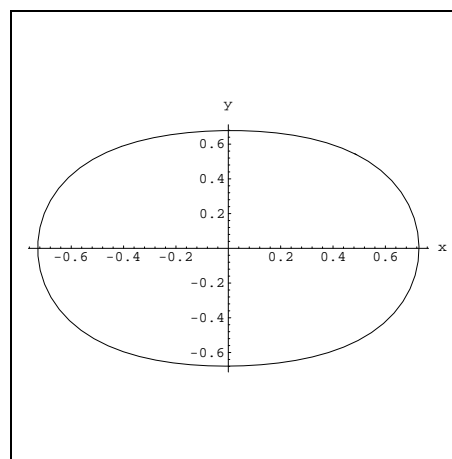


Figure 2.1 A limit cycle.

In nonlinear dynamical theory, the number of *degrees of freedom* is usually defined as the number of dynamic variables needed to specify the dynamical state of the system, or equivalently as the number of independent initial conditions that can be specified for the system.

An  $n$ th order autonomous continuous time system is defined as

Chapter 2 - Nonlinear Dynamics

$$\frac{dx_i}{dt} = g_i(x_1, \dots, x_n, p_i), \quad (i = 1, \dots, n) \quad (\text{II.1})$$

where  $t$  is time,  $x = (x_1, \dots, x_n)$  is a vector in  $n$ -dimensional state space, i.e.  $x_i$  are the dynamic variables,  $g = (g_1, \dots, g_n)$  is a vector field in the state space, i.e.  $g_i$  are functions of  $x_i$ , and  $p_i$  are the corresponding vectors of control parameters. As the vector field does not depend on time, the initial time may be taken as  $t_0 = 0$ .

If  $t$  appears in  $f_i$ , then such a system is said to be *non-autonomous*. If there exists  $T > 0$  such that  $g(x, p, t) = g(x, p, t + T)$  for all  $x$  and  $t$ , then the system is *time periodic* with period  $T$ . A  $d$ th order non-autonomous system with period  $T$  can be written as a  $(d + 1)$ th order autonomous system by adding an extra state  $\theta = 2\pi t/T$ . Since  $g$  is time periodic with period  $T$ , the system is periodic in  $\theta$  with period  $2\pi$ . Since the vector field of an autonomous system is independent of time, the autonomous system can be considered as a time periodic non-autonomous system with period  $T$ . For example the Duffing oscillator is usually written as a non-autonomous system [Parlitz 1985] but for sufficiently large values of  $f$  the periodic oscillation occurs in units of  $2\pi/\omega$ , where  $f$  and  $\omega$  are the control parameters of the model. Therefore it can be written as an autonomous system.

A non-autonomous system that is not time periodic can also be written as an autonomous system by choosing any  $T > 0$ . However, the solution is unbounded i.e.  $\theta \rightarrow \infty$  as  $t \rightarrow \infty$ , thus the steady state behaviour of autonomous systems does not apply.

We distinguish between *conservative* and *dissipative* dynamic systems. In conservative systems, described in section 3.2, volume elements in the state space are conserved, whereas in a dissipative system the volume elements contract as the system evolves.

The terms are best understood with examples. A well known nonlinear dissipative system called the Lorenz model [Lorenz 1963], described in section 3.3.1, is used for this purpose.

The Lorenz model is defined by a set of differential equations as

$$\begin{aligned} \dot{x} &= \sigma (y - x) \\ \dot{y} &= x (R - z) - y \\ \dot{z} &= x y - b z \end{aligned} \quad (\text{II.2})$$

This system has three degrees of freedom as there are three dynamic variables  $x$ ,  $y$  and  $z$ . The control

parameters are  $\sigma$ ,  $R$  and  $b$ . For  $R$  less than 1, all trajectories, no matter what their initial conditions, eventually end up approaching the origin of the  $xyz$  state space. That is for  $R < 1$ , all of the  $xyz$  space is the *basin of attraction* for the *attractor* at the origin. Figure 2.2 illustrates a trajectory of the model with  $\sigma = 10.0$ ,  $R = 0.5$ ,  $b = 8/3$ ,  $x = 1.0$ ,  $y = 2.0$  and  $z = 3.0$ .

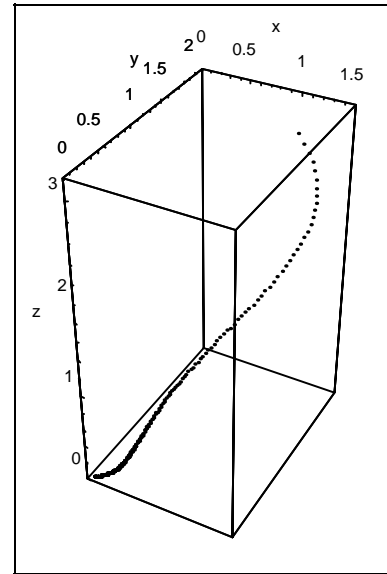


Figure 2.2 Stable attractor.

For dissipative systems, the effects of transients associated with initial conditions disappear in time. The trajectory in state space will head for some final attracting region, or regions, which might be a point, curve, area, and so on. Such an object is called the *attractor* for the system, since a number of distinct trajectories will be attracted to this set of points in the state space. The properties of the attractor determine the long term dynamical behaviour of the system. For the Lorenz model (illustrated in Figure 2.2), the attractor is a *point attractor* and it is stable once the trajectory reaches the origin.

The set of all initial conditions giving rise to trajectories that approach a given attractor is called the *basin of attraction* for that attractor. If more than one attractor exists for a system with a given set of control parameter values, there will be some initial conditions that lie on the border between the two or more basins of attraction.

### 2.3 Stability of limit sets

Stability of a limit set is important in studying the behaviour of an autonomous system. An *equilibrium point*  $x_F$ , often referred to as a *critical point* or a *singular point*, is a point in the state space where stability exists. In Figure 2.3, the equilibrium point  $x_F$  is indicated by the dot in middle of each diagram.

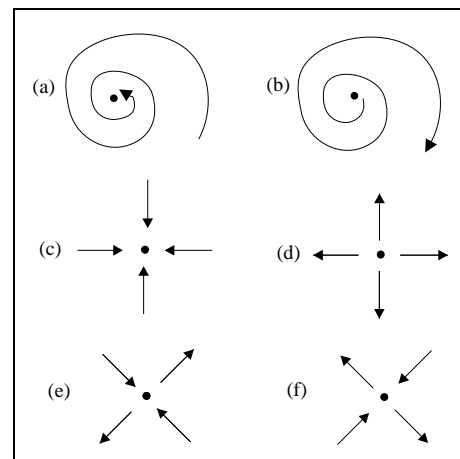


Figure 2.3 Types of fixed points.

The set of points that approach a limit set is called the *stable manifold* of the limit set. The set of points that repel from it is called the *unstable manifold*.

The arrows pointing to the equilibrium point  $x_F$  are the stable manifolds and the arrows pointing away are

the unstable manifolds. The basic types of stability in a multi-dimensional state space are illustrated in Figure 2.3 and are as follows:

- (a) *Asymptotically stable* - The equilibrium point is called a *spiral node*. The trajectories spiral around the node on a surface (submanifold) as they approach  $x_F$ .
- (b) *Asymptotically unstable* - The equilibrium point is called a *spiral repeller*. Trajectories spiral around the repeller as they are repelled away from  $x_F$ .
- (c) *Stable* - The equilibrium point is called a *node*. All trajectories in the neighbourhood of the node are attracted toward  $x_F$  without looping.
- (d) *Unstable* - The equilibrium point is called a *repeller*. All trajectories in the neighbourhood of the repeller diverge away from  $x_F$ .
- (e) *Non-stable type 1* - The equilibrium point is called a *saddle point*. Trajectories approach  $x_F$  on a surface and diverge from it along a curve, or the trajectories approach  $x_F$  on a curve and diverge from it on a surface.
- (f) *Non-stable type 2* - The equilibrium point is called a *spiral saddle point*. Trajectories spiral around  $x_F$  as they approach on a surface, or trajectories spiral around  $x_F$  on a surface as they diverge from  $x_F$ .

The local behaviour near  $x_F$  can be determined by linearising the equations describing the dynamic system at  $x_F$ . This is done by evaluating the eigenvalues of *Jacobian matrix*  $J$ , of partial derivatives at  $x_F$ .

The Jacobian matrix  $J$  of an autonomous system described by  $d$  first-order differential equations, is a  $d \times d$  matrix with the elements defined as

$$j_{l,m} = \frac{\partial g_l}{\partial x_m} \quad (1 \leq l, m \leq d) \quad (\text{II.3})$$

If the determinant of the Jacobian matrix,  $\det J$ , is one at all points the system is conservative. If the average of  $|\det J| < 1$  then the system is dissipative. If the average of  $|\det J| > 1$  then volumes in state space expand with time.

Suppose the Jacobian matrix at an equilibrium point  $x_F$  has  $d$  eigenvalues  $\lambda_i$ ,  $i, j, k \leq d$ ,  $i, j, k \in \mathbb{N}$ . Table 2.1 summarises the type of the equilibrium point  $x_F$ .

**Table 2.1** Conditions on the types of equilibrium points.

Conditions on $\text{Re}[\lambda]$	Conditions on $\text{Im}[\lambda]$	Equilibrium point type	Stability
$\text{Re}[\lambda_i] < 0$ for all $i$	$\text{Im}[\lambda_i] = 0$ for all $i$	Node	Stable
$\text{Re}[\lambda_i] < 0$ for all $i$	$\text{Im}[\lambda_i] \neq 0$ for some $i$	Spiral node	Asymptotically stable
$\text{Re}[\lambda_i] > 0$ for all $i$	$\text{Im}[\lambda_i] = 0$ for all $i$	Repeller	Unstable
$\text{Re}[\lambda_i] > 0$ for all $i$	$\text{Im}[\lambda_i] \neq 0$ for some $i$	Spiral repeller	Asymptotically unstable
$\text{Re}[\lambda_i] > 0$ & $\text{Re}[\lambda_j] < 0$ for some $i$ & $j$	$\text{Im}[\lambda_k] = 0$ for all $k$	Saddle point	Non-stable type 1
$\text{Re}[\lambda_i] > 0$ & $\text{Re}[\lambda_j] < 0$ for some $i$ & $j$	$\text{Im}[\lambda_k] \neq 0$ for some $k$	Spiral saddle point	Non-stable type 2

## 2.4 Chaos

There is currently great excitement and much speculation about chaos theory and its potential role in understanding the world. A brief introduction to the history of the mathematical foundations of the subject can be cited in [Holmes 1990]. A chaotic system will remain *apparently* noisy regardless of how well experimental conditions are controlled.

For the Duffing oscillator model, different values of  $d$ ,  $f$  and  $\omega$  exhibit completely different system behaviours. In Figure 2.4, a time series of a periodic behaviour of the model for  $d = 0.15$ ,  $f = 0.3$  and  $\omega = 1.0$  is shown.

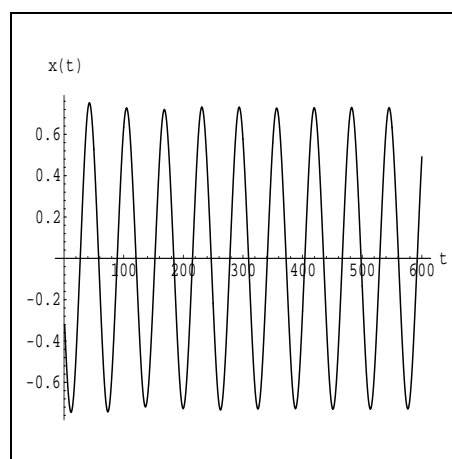


**Figure 2.4** A periodic time series.

In Figure 2.5, a typical time series of the chaotic behaviour of the model for  $d = 0.2$ ,  $f = 36$  and  $\omega = 0.665$  is illustrated. As can be seen, the chaotic time series is more complicated in appearance, but there is a boundary within which the system stays.

If a system displays *divergence of nearby trajectories* or *sensitive dependence on initial conditions* for some range of its control parameter, then the long term behaviour of that system becomes essentially

unpredictable<sup>1</sup>, i.e. the long term future of a chaotic system is in practice indeterminable even though the system is theoretically deterministic.

The effect of divergence of nearby trajectories on the behaviour of nonlinear systems is known as the *butterfly effect*. The term was introduced by Lorenz based on the picturesque notion that if the atmosphere displays chaotic behaviour with divergence of nearby trajectories, then even the flapping of a butterfly's wings would alter any long term prediction of atmospheric dynamics. This phenomenon is illustrated in Figure 2.6 for the  $x$ -coordinate of the Lorenz model with one trajectory starting at  $x = 1.0$ ,  $y = 2.0$  and  $z = 3.0$  in black, and another at  $x = 1.01$ ,  $y = 2.01$  and  $z = 3.01$ , in grey. Instead of  $R = 0.5$ , we have used  $R = 28.0$  as the model exhibits a chaotic behaviour with this value.

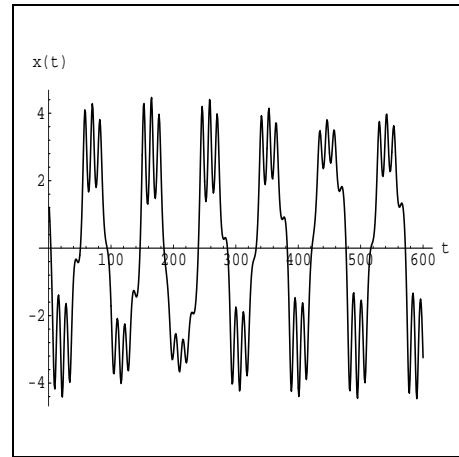


Figure 2.5 A chaotic time series.

For many nonlinear systems, we must integrate the equations step by step to find future behaviour. Any small error in specifying the initial conditions will be magnified, thus leading to grossly different long term behaviour of the system, therefore we cannot predict that long term behaviour in practice. Thus, chaotic behaviour is characterised by the divergence of nearby trajectories in state space. As a function of time, the separation between two nearby trajectories increases exponentially, at least for short time. (For short time because the trajectories stay within some bounded region of the state space.)

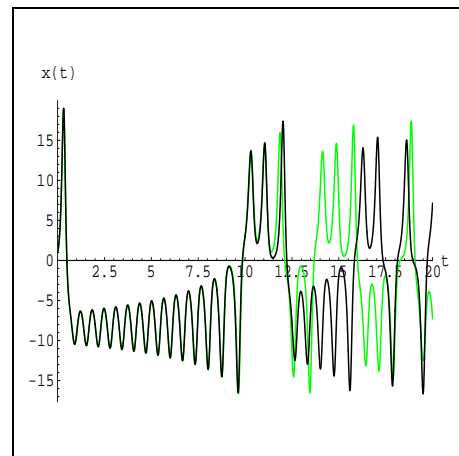


Figure 2.6 The butterfly effect.

In three or more dimensions, initially nearby trajectories can continue to diverge by wrapping over and under each other. The crucial feature of state space with three or more dimensions which permits chaotic behaviour is that trajectories remain within some bounded region by intertwining and wrapping around each other, without intersecting and without repeating themselves exactly. The geometry created by such trajectories is strange. Such attractors are thus called *strange attractors* [Ruelle 1980], i.e. if nearby trajectories on average diverge exponentially then we say the attractor is *strange* or *chaotic*.

<sup>1</sup> In the sense previously discussed.

## 2.5 Lyapunov exponent

The exponential divergence of nearby trajectories is calculated by the *Lyapunov exponent*. It is a measure of the rate of attraction or repulsion.

If two nearby trajectories on a chaotic attractor start off with a separation  $d_0$  at time  $t = 0$ , then the trajectories diverge so that their separation at time  $t$ , denoted by  $d(t)$  satisfies the expression

$$d(t) = d_0 e^{\mu t} \quad (\text{II.4})$$

where  $\mu$  is called the *Lyapunov exponent* for the trajectories.

There are two aspects of the time evolution of a system which are of particular interest for continuous time systems.

The first aspect relates to the evolution of volume elements in state space. For a continuous time system described by a system of differential equations such as (II.1), an element of volume  $V$  will evolve over time according to the divergence equation

$$\frac{1}{V} \frac{dV}{dt} = \sum_{i=1}^n \frac{\partial g_i}{\partial x_i} \equiv \text{div } g \quad (\text{II.5})$$

see, for example [Hilborn 1994], page 100.

We first note that  $\text{div } g = \text{Trace } J$ , where  $J$  is the Jacobian matrix of the system. Thus if the average over time of  $\text{Trace } J < 0$ , then volume elements will contract and the system will be dissipative, whereas if the average over time of  $\text{Trace } J = 0$  the system is conservative.

Now

$$\text{Trace } J = \sum_{i=1}^n \lambda_i \quad (\text{II.6})$$

where the  $\lambda_i$  are the eigenvalues of  $J$ . Thus the dissipative or conservative properties of a system are determined by the average over time of the sum of the eigenvalues of  $J$ .

We are primarily interested in dissipative systems which are chaotic, so that the second aspect of time

evolution which concerns us is whether nearby trajectories have a tendency to diverge exponentially on average.

The Lyapunov exponents provide a coordinate-independent measure of the asymptotic local stability of properties of a trajectory. The concept is very geometrical. Imagine a small infinitesimal ball of radius  $\epsilon(0)$  centred on a point  $\Phi(0)$  in state space. Under the action of the dynamics the centre of the ball may move, and the ball become distorted. Since the ball is infinitesimal, this distortion is governed by the linear part of the flow. The ball thus remains an ellipsoid. Suppose the principal axes of the ellipsoid at time  $t$  are of length  $\epsilon_i(t)$ . The spectrum of Lyapunov exponents for the trajectory  $\Phi(t)$  is defined as

$$\mu_i = \lim_{t \rightarrow \infty} \lim_{\epsilon(0) \rightarrow 0} \frac{1}{t} \log \frac{\epsilon_i(t)}{\epsilon(0)} \quad (\text{for } 1 \leq i \leq n) \quad (\text{II.7})$$

Note the Lyapunov exponents depend on the trajectory  $\Phi(t)$ . Their values are the same for any state on the same trajectory, but may be different for states on different trajectories. The trajectories of an  $n$ -dimensional state space have  $n$  Lyapunov exponents. This is often called the *Lyapunov spectrum*. It is conventional to order them according to size. The qualitative features of the asymptotic local stability properties can be summarised by the sign of each Lyapunov exponent; a positive Lyapunov exponent indicating an unstable direction, and a negative exponent indicating a stable direction. The motion will be dissipative if

$$\sum_{i=1}^n \mu_i < 0 \quad (\text{II.8})$$

and chaotic if at least one  $\mu_i > 0$ .

Trajectory divergence properties can also be expressed in terms of the eigenvalues of  $J$ , since the eigenvalues will determine the form of the solution to the locally linear differential equations which determine the trajectory at any particular point of the state space. In general terms these locally linear solutions for the  $x_i$  will be of the form

$$A_1 e^{\lambda_1 t} + A_2 e^{\lambda_2 t} + \dots + A_d e^{\lambda_d t} \quad (\text{II.9})$$

If for a particular trajectory we write the time average

$$\lim_{T \rightarrow \infty} \frac{1}{T} \int_{t=0}^T \ln |e^{\lambda_i(t)}| dt \quad (1 \leq i \leq d) \quad (\text{II.10})$$

one might conjecture that this provides an alternative route to the Lyapunov exponents.

The geometrical meaning of the positive Lyapunov exponents is that there exist directions in which the motion on average is unstable such that nearby trajectories in these directions will diverge from the original orbit. Although the orbit is unstable, its stable directions provide sufficient volume contraction so that the orbit is confined to some bounded region in state space. At least one Lyapunov exponent must be zero for any limit set other than an equilibrium point. It follows that the number of zero Lyapunov exponents of a non-chaotic attractor indicates the dimension of the attractor. An equilibrium point has dimension 0, a limit cycle has dimension 1 and a  $K$ -torus has dimension  $K$ .

To produce a strange attractor the system must be dissipative and hence must have at least one negative Lyapunov exponent. Furthermore, at least one Lyapunov exponent must be zero for any limit set other than an equilibrium point. Also for a chaotic system, at least one Lyapunov exponent must be positive. It follows that a strange attractor must have at least three Lyapunov exponents. Hence, chaos can only occur in third-order autonomous, second-order non-autonomous or higher order continuous time systems.

## 2.6 The Poincaré map

When studying a continuous nonlinear dynamic system, it is often desirable to reduce it to a discrete time system. The *Poincaré map* is a technique which models a continuous time system as a discrete system. A specified submanifold of the state space, called the *Poincaré section*, is selected. As the system evolves through time the trajectory repeatedly intersects the Poincaré section. Plotting the points of intersection  $X_n$  creates a lower dimensional portrait of the system behaviour. Successive crossing points are determined by integrating the time evolution equations describing the system. This determines a function  $F: X_n \rightarrow X_{n+1}$ . A detailed knowledge of the function  $F$  can prove a useful tool in the study of the dynamic system.

In general, we write

$$X_{n+1} = F(X_n), \quad F = (F_1, \dots, F_m) \quad (\text{II.11})$$

To analyze the nature of the attractor, one can analyze the nature of the function  $F$  and its derivatives. This technique reduces an  $m$ -dimensional problem to a  $(m-1)$ -dimensional one and also states an iterative relation rather than a differential one. The time interval between the two points is roughly the time to go

around the attractor once, which is a relatively big jump in time. As such, the location of successive iterates generated by the trajectories on the section is generally unpredictable. Note that finding such a function  $F$  is equivalent to solving the original set of equations and that may be impossible in actual practice.

A Poincaré section can be obtained by plotting the points generated by the Poincaré map (II.11). The section simplifies the geometric description of the dynamics by removing one of the state space dimensions. The important point is that this simplified geometry contains much essential information about the system behaviour.

In practice the Poincaré section can be generated by choosing a Poincaré plane and when a trajectory crosses that plane, that crossing point is recorded. One of the easiest method for choosing the plane is to set one of the dynamic variable as a constant. The plane should be chosen so that the trajectories cut the surface transversely, that is the trajectories do not run parallel to the surface as they pass through.

A chaotic attractor is an *indecomposable (ergodic), invariant* and closed set which attracts all orbits starting at points in some neighbourhood. Indecomposable means that every point in the set will be visited at some time, therefore no points in the set can be omitted without it ceasing to be the attractor. The existence of a dense orbit, typically a horseshoe shape, in a Poincaré section, usually implies indecomposability. Invariant means that the orbits starting in the set remain in it for all forward and backward time. The consequence of indecomposability and invariance is that typical orbits attracted to the set continually wander about, exploring its entirety, and not settling down to some simpler subset.

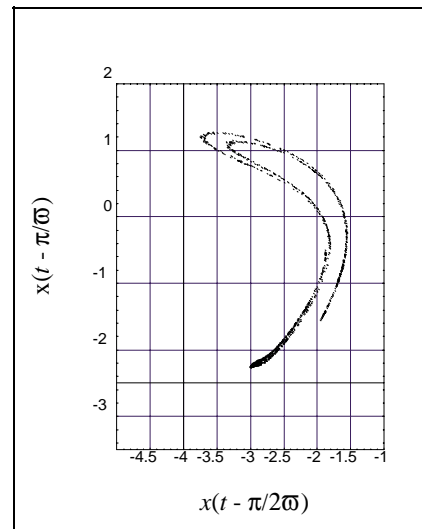


**Figure 2.7** A surface of section.

If the system has a natural periodic forcing associated with it, as for the Duffing oscillator, then the Poincaré plane could be a surface corresponding to a definite phase of the forcing. In such a case the Poincaré section is same as a *stroboscopic portrait* or a *stroboscopic map* e.g. in the case of a mechanical system recorded with a flash lamp fired once every period of the motion.

A *return map* is a plot of pairs of points  $(x_n, x_{n+1})$  where  $x_n$  is the  $n$ th point in the Poincaré map or, in the case of embedding technique described in chapter four, the pairs of the points are separated by one unit of delay time. Any plot of a Poincaré section, a stroboscopic map or a return map is often referred

to as a *surface of section*. In Figure 2.7, a surface of section of the Duffing oscillator is illustrated. The plot was obtained by the conditions  $x(t) = 1$ ,  $y(t) > 1$  and  $x(t - \pi/2\omega) < 0$ , and plotting  $x(t - \pi/2\omega)$  versus  $x(t - \pi/\omega)$ .

A *fixed point* in a surface of section say  $\xi_F$ , is a point of a map  $F$ , where  $\xi_F = F(\xi_F)$ . The nature of a fixed point is determined by the eigenvalues of Jacobian matrix at  $\xi_F$ . An eigenvalue of the Jacobian matrix at a fixed point is called a *characteristic multiplier* or a *Floquet multiplier*. The stability type of a fixed point of a Poincaré map corresponds to the stability type of the underlying equilibrium point.

Suppose the Jacobian matrix at a fixed point  $\xi_F$  has  $m$  real eigenvalues  $\lambda_1, \dots, \lambda_d$ .

The point  $\xi_F$  is:

Stable if  $|\lambda_i| < 1$  for all  $1 \leq i \leq m$ .

Unstable if  $|\lambda_i| > 1$  for all  $1 \leq i \leq m$ .

Non-stable if  $|\lambda_i| > 1$  and  $|\lambda_j| < 1$  for some  $1 \leq i, j \leq m$ .

For an iterative map function of the form (II.11) with Jacobian

$$J = \left( \frac{\partial F_i}{\partial X_j} \right) \quad (1 \leq i, j \leq m) \quad (\text{II.12})$$

volume elements will locally contract or diverge according as  $|\det J|$  is less than or greater than 1, respectively. Thus in this case the condition for a dissipative system depends on the average of  $|\det J|$ , rather than Trace  $J$  as in the continuous case.

We can still speak of an average rate of divergence: if the system is allowed to evolve from two slightly differing initial states  $X$  and  $X + \varepsilon$  after  $n$  iterations the divergence of the two points may be characterised as

$$\varepsilon(n) = (\varepsilon(0)) e^{m\mu_1}, \dots, \varepsilon(0) e^{m\mu_d} \quad (\text{II.13})$$

where the Lyapunov exponents  $\mu_i$  give the average rate of divergence/convergence over a large number of iterations. For small  $\varepsilon$  we can express this as

$$\mu_i = \lim_{n \rightarrow \infty} \lim_{\varepsilon(n) \rightarrow 0} \frac{1}{n} \sum_{k=1}^n \ln \left| \frac{\partial F_i}{\partial X_i} \right|_{X=X_k} \quad (1 \leq i \leq m) \quad (\text{II.14})$$

which is analogous to (II.10) for a continuous system.

## 2.7 Fractal dimension

There are several different techniques for quantifying the dimension of point sets which are not Lebesgue measurable, or have Lebesgue measure zero. For example, the dimension of a dynamical system is the number of state variables that are required to describe the dynamics of the system. What is the dimension of a strange attractor? Since the volume (Lebesgue measure) of the attractor is zero, its dimension must be smaller than the dimension of the state space. The generic term for a dimension that allows non-integer values is *Hausdorff* or *fractal dimension* (actually a special case of the Hausdorff dimension) and it is widely used to define the dimension of an attractor. Strange attractors have non-integer dimension while the dimension of a non-strange attractor is always an integer.

There are a number of ways in which the fractal dimension can be estimated. We will introduce three such methods.

### 2.7.1 Capacity dimension

Strange attractors are often characterised by capacity dimensionality  $D_{Ca}$  which is smaller than the number of degrees of freedom  $d$ ,  $D_{Ca} < d$ . A formula to calculate the capacity dimension using a *box-counting algorithm*, which stems from the definition of the dimensionality was presented [Russel 1980] as

$$D_{Ca} = - \lim_{\alpha \rightarrow \infty} \frac{\ln n(\alpha)}{\ln \alpha} \quad (\text{II.15})$$

where  $n(\alpha)$  is the number of  $m$ -dimensional cubes of side  $\alpha$  needed to cover the attractor.

The capacity dimension is calculated by successively dividing the state space into equal hypercubes. We then calculate the  $n(\alpha)$  hypercubes required to contain all the points of the geometric object.  $n(\alpha)$  is expected to increase as  $\alpha$  is decreased.

The number of computations required for this method increases exponentially with the state space dimension. The method requires the state space to be partitioned with hypercubes and then to locate the trajectory points within them. This is a time consuming process.

### 2.7.2 Lyapunov dimension

To calculate the fractal dimension using the box counting method is more time and much more memory

consuming than to calculate the average Lyapunov exponents.

Another method of approximating the dimension of the attractor has been proposed by J. Kaplan and J. A. Yorke [Kaplan 1979]. They suggested that the dimension of an attractor in a multi-dimensional state space can be defined in terms of the average Lyapunov exponents in the space. First rank the Lyapunov exponents from the largest  $\mu_1$  to the smallest  $\mu_d$  for a  $d$ -dimensional space, where  $\mu_1 \geq \mu_2 \geq \dots \geq \mu_d$  and then choosing  $j$  as the largest integer such that  $\mu_1 + \mu_2 + \dots + \mu_j \geq 0$ . The Lyapunov dimension  $D_L$  is defined as

$$D_L = j - \frac{\sum_{i=1}^j \mu_i}{\mu_{j+1}} \quad (\text{II.16})$$

If no such  $j$  exists,  $D_L$  is defined to be zero, which means the system is not chaotic.

There is some evidence [Russell 1980] that  $D_L$  is numerically close to the correlation dimension (defined below) and thus it can be used as an estimate for the dimension of the attractor [Lathrop 1989], [Sano 1985].

### 2.7.3 Correlation dimension

A major drawback of the box counting algorithm based on (II.15) is that it is very difficult to compute whenever  $D_{Ca} > 2$  [Greenside 1982]. Most recent work to estimate the dimension of the attractor has focused on the evaluation of the *correlation dimension*  $D_C$  [Grassberger 1982], described in more detail in section 4.5.1.

In this method, a new data point is taken with each pass through the data, and a hyperdimensional sphere of embedding dimension  $m$  and radius  $r$  is centred on that point. The fraction of subsequent data points in which fall within the sphere is then calculated for various values of  $r$ , and a plot is made of the logarithm of this number versus the logarithm of the radius. The correlation dimension is taken as the average slope of the cumulative curve over the middle one-quarter of the vertical scale, and the error is taken as half the difference of the maximum and minimum slope over the same range.

In a plot of the correlation dimension versus the embedding dimension, as the embedding dimension increases the correlation dimension should initially increase but eventually saturate at the correct value. The correlation dimension is found to be more reliable than the capacity dimension for high dimensional systems.

## 2.8 Routes to chaos

It is important to know how system behaviour changes from order to chaos. For some nonlinear systems, a small change in a control parameter could lead to sudden and dramatic changes in both the qualitative and quantitative behaviour of the system. This is demonstrated by the Duffing oscillator model in section 3.3.4. Due to the effect of a perturbation, the trajectories may undergo various changes. For one value, the behaviour might be periodic, for a slightly different value, the behaviour might be chaotic.

Some nonlinear models behave quite differently, depending on both the parameter values and initial conditions. These complications arise since a nonlinear system may have several attractors that coexist for a given range of control parameter values. The system changes its behaviour as the attractors change their characters or the basins of attraction interact in such a way as to give rise to chaotic dynamics.

*Bifurcation* is the word used to describe any sudden change in the nature of the system as a control parameter is varied. It refers to a splitting of the behaviour of the system into two regions, one above the particular parameter value at which the change occurs and the other below. The value of a control parameter at which a bifurcation occurs is called a *bifurcation value*. A bifurcation value of a control parameter is necessarily a value for which the system is structurally unstable. Therefore, at least one of the Lyapunov exponents is zero at a bifurcation value. The *bifurcation diagram* is a plot of the position of the fixed points versus the control parameter and an example of which is in Figure 2.8.

**Table 2.2** Routes to chaos.

Local bifurcation	Global bifurcation
Period-doubling (Flip) Quasi-periodicity (Hopf)	Intermittency Crisis Chaotic transient

When a control parameter of a system is changed, chaotic behaviour may appear and disappear in several different ways, thus there are several *routes to chaos*. Well known routes to chaos are listed in Table 2.2. These routes can be divided into two categories, with several subdivisions within each of them. One category includes sequences of bifurcations involving limit cycles, which are called *local bifurcations*. The other category involves changes in trajectories associated with several limit cycles. Since these changes involve the properties of trajectories ranging over a significant volume of state space, they are called *global bifurcations*. Sudden changes from regular to chaotic behaviour are characteristic of these global

bifurcations.

The *period doubling* route to chaos, also known as the *Feigenbaum scenario*, begins with a limit cycle. As a control parameter changes, the limit cycle becomes unstable. If the limit cycle becomes unstable by having one of its eigenvalues become smaller than minus one, then in many situations, the new motion remains periodic but has a period twice as long as the period of the original motion. In the Poincaré section, this new limit cycle becomes two points, one on each side of the original Poincaré section point. The trajectory's map points are repelled by the original map point. The minus sign signifies that they alternate from one side to the other. Thus, this type of bifurcation is also called a *flip bifurcation*. As the control parameter is changed further, this period-two limit cycle may become unstable again and give birth to a period-four cycle. This process may continue until the period becomes infinite, thus becoming a chaotic system.

The route to chaos via an infinite sequence of period doubling bifurcations has the universal property that the bifurcation parameters are related to each other by the *Feigenbaum constant*. The Feigenbaum constant 4.669201609... is the ratio of successive differences between bifurcation values of a period doubling sequence.

Consider a one-dimensional discrete time system in the form of the *Logistic map*, which is defined as

$$x_{n+1} = 4rx_n(1 - x_n) \tag{II.17}$$

For  $0 \leq r \leq 1$ , the function maps the unit interval to itself.

The bifurcation diagram of the logistic map is illustrated in Figure 2.8. For  $r < 0.7494$ , the system has only one fixed point. At  $r \approx 0.7494$ , a period doubling bifurcation occurs so that the system becomes a periodic system of period two. At  $r \approx 0.8621$  another period doubling bifurcation occurs so that the periodicity doubles again. The subsequent bifurcation values are approximately 0.8858, 0.8910,

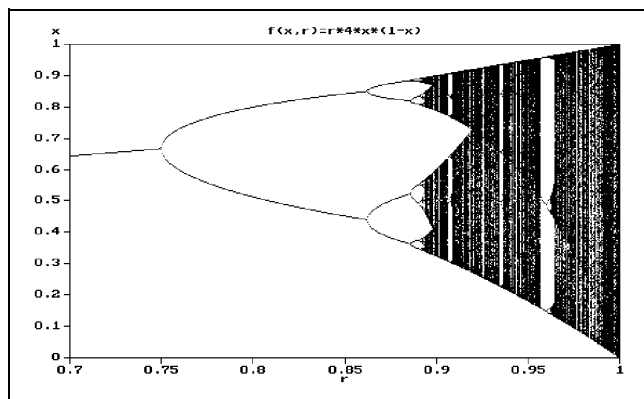


**Figure 2.8** Bifurcation diagram - Logistic map.

0.8921 and so on. There are regions of periodic behaviour between regions of chaotic behaviour for  $0.8921 \leq r \leq 1.0000$ , such *periodic windows* occur frequently in chaotic systems.

## Chapter 2 - Nonlinear Dynamics

In *quasi-periodicity* or *Hopf bifurcation*, the system begins again with a limit cycle trajectory. As a control parameter is changed, a second periodicity appears in the behaviour of the system. If two periodic motions whose periods have a common measure are combined, the resulting motion is still periodic. However, if the ratio of the period of the second type of motion to the period of the first is not a rational number, then the resulting motion is said to be quasiperiodic as the motion never repeats exactly but almost repeats itself. Under some circumstances, if the control parameter is changed further, the motion becomes chaotic.

The *intermittency* route to chaos is characterised by dynamics with irregularly occurring bursts of chaotic behaviour with intervals of apparently periodic behaviour [Grebogi 1987]. As a control parameter is varied, the chaotic bursts become longer and occur more frequently until the whole system becomes chaotic.

A *crisis* [Grebogi 1982] is a bifurcation event in which a chaotic attractor and its basin of attraction suddenly disappear or reduce in size as a control parameter is changed. If the control parameter is changed in opposite direction, the chaotic attractor suddenly appears or the size of the attractor increases.

Although the nature of an attractor changes suddenly as a parameter is varied, these sudden changes are often hidden by chaotic transients. In a *chaotic transient*, the system's trajectory wanders through state space, in an apparently chaotic fashion [Grebogi 1986]. Eventually the trajectory approaches a regular, periodic attractor. As the control parameter is changed, the chaotic transient lasts longer and longer until finally the motion becomes chaotic.

### 2.9 Other key areas of chaos theory.

*Embedding techniques* are widely used to model chaotic systems in experiments when mathematical descriptions are unavailable. These techniques are used to reconstruct the attractor, estimate fractal dimension, estimate Lyapunov exponents, locate fixed points and so on. This is one of the most important techniques in chaos theory and is described fully in chapter four.

*Control of chaotic systems* is the main theme of this report and it is discussed in chapter five.

There are a number of key aspects of chaos theory which are out of the scope of this report. Some of the most well studied questions concern *entropy*, *universality*, *Quantum chaos*, *Hamiltonian chaos* and *fractals*. Readers interested in these theories may refer to section 2.13.

## 2.10 Detecting chaos

How can we know a system is exhibiting chaotic behaviour? A detection of chaos subjects the system output to several tests, each of which determines some characteristic signature of chaos. W. R. Derrick [Derrick 1993] provides a good basis for detecting chaos. He describes the main tests involving: time series, Poincaré section, return and stroboscopic maps, fractal dimension, Lyapunov exponents, power spectra and autocorrelation.

### 2.10.1 Test 1: Time series

Chaotic time series appear noisy and random as in Figure 2.5, but systems with a high periodicity may also offer a similar appearance to the external observer. It is therefore ill advised to look for chaos only in a time series plot, though it is almost always the initial test to be carried out. A time series plot illustrates the system behaviour to some extent, but is difficult to interpret if a long time period is chosen, as the fine detail cannot be observed. However, for a system displaying intermittency we need to plot the time series for a long period. This dilemma is another reason why a simple time series test is often unreliable.

If a mathematical description of the system is available, it is useful to plot trajectories starting at nearby initial conditions and compare the resulting time series. Chaos is probably present if these trajectories diverge.

### 2.10.2 Test 2: Poincaré section

A state space plot generally does not distinguish between noisy and chaotic data. For this purpose it is useful to take some sort of cross section of the state space in order to reduce its dimension by one. After such an operation, chaotic data will often appear in the form of a strange attractor having a fractal structure with a fractal dimension.

If the Poincaré section consists of just a few points, it is a good indication that the orbit is periodic with period equal to the number of points. When the section describes a locus such as a closed curve or a line, it gives evidence of *quasi-periodicity* and possibly of chaos. Quasi-periodicity means a periodic orbit with a very high period. When the section fills a region containing a strange object, there is a good evidence of chaos.

It is often useful to look for horseshoe shapes in the Poincaré section, as these can be indications of chaos.

Any folding should be carefully analyzed as this flow mixing is the principle that leads to chaos in some systems, an example of which is the Lorenz model. Random data will fill the dimensional volume, whereas chaotic data may yield a structure with less than the state space dimension. With random data dominated by noise, no discernible pattern emerges.

### 2.10.3 Test 3: Return and stroboscopic maps

The return map and the stroboscopic map can also be used to detect chaos. In these maps, points which fall on the line of identity signify periodic orbits of period one. By increasing the time between successive coordinates of the plot, it is possible to locate periodic orbits of higher order. For example, by increasing the time by twice, the points which fall on the line of identity signify periodic orbits of two.

It should be noted that increasing the delay time will make the points in the map spread, thus making them less easy to interpret. Again, if the map consist of a strange object, this is good evidence of chaos.

### 2.10.4 Test 4: Fractal dimension

When the fractal dimension of the system is not an integer, this is an indication that the system is chaotic, as the attractor of the system is strange. However, periodic systems could also yield non-integer fractal dimensions if the signal to noise ratio is high, for example in the measurements obtained from a physical system.

### 2.10.5 Test 5: Lyapunov exponents

This test measures sensitivity of the system to changes in initial conditions. The Lyapunov exponent is a measure of the rate at which nearby trajectories in state space diverge. If at least one of the Lyapunov exponents is positive, it means that the system is chaotic. (Recall that the fundamental mathematical definition of a chaotic system is that it has at least one positive Lyapunov exponent.) For periodic systems, all Lyapunov exponents are negative or equal to zero. Unlike test 4, this test is fairly robust in the face of noise, as a periodic system always exhibits periodicity even when the measurements have a high noise level. Such systems will not, of course, display the butterfly effect.

### 2.10.6 Test 6: Power spectra

The power spectrum of a time series is calculated by the *fast Fourier transformation*, FFT. The result of applying a one dimensional FFT consists of a sequence of frequencies with associated intensities. This set

of pairs of numbers is best presented graphically, displaying intensity versus frequency. Such a diagram is referred to as a *power spectrum* or *Fourier spectrum*. Construction of power spectra has been utilised as a standard means for characterising chaos.

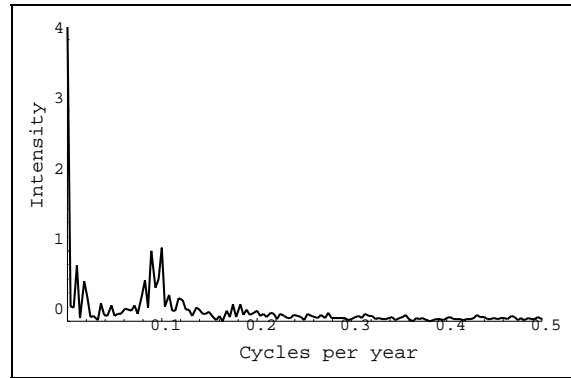


**Figure 2.9** A power spectrum for Sun spot data.

The power spectra for a periodic systems with small periods usually produce a few sharp peaks, for a chaotic system it is broad.

A power spectrum of the Sun spot data is illustrated in Figure 2.9. As the signal to noise ratio increases, the plateau of the spectrum rises and the peaks begins to vanish. A difficulty in detecting chaos using the power spectrum is that noisy experimental data for quasi-periodic systems may also appear as chaotic. In [Crutchfield 1980], the relationship between the spectra and the associated attractor topology are discussed.

### 2.10.7 Test 7: Autocorrelation

The *autocorrelation function* measures the linear dependence of a variable separated in time. It is defined as

$$g(l) = \frac{\sum_k x_k \tau x_{(l+k)\tau}}{\sum_k |x_k \tau|^2} \quad (\text{II.18})$$

$g(l)$  compares a data point in a time series with a data point located  $l$  units of time away. If, on the average, they are uncorrelated then  $g(l) = 0$ . If they are the same, then  $g(l) = 1$ . For data sets from chaotic systems, initially the autocorrelation function is expected to fall off exponentially with  $l$ ,  $g(l) = ae^{-l\beta}$  where  $\beta$  is called the autocorrelation time.  $\beta$  is estimated as the slope of the graph  $\ln g(l)$  vs  $l$ .

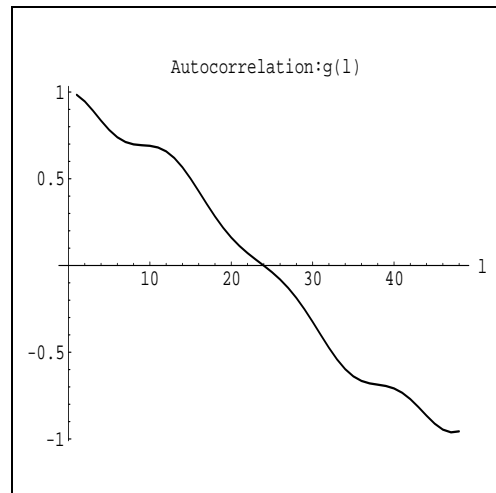


**Figure 2.10** Autocorrelation of a chaotic system.

The autocorrelation function is very simply calculated but may be misleading if the data is noisy. If chaos is present, the autocorrelation function is expected to reach zero. As the signal to noise ratio increases, some quasi-periodic systems may also reach zero. This could lead to a false conclusion regarding the system under study.

In Figure 2.10, the autocorrelation function for the Duffing oscillator is plotted as a function of delay time. As can be seen, initially the curve almost fits  $ae^{-l\beta}$  for  $g(l) > 0$ . The autocorrelation function reaches zero at  $23\tau$ , and the local minimum occurs at  $47\tau$ . Subsequently,  $g(l)$  oscillates between 1 and -1.

### 2.10.8 Conclusion

At least some of the tests mentioned in this section should be used to detect chaos when the class of a system is unknown. In experiments, noise is always present either in the form of instrumental or truncation error. The effect of noise is significant and some of the issues are addressed in [Crutchfield 1981], [Belmonte 1988] and [Provenzale 1992]. It is therefore necessary for experimental data to make sure that the noise level is kept as low as possible, possibly by use of a noise reduction method [Pfister 1992].

In many experiments, the mathematical models are not available. In such situations, the embedding techniques described in chapter four should be used.

Tests one, four and five are conclusive when a mathematical description of the system is used. Where a mathematical description is not available and real data is used, one should apply as many of the tests as possible in an attempt to counteract the effects of noise.

## 2.11 Numerical integration

Since digital computers work in discrete time, a numerical integration algorithm models a continuous time system by a discrete time system. Integration algorithms differ in that they model the same differential equation into different discrete time systems.

When we study chaotic models, we need to use a numerical integration algorithm. Therefore it is desirable to choose an algorithm which is as accurate as possible with respect to computational expense. It is quite common for end users to treat an integration algorithm as a *black box*, so that given the initial conditions, the final time and the error tolerance, out comes the final state. We must be satisfied that the results of the integration represents the true nature of the model.

In this section we will introduce different types of numerical integration algorithms, the associated types of errors and justify the use of the particular numerical integration algorithms employed in the simulations of chaotic models.

### 2.11.1 Types of integration algorithms

Perhaps the most important numerical task in simulations of continuous time systems is the calculation of trajectories. The effect of integration algorithm used is often overlooked. There are several types of integration algorithms to choose from. Commonly used numerical integration algorithms can be divided into two types, *single-step* and *multi-step*.

The single-step algorithms include *Forward Euler*, *Backward Euler*, *Trapezoidal* and *k th-order Runge-Kutta*. These algorithms require only one input point at each step. Higher order single-step algorithms are used to increase accuracy but tend to be computationally inefficient. For example *k th-order Runge-Kutta* requires *k* evaluations of the function per step. Furthermore, the function evaluation performed during a step is not used in any of the succeeding steps.

The multi-step algorithms include *Adams-Bashforth*, *Adams-Moulton* and *Gear's algorithm*. An *m*-step algorithm uses the *m* previous points and the value of the function at these points to estimate the next point.

There are many books [Atkinson 1978], [Pearson 1986], [Smith 1986] with detailed analyses of these algorithms and the interested reader may refer to them.

### 2.11.2 Integration error

The output of a continuous time system is a time waveform and the output of an integration algorithm is a sequence of points. There are two types of *integration error*: *local* and *global* errors. The local error is the error introduced by a single step of the integration algorithm. The global error is the accumulation of the local errors. The errors can further be divided into two categories : *round-off* and *truncation* errors.

#### 2.11.2.1 Round-off error

The local round off error is the inevitable error that results from performing 'real' fixed length precision arithmetic on a digital computer. The error depends on the fixed length precision and the number and type of arithmetic operations per step, and is independent of the integration step size.

The only way to reduce round off error is to choose superior hardware or increase the precision of the floating point representation. For each calculation, a typical single precision representation uses 32 bits and is accurate to about seven decimal places. Most double precision representations use 64 bits and are

accurate to about fifteen decimal places for each integration step.

Global round-off error is the accumulation of the local round-off errors. Therefore, a larger step size leads to a smaller global round-off error.

Some packages such as *Mathematica*<sup>™</sup> by Wolfram research, allow the user to specify the number of digits of precision of the final numerical integration result (Mathematica will then compute to the requisite precision length) or to set the number of digits of precision to use in internal computations. These features are useful in minimising the local and global round-off errors. Of course, the price that the user must pay for the enhanced accuracy is in increased memory requirement and actual computing time.

### 2.11.2.2 Truncation error

Truncation error is the error which occurs assuming there is no round-off error. This error depends only on the algorithm and is therefore hardware independent.

For an algorithm of a given order, the truncation error decreases with the step size. This is expected as a discrete time system approximates a continuous one more closely as the sampling time is decreased. However, decreasing the step size increases both global round-off error and the computation time.

For a given step size the higher order algorithms are more accurate than the lower order algorithms. Most multi-step routines, including those used in *Mathematica*<sup>™</sup>, automatically adjust both their step size and the order to achieve the desired accuracy with the largest possible step size.

### 2.11.3 Integration routines

Any useful integration routine should automatically adjust the step size to use the largest step size which satisfies the error tolerance, also it should adjust the order of the integration algorithm as well to reduce the computation time. Since we are interested in the reduction of integration error and not of the step size when simulating chaotic systems, an ideal routine should take an error tolerance as an input. Typically such an algorithm (*variable step size* routine) works as follows. The user supplies an integration error tolerance  $E$ . The routine chooses a step size, calculates  $x_{k+1}$  and then estimates the error. If the error exceeds  $E$ , the step size is reduced and new  $x_{k+1}$  is calculated. The process is repeated until the error is less than  $E$ . If the error is much less than  $E$ , the step size is increased for the next step.

Suppose the current time is  $t_k$  and the current step size is  $s_k$ . The next point a variable step size routine

calculates  $x_{k+1}$  at time  $t_{k+1} = t_k + s_k$ , assuming that the error was less than  $E$ . Suppose the user requests an output point at time  $t'$  where  $t_k < t' < t_{k+1}$ . There are two common ways to estimate the output point. The first approach is to set  $t_{k+1} = t'$ . Routines of this type are called *extrapolating* routines. The second is to calculate the solution at time  $t_{k+1}$  and then use an interpolation formula to calculate the solution at time  $t'$ . Routines of this type are called *interpolating* routines. Most routines which use multi-step algorithms such as Adam-Moulton are interpolating routines. Routines which use single-step algorithms such as Runge-Kutta are extrapolating routines.

Extrapolating routines are not suitable for applications which require closely spaced output points. Consider that  $s_k = 0.1$  and the user requests output points at intervals of 0.01. An interpolating routine takes an integration step with the natural step-size of 0.1, and then uses interpolation nine times to calculate the output points requested. An extrapolating routine takes ten integration step of 0.01 instead, therefore the extra computation for the integration takes ten times as long. The accuracy of the output point is increased, however since the larger step-size of 0.1 meets the error tolerance, the additional accuracy is not required.

#### 2.11.4 Integration of chaotic systems

The integration of a chaotic system poses a special difficulties, as the butterfly effect implies that an arbitrarily small error eventually affects the global behaviour of the system, and error is inherent in any integration algorithm. Therefore the simulations of chaotic systems require careful interpretation and should always be verified. Ideally, two or more different routines should be used to integrate the same system so as to validate the calculations.

An integration routine cannot estimate the state of a chaotic system with any accuracy after a long period of integration. So how can we be confident in simulations of chaotic systems?

If the local error is reasonably small, then the output points  $x_i$  of the integration routine may not lie on the trajectory, but they do still approach the attractor. When stepping from  $x_n$  to  $x_{n+1}$ , the effect of the error is to switch from the trajectory  $\Phi_t(x_n)$  passing through  $x_n$  to the trajectory  $\Phi_t(x_{n+1})$  passing through  $x_{n+1}$ . If the error is small,  $x_{n+1}$  will still be in the same basin of attraction and the new trajectory approaches the attractor. This is known as a *trajectory hopping* and is illustrated in Figure 2.11. In any strange attractor, the contraction outweighs the expansion and it follows that the sequence of integration points approaches the attractor.

In simulations of chaotic systems we are mostly concerned with the long-term behaviour and not in the

exact location of a trajectory. Therefore applications that do not require one specific trajectory to be followed, but only the points which lie on the attractor, are possible by numerical integration. Even when estimating the Lyapunov exponents, though it may appear that precisely one trajectory should be followed, the trajectory hopping caused by the local error in most cases does not significantly affect the final result as the trajectories in a same basin of attraction have same Lyapunov exponents.

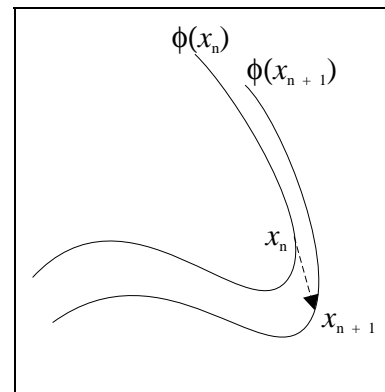


Figure 2.11 Trajectory Hopping.

## 2.12 Chapter summary

In this chapter we have first described commonly used terms in nonlinear dynamics. These were dynamic and static variables, state space, trajectory, limit set, limit cycle, stable and unstable manifolds, phase portrait, degrees of freedom, and dissipative and conservative systems.

The stability of limit sets were described by using the Jacobian matrix and the associated eigenvalues. The types of equilibrium points in a multi-dimensional system were defined as node, spiral node, repeller, spiral repeller, saddle point and spiral saddle point.

Descriptions of chaotic systems were given using these properties. We have seen that a chaotic system is sensitive to initial conditions, has at least one positive Lyapunov exponent, has a non-integer fractal dimension and that a Poincaré section could be used to study chaos. The stability of fixed points in a surface of section were defined.

Three different methods of estimating the fractal dimension were presented in the forms of capacity, Lyapunov and correlation dimensions.

We saw that there are a number of ways in which a periodic system can change into a chaotic system. The routes to chaos introduced were period-doubling bifurcation, quasi-periodicity bifurcation, intermittency, crisis and chaotic transient. Some routes to chaos were defined as local since changes involve bifurcations of limit cycles and others were defined as global as changes involve a considerably larger fraction of the attractor.

The usefulness of the tests was discussed in order to distinguish chaotic from non-chaotic systems. The tests suggested to detect chaos were: time series, Poincaré section, return and stroboscopic maps, fractal dimension, Lyapunov exponents, power spectra and autocorrelation.

Some of the issues involved in using a numerical integration algorithm were discussed. These included the types of the algorithms, integration error and integration of chaotic systems. Use of a numerical integration algorithm for most simulations of chaotic systems was justified.

### **2.13 Further reading**

We have introduced only a few aspects of the fast growing science of nonlinear dynamics and chaos. In this section interested readers are pointed to various books and papers.

For readers new to nonlinear dynamics and chaos, following books give good account of the subject. [Gleick 1987] is a well publicised book which became a best seller, and is a nice introductory book including a history of chaos. Books by Ian Stewart [Stewart 1989], [Stewart 1996] are also best sellers. The first book is easy to read yet covers most of the key topics of chaos. [Hall 1992] is a collection of easy to read introductory papers to different areas of research in chaos. For readers who wish to study the behaviours of nonlinear dynamics (including chaos) geometrically, a series of visual mathematics books by Abraham and Shaw [Abraham 1982], [Abraham 1983], [Abraham 1985] are good starting points with many pictures which describe the concepts in dynamical systems well. The first book is on periodic behaviour, the second is on chaotic behaviour and the third is on global behaviour. Edward N. Lorenz is one of the leading figure of chaos theory. His book [Lorenz 1993] is a good survey of chaos which includes a brief list of the terminology of dynamical systems and chaos.

There are a number of books which cover most key topics. [Hilborn 1994] is a highly recommended book which covers most of the theory in depth. [Peinke 1992] was partly written by O. E. Rössler (see chapter III) with a good mixture of theory and experimental results.

[Cvitanovic 1989], [Hao 1990] are collections of the significant papers along the road towards understanding chaos. [Eckmann 1985] is a classic paper which summarised the main mathematical ideas and analysis of experimental data which are still useful today. Contemporary chaos research areas with strong emphasis on experiments are described well in [Kim 1992], [Ott 1994], [Thompson 1994].

For readers who are interested in implementing the algorithms often used in nonlinear dynamics and chaos, [Parker 1989] is particularly good with its easy to follow pseudo-code descriptions of the algorithms with appropriate theoretical justifications. This books come with a collection of IBM PC programs.

### **Chapter references**

[Abraham 1982] R. H. Abraham and C. D. Shaw, *Dynamics - The geometry of behavior Part One* :

## Chapter 2 - Nonlinear Dynamics

*Periodic Behavior*, Aerial Press, California, 1982.

[Abraham 1983] R. H. Abraham and C. D. Shaw, *Dynamics - The geometry of behavior Part Two : Chaotic Behavior*, Aerial Press, California, 1983.

[Abraham 1985] R. H. Abraham and C. D. Shaw, *Dynamics - The geometry of behavior Part Three : Global Behavior*, Aerial Press, California, 1985.

[Atkinson 1978] K. E. Atkinson, *An introduction to numerical analysis*, John Wiley & Sons, Canada, 1978.

[Belmonte 1988] A. L. Belmonte, M. J. Vision, J. A. Glazier, G. H. Gunaratne and B. G. Kenny. *Trajectory Scaling Functions at the Onset of Chaos: Experimental Results*, Physical Review Letters 61, 5, 539-542, 1988.

[Crutchfield 1980] J. Crutchfield, D. Farmer, N. Packard, R. Shaw, G. Jones and R. J. Donnelly. *Power spectral analysis of a dynamical system*, Physics Letters A 76, 1-4, 1980.

[Crutchfield 1981] J. Crutchfield, M. Nauenberg and J. Rudnick. *Scaling for External Noise at the Onset of Chaos*, Physical Review Letters 46, 933-935, 1981.

[Cvitanovic 1989] P. Cvitanovic. *Universality in Chaos : second edition*, Adam Hilger, Bristol, 1989.

[Derrick 1993] W. R. Derrick in *Chaos in chemistry and biochemistry*, Ed R. J. Field and L. Györgyi, World Scientific Publishing, 1993.

[Eckmann 1985] J. P. Eckmann and D. Ruelle. *Ergodic theory of chaos and strange attractors*, Rev. Modern Physics 57, 3, 617-656, 1985.

[Gleick 1987] J. Gleick. *CHAOS : Making a new science*, Abacus book, London, 1987.

[Grassberger 1983] P. Grassberger and I. Procaccia, *Characterization of Strange Attractors*, Physical Review Letters 50, 5, 346-349, 1983.

[Grebogi 1982] C. Grebogi, E. Ott, J. A. Yorke. *Chaotic Attractors in Crisis*, Physical Review Letters 48, 1507-1510, 1986.

[Grebogi 1986] C. Grebogi, E. Ott, J. A. Yorke. *Critical Exponent of Chaotic Transients in Nonlinear Dynamical Systems*, Physical Review Letters 57, 1284-1287, 1986.

[Grebogi 1987] C. Grebogi, E. Ott, J. A. Yorke. *Critical exponents for crisis-induced intermittency*, Physical Review A 36, 5365-5380, 1987.

[Greenside 1982] H. S. Greenside, A. Wolf, J. Swift and T. Pignataro. Physical Review A 25, 3453, 1982.

[Hall 1992] N. Hall. *The new scientist guide to chaos*, Penguin books, London, 1992.

[Hao 1990] B. Hao, *Chaos II*, World Scientific, 1990.

[Hilborn 1994] R. C. Hilborn. *Chaos and Nonlinear Dynamics : An introduction for scientists and engineers*, Oxford University press, New York, 1994.

[Holmes 1990] P. Holmes. *Poincaré. celestial mechanics, dynamical-systems theory and "chaos"*, Physics

Reports 193, 3, 137-163, 1990.

[Kaplan 1979] J. Kaplan, J. A. Yorke in *Chaotic behavior of multidimensional difference equations*, H. O. Peitgen et al., Eds., "Springer Lecture, Notes in Mathematics", Springer-Verlag, Berlin, Volume 730, 204-227, 1979.

[Kim 1992] J. H. Kim and J. Stringer, *Applied Chaos*, John Wiley & Sons, Canada, 1992.

[Lorenz 1963] E. N. Lorenz. *Deterministic Nonperiodic Flow*, J. Atmospheric Sciences 20, 130-141, 1963.

[Lorenz 1993] E. N. Lorenz, *The essence of chaos*, University of Washington press, 1993.

[Ott 1994] E. Ott, T Sauer and J. A. Yorke, *Coping with Chaos*, John Wiley & Sons, Canada, 1994.

[Parker 1989] T. S. Parker and L. O. Chua. *Practical Numerical Algorithms for Chaotic Systems*, Springer-Verlag, New York, 1989.

[Pearson 1986] C. E. Pearson, *Numerical methods in engineering and science*, Van Nostrand Reinhold Company Inc, England, 1986.

[Peinke 1992] J. Peinke, J. Parisi, O. E. Rössler and R. Stoop, *Encounter with Chaos : Self-Organized Hierarchical Complexity in Semiconductor Experiments*, Springer-Verlag, 1992.

[Pfister 1992] G. Pfister, Th. Buzug and N. Enge. *Characterization of experimental time series from Talyor-Couette flow*, Physica D 58, 441-454, 1992.

[Provenzale 1992] A. Provenzale, L. A. Smith, R. Vio and G. Murante. *Distinguishing between low-dimensional dynamics and randomness in measured time series*, Physica D 58, 31-49, 1992.

[Ruelle 1980] D. Ruelle. *Strange Attractors*, The Mathematical Intelligence 2, 126-137, 1980.

[Russell 1980] D. A. Russell, J. D. Hansen, and E. Ott. *Dimensions of Strange Attractors*, Physical Review Letters 45, 1175-1178, 1980.

[Sano 1985] M. Sano and Y. Sawada. *Measurement of the Lyapunov Spectrum from a Chaotic Time Series*, Physical Review Letters 55, 10, 1082-1085, 1985.

[Smith 1986] W. A. Smith, *Elementary Numerical Analysis*, Prentice-Hall, England, 1986.

[Stewart 1989] I. Stewart, *Does God Play Dice : The new mathematics of chaos*, Penguin books, England, 1989.

[Stewart 1996] I. Stewart, *From Here to Infinity : A guide to today's mathematics*, Oxford University Press, England, 1996.

[Thompson 1994] J. M. T. Thompson and S. R. Bishop, *Nonlinearity and Chaos in Engineering Dynamics*, John Wiley & Sons, England, 1994.

## CHAPTER III

### CHAOTIC MODELS

---

#### 3.1 Introduction

In this chapter we will briefly introduce Hamiltonian systems and move onto studies of four dissipative systems: the Lorenz model, the Hénon map, the Rössler model and the Duffing oscillator model.

These models exhibit chaotic behaviour for some range and combinations of the control parameters. Our aim is to define the range and the combination so that the systems behave chaotically. We will use some of these systems in chaotic modes to demonstrate the embedding techniques and the control method described in Chapter IV and Chapter VI, respectively.

#### 3.2 Hamiltonian systems

The important feature of a dissipative system from the state space point of view is the collapse of a volume of initial conditions in state space. That is, we need to consider only the attractors to understand the long-term dynamics of the system.

If the rate of dissipation is small it takes longer for a volume of initial conditions to collapse onto the attractor. When there is no dissipation at all, we would expect a volume of initial conditions to remain constant for all time and there then exist no attractors for the trajectories.

Systems with no dissipation are called conservative or Hamiltonian systems. The term conservative means that certain physical properties of the system remain constant in time. These quantities are called *conserved quantities*. Unlike a dissipative system, a Hamiltonian system does not settle down to an attractor, although they may exhibit chaotic behaviour in the sense that the set of points visited is everywhere dense in the state space.

In practice, many real systems are nearly conservative. The most famous *almost* conservative system is the solar system. Over the time periods of concern we can neglect most aspects of dissipation. To a high degree of approximation these dissipative effects can be neglected if we limit ourselves to time periods of a few millions years. Based on these assumptions, we can model the dynamics of the solar system with

a Hamiltonian model.

Further discussions of Hamiltonian systems is out of scope of this report. In the remaining chapters we will consider only dissipative systems.

### **3.3 Dissipative systems**

In comparison with Hamiltonian systems the structure of state space is much richer and the dynamics more diverse in dissipative systems. One of the distinctive features of dissipative systems is the existence of attractors and repellers.

In this section, we study four classic models which are known to exhibit chaos. These models are used in later chapters for demonstration purposes.

The numerical integrations were performed by using the *Mathematica*<sup>™</sup> running under *Windows*<sup>™</sup> 3.1.

#### **3.3.1 The Lorenz model**

The Lorenz model [Lorenz 1963] is based on a simplification of the fundamental Navier-Stokes equations for fluids in the context of weather prediction. The fluid motion and resulting temperature differences can be expressed in terms of three variables  $x$ ,  $y$  and  $z$ , where  $x$  is related to the time dependence of the fluid stream function. Taking the derivatives of the stream function with respect to the spatial variables gives the components of the fluid flow velocity. In the model, the spatial dependence of the stream function is chosen to match the simple pattern of convective rolls. Thus the model cannot apply to fluids that develop more complex spatial patterns. The variables  $y$  and  $z$  are related to the time dependence of temperature deviations away from the assumed linear temperature drop from bottom to top, which obtains for the nonconvective steady-state situation. The variable  $y$  is proportional to the temperature difference between the rising and falling parts of the fluid at a given height, while  $z$  is proportional to the deviation from temperature linearity as a function of vertical position.

The Lorenz model does not have any external periodic forcing to determine the fundamental period. Although the Lorenz model is based on a simple set of differential equations, it exhibits very complex behaviour, including period-doubling bifurcation and intermittency.

Recall from Chapter 2 that the Lorenz equations are defined as

$$\begin{aligned} \dot{x} &= \sigma (y - x) \\ \dot{y} &= x (R - z) - y \\ \dot{z} &= x y - b z \end{aligned} \tag{III.1}$$

where  $\sigma$ ,  $R$  and  $b$  are the control parameters. The parameter  $\sigma$  is defined to be the ratio of the kinetic viscosity (friction) of the fluid to its thermal diffusion coefficient. It roughly compares the rate of energy loss from a small packet of fluid due to viscosity to the rate of energy loss from the packet due to thermal conduction. The parameter  $R$  is proportional to the Rayleigh number, which is a measure of the temperature difference between the bottom and top of the fluid layer. Finally,  $b$  is related to the ratio of the vertical height of the fluid layer to the horizontal size of the convection rolls. It turns out that for  $b = 8/3$ , the convection begins

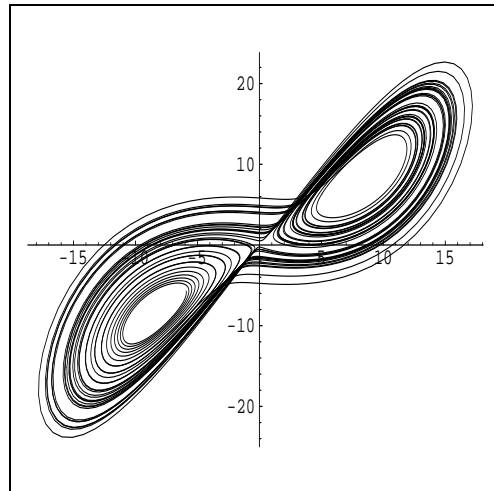


Figure 3.1 Lorenz attractor :  $x$  vs  $y$ .

for the smallest value of  $R$ . This is the value usually chosen for the study of the Lorenz model. The parameter  $\sigma$  is then chosen for the particular fluid under study. E. N. Lorenz [Lorenz 1963] used the value  $\sigma = 10$ , which corresponds roughly to cold water and  $R$  was chosen to be the adjustable control parameter which is varied to study different behaviours of the model.

For small values of  $R$ , the model predicts that the nonconvecting state is stable. This state is described by  $x = 0$ ,  $y = 0$  and  $z = 0$ . For values of  $R$  just greater than 1, steady convection sets in. There are two possible convective states, one corresponding to clockwise rotation, the other to anticlockwise for a given convective roll. Some initial conditions lead to one state, other conditions to the other state. If  $\sigma > b + 1$ , then this steady convection becomes unstable for large  $R$  and gives way to more complex behaviour. As  $R$  increases, the behaviour has regions of chaotic behaviour intermixed with regions of periodicity and regions of intermittency, which cycle back and forth, apparently randomly, between chaotic and periodic behaviour.

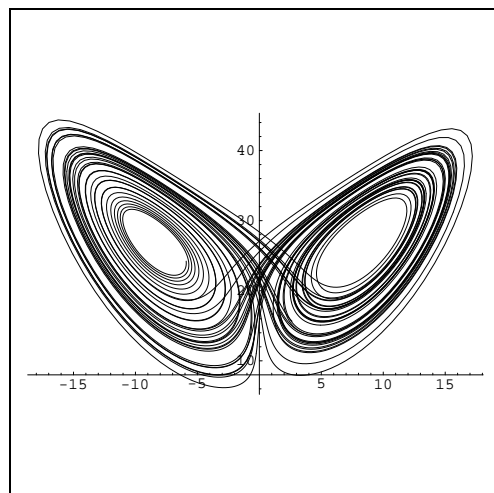
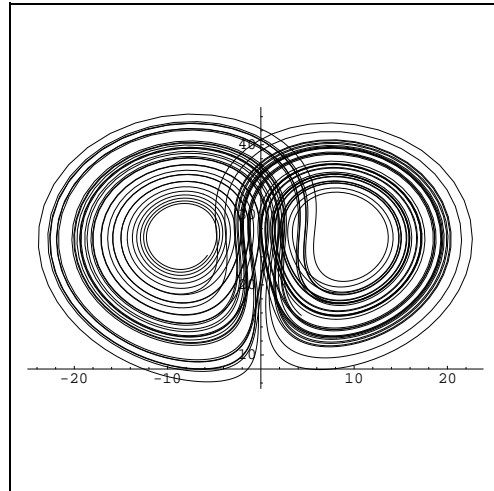


Figure 3.2 Lorenz attractor :  $x$  vs  $z$ .

The behaviour of the system for values of  $R = 0.5$  is illustrated in Figure 2.2, page 10. The system settles into the steady nonconvective state at the origin of the state space.

For  $R > 1$ , there are three fixed points. The one at the origin becomes a repeller. A slightest deviation from the conditions  $x = 0$ ,  $y = 0$  and  $z = 0$  repels the state space trajectory away from the origin. The other two fixed points are spiral nodes if  $R$  is not too large. Some initial conditions give rise to trajectories that approach one of the fixed points, other initial conditions give rise to trajectories that approach the other fixed point. For  $R$  just greater than 1, the other two fixed points become the attractors in the state space. Thus  $R = 1$  is a bifurcation value for the model.



**Figure 3.3** Lorenz attractor :  $y$  vs  $z$ .

When  $R$  is close to 144 the period-doubling route to chaos occurs. The behaviour is not simple harmonic, but it is aperiodic. We can understand the physical nature of the system's behaviour by looking at the graphs of  $x$  and  $y$  as functions of time in Figure 3.1. We see that  $x$  and  $y$  oscillate nearly symmetrically around the values  $x = 0$  and  $y = 0$ , respectively. This tells us that the fluid is convecting first in the clockwise direction, then anticlockwise, continually reversing as time goes on. The temperature difference between up flow and down flow  $y$ , also oscillates symmetrically around  $y = 0$ . However,  $z$  oscillates around a nonzero value, see Figure 3.2 and Figure 3.3.

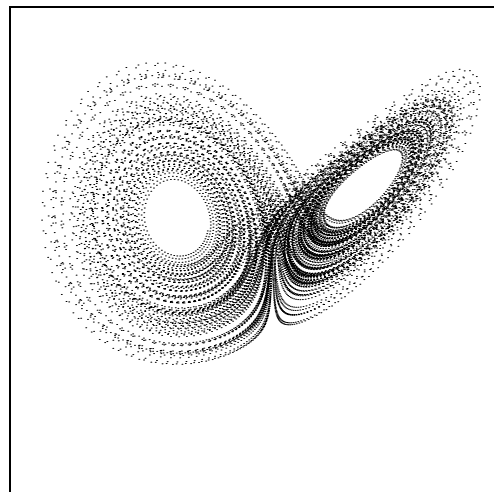


**Figure 3.4** Chaotic Lorenz attractor

The three dimensional Lorenz attractor can be seen in Figure 3.4. This graph synthesises the information of Figure 3.1, Figure 3.2 and Figure 3.3. The control parameters used for these plots were  $R = 144$ ,  $b = 8/3$  and  $\sigma = 10$ .

In [Sano 1985] the average Lyapunov exponents for these trajectories were found to be  $\mu_1 = 1.37$ ,  $\mu_2 = 0.00$  and  $\mu_3 = -22.37$ . The dimension of the attractor can be estimated by the Lyapunov dimension  $D_L$ , equation (II.16) in section 2.7.2, page 20.

As  $\mu_1 + \mu_2 \geq 0$ , it follows that

$$D_L = 2 - \frac{\mu_1 + \mu_2}{\mu_3} = 2 - \frac{1.37 + 0.00}{(-22.37)} = 2 + 0.06 = 2.06 \quad (\text{III.2})$$

This estimate compares favourably with the correlation dimension of 2.05 [Grassberger 1983].

### 3.3.2 The Hénon map: A two-dimensional Iterated Map

The motivation for studying iterated maps stems from the description of intersections of state space trajectories with Poincaré sections described in section 2.6.

In many cases, we can use the maps as models for physical systems even if we do not know the underlying differential equation models, so that this approach to modelling can give us useful insights for the dynamics of complex systems.

A one-dimensional iterated map is based on a function of a single variable and takes the form

$$X_{n+1} = f(X_n) \quad (\text{III.3})$$

The mathematical theory of one-dimensional iterated maps has played an important role both historically and conceptually in the development of chaos theory, and these maps can be studied in depth. An example of such a map, the Logistic map, was introduced in section 2.8.

Increasing the number of dimensions for iterated maps greatly increases the range of possible dynamic behaviours. At present very few systematic studies of two or more dimensional iterated map functions have been reported in depth.

To illustrate the behaviour of a two-dimensional map, let us consider the Hénon map [Hénon 1976]. This function is a simplified model of the Poincaré map for the Lorenz model, which exhibits the same essential properties. The Hénon map function is a two-dimensional extension of the one-dimensional quadratic map

$$\begin{aligned} X_{n+1} &= 1 + Y_n - aX_n^2 \\ Y_{n+1} &= bX_n \end{aligned} \quad (\text{III.4})$$

The Hénon map is an *invertible map function*, so that if we are given  $X_n$  and  $Y_n$ , we can find the unique pair of values  $X_{n-1}$  and  $Y_{n-1}$ , which gave rise to these values. Thus, we can follow both the forward and

backward iterations of the Hénon map. When  $b = 0$ , it becomes a quadratic map function.

$b$  should be small enough for the folding to occur, but not too small to observe the fine structure of the attractor. The standard values used are  $a = 1.4$  and  $b = 0.3$ . For these values the system is well studied in the literature [Hénon 1976], [Cvitanovic 1988], thus we have used them for our study. Depending on the initial condition, the sequence of points obtained by iteration of the equations either diverges to infinity or tends to a strange attractor. The Hénon attractor is illustrated in Figure 3.5.

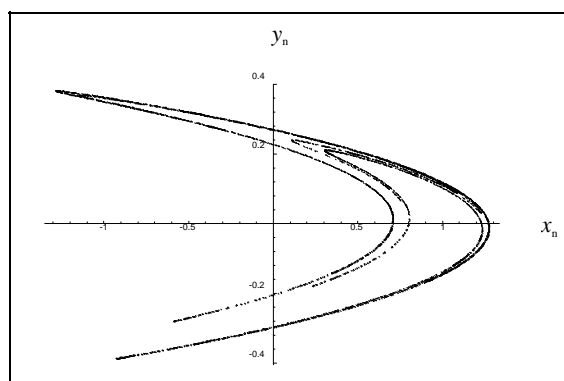


Figure 3.5 The Hénon attractor.

Given a suitable set of initial conditions, e.g.  $X_0 = 1.4$  and  $Y_0 = 0$ , the iterations of the Hénon map collapse the attractor in the  $Y$  direction. Once a point is in the attractor, the succeeding points will stay in the horseshoe like cluster for all time. If a section of the attractor is magnified, the structure will be that of a fractal, as in a Poincaré section of a continuous time system.

Recall that although we can be sure that the next point will fall in the attractor in a return map, we cannot predict the location. The only exception is if a point lies on the line of identity, we can then predict with some confidence that the next point could be located nearby. The reason is that as the attractor plots are essentially a stroboscopic maps in discrete time systems, any points which fall near the line of identity are saddle points. We know they are saddle points as the attractor is strange.

In [Sano 1985] the average Lyapunov exponents for these trajectories were found to be  $\mu_1 = 0.42$  and  $\mu_2 = -1.58$ . Repeating a similar procedure to (III.2), we estimate  $D_L \approx 1.27$ , which compares reasonably well with the reported correlation dimension of 1.25 [Grassberger 1983] and the capacity dimension of 1.26 [Russell 1980].

### 3.3.3 The Rössler model

Chemistry provides some very well known examples of chaos [Field 1993]. The dynamics of chemical reactions can display the same kind of periodic and chaotic behaviour that appears in other sciences but the transition from order to chaos is easier to study as the conditions of the experiments can be readily controlled.

The Rössler model [Rössler 1976] is based on abstract chemical kinetics. The equations are similar in appearance to that of the Lorenz model but the system behaviour is quite different, as can be seen from the three dimensional attractor in Figure 3.6.

The model is defined as

$$\begin{aligned} \dot{x} &= -z - y \\ \dot{y} &= x + ay \\ \dot{z} &= b + z(x - c) \end{aligned} \tag{III.5}$$

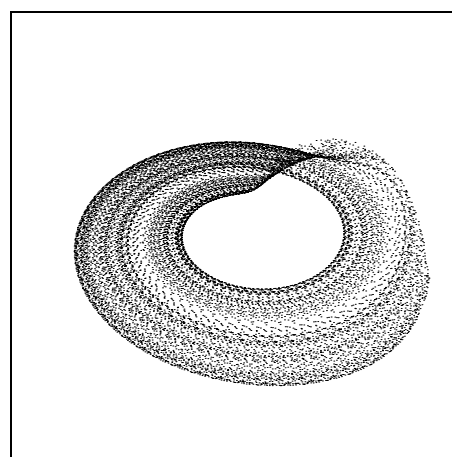


Figure 3.6 Chaotic Rössler attractor.

For  $x < c - a$ , any volume element shrinks continually as it flows through space. The model has a limit cycle for some choice of the parameters, for example  $a = 0.2$ ,  $b = 0.2$ , and  $c = 2.6$ . As  $c$  is varied period doubling bifurcations occur and finally when  $c = 5.7$ , the model becomes chaotic.

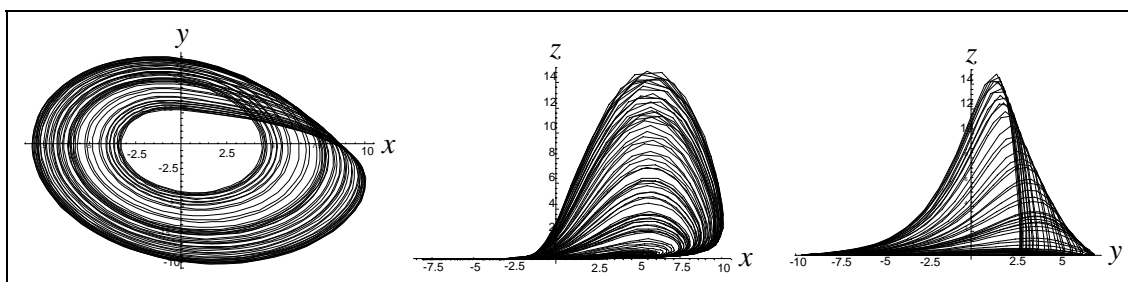


Figure 3.7 Two dimensional chaotic Rössler attractors.

For  $b = 0.4$ , the model also behaves chaotically. In Figure 3.7, the chaotic Rössler attractor is illustrated as three two-dimensional plots for  $a = 0.2$ ,  $b = 0.4$  and  $c = 5.7$ .

Let us now look at the plot of the autocorrelation function against the delay time, illustrated in Figure 3.8. The autocorrelation functions were calculated using 500 data points of the  $x$ -coordinate after the transients have disappeared, with the sampling time of  $\tau = 0.1$ . We observe from the plot that the function drops to zero when the delay time is  $14\tau$  and reaches the minimum value at  $30\tau$ .

We can say with some confidence that the model exhibits a chaotic behaviour as described in section 2.10.7.

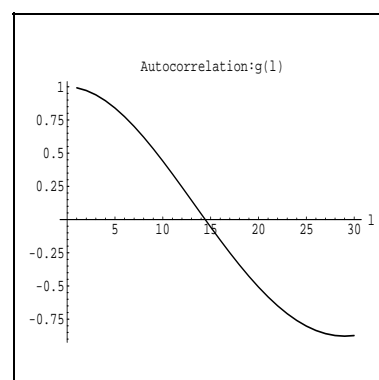
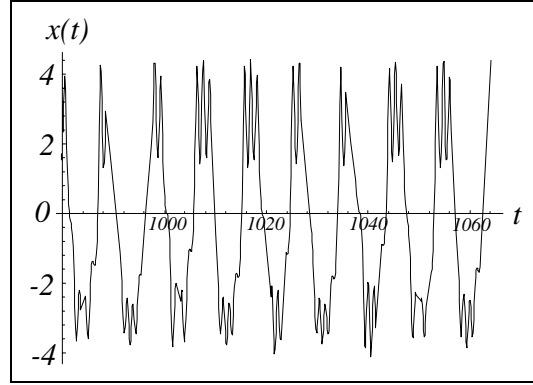


Figure 3.8 Autocorrelation of the Rössler model.

In [Sano 1985] the average Lyapunov exponents for these trajectories were found to be  $\mu_1 = 0.007$ ,  $\mu_2 = 0.00$  and  $\mu_3 = -4.98$ . Repeating the same procedure as (III.2) once again, we estimate  $D_L \approx 2.01$ .

### 3.3.4 The Duffing oscillator model

Duffing's model discussed in [Parlitz 1985] is based on a nonlinear electronic oscillator. Its solutions have a wide range of dynamical behaviour as the parameters are varied. The model is a nonlinear oscillator displaying *secondary resonances*. The secondary resonances signify the existence of a number of higher order periodicities of the nonlinear oscillations within the main periodic oscillation. This is illustrated in Figure 3.9 in the form of a time series plot of the  $x$ -coordinate.



**Figure 3.9** The Duffing oscillator time series displaying the secondary resonances.

The Duffing equations are defined as

$$\begin{aligned}\dot{x} &= y \\ \dot{y} &= -d y - x - x^3 + f \cos(2\pi z) \\ \dot{z} &= \omega/2\pi\end{aligned}\tag{III.6}$$

where  $\omega$  is the excitation frequency and  $f$  is the excitation amplitude. If  $f$  is sufficiently large the periodic oscillation occurs in units of  $2\pi/\omega$ .

The nonlinear term  $x^3$  in the equation makes the model chaotic. Without this term the model is a harmonic oscillator. The Duffing oscillator has been successfully used to model a variety of physical processes such as stiffening springs, beam buckling, nonlinear electronic circuits, ionisation waves in plasma etc.

In order to study the behaviour, we have study the model by fixing  $d = 0.2$  and  $\omega = 0.665$ . The amplitude  $f$  was taken to be 35, 35.28, 36, 37 and 38. For each value of  $f$  in ascending order, a stroboscopic map was created by using the values from  $x$ -coordinate sampled at  $2\pi/\omega$ . These maps are illustrated in Figure 3.10 (a) - (e), respectively.

It is interesting to observe that the regions visited by the trajectories expands between  $f = 35$  and  $f = 36$ . At  $f = 37$ , the attractor retains similar shape but at  $f = 38$ , there are only three regions visited. That is, for

this value of  $f$ , the system is almost periodic. What we are observing is the period-doubling route to chaos. The attractor gradually expands from  $f = 35$  to  $f = 37$  exhibiting complex behaviour but when  $f = 38$ , the system enters a periodic window.

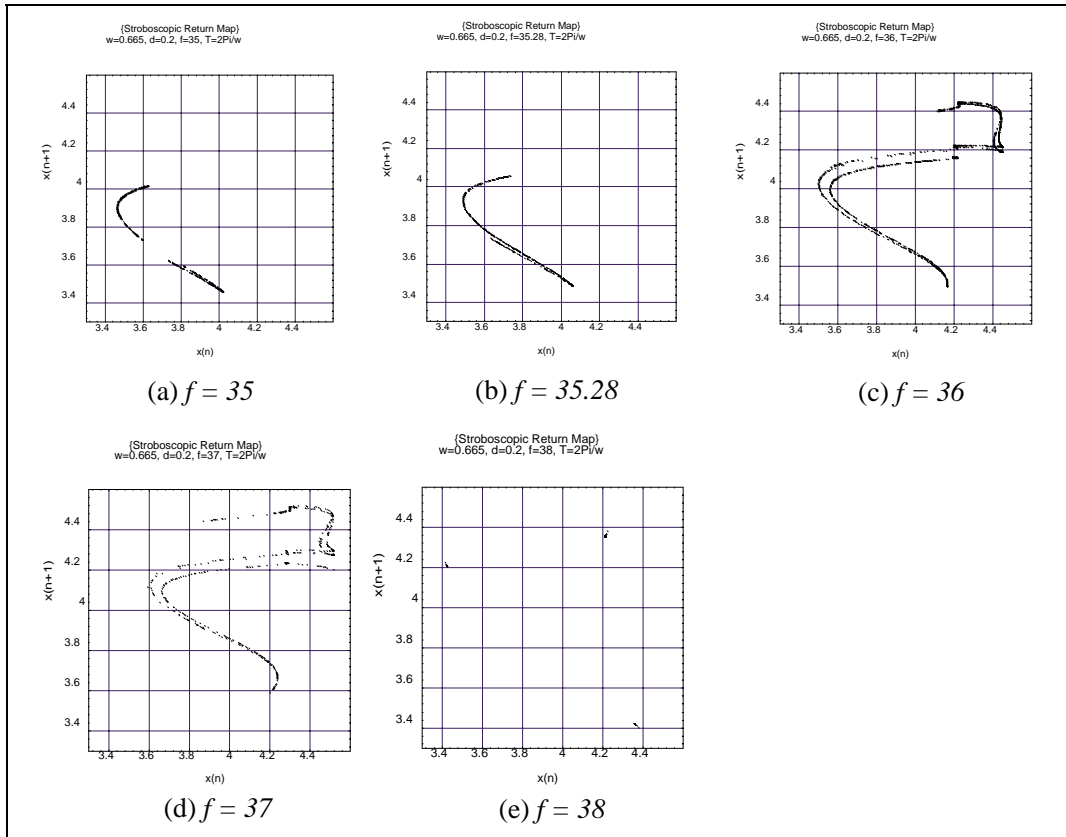


**Figure 3.10** Stroboscopic maps of the Duffing oscillator for different value of  $f$ .

It should be noted that the Duffing oscillator exhibits extremely rich dynamical behaviour and research on this model continues. A complete understanding of the system for all values of the control parameters has not yet been achieved. The best studied case is  $\omega = 1$ . The model is often referred to as the Ueda oscillator.

### 3.4 Chapter summary

In this chapter we have briefly introduced Hamiltonian systems followed by studies of four well known dissipative systems exhibiting chaos. These were the Lorenz model, the Hénon map, the Rössler model and the Duffing oscillator model. Higher dimensional systems were not studied as such systems are out of scope of this report, also there is a difficulty in understanding graphical representations of the attractors.

Model	Control parameters	Sampling period
Lorenz	$R = 144, b = 8/3 \text{ \& } \sigma = 10$	0.01
Hénon map	$a = 1.4 \text{ \& } b = 0.3$	-
Rössler	$a = 0.2, b = 0.4 \text{ \& } c = 5.7$	0.1
Duffing's oscillator	$d = 0.2, \omega = 0.665 \text{ \& } f = 36$	0.1

**Table 3.1** The control parameter combinations for chaotic behaviours.

The combinations of values of the control parameters, which make the models studied in this chapter chaotic are summarised in Table 3.1, Table 4.2. The sampling period was the time difference from a data point to the next.

### Chapter references

[Cvitanovic 1988] P. Cvitanovic, G. H. Gunaratne and I. Procaccis, *Topological and metric properties of Hénon-type strange attractors*, Physical Review A 38, 1503-1520, 1988.

[Field 1993] R. J. Field and L. Györgyi. *Chaos in chemistry and biochemistry*, World Scientific Publishing, 1993.

[Grassberger 1983] P. Grassberger and I. Procaccia, *Characterization of Strange Attractors*, Physical Review Letters 50, 5, 346-349, 1983.

[Hénon 1976] M. Hénon. *A Two-dimensional Mapping with a Strange Attractor*, Communications in Mathematical Physics 50, 69-77, 1976.

[Lorenz 1963] E. N. Lorenz. *Deterministic Nonperiodic Flow*, J. Atmospheric Sciences 20, 130-141, 1963.

[Parlitz 1985] U. Parlitz and W. Lauterborn. *Superstructure in the bifurcation set of the Duffing equation*, Physics Letters A 107, 8, 351-355, 1985.

[Rössler 1976] O. E. Rössler. *An Equation for Continuous Chaos*, Physics Letter A 57, 397-398, 1976.

[Russell 1980] D. A. Russell, J. D. Hansen, and E. Ott. *Dimensions of Strange Attractors*, Physical Review Letters 45, 1175-1178, 1980.

[Sano 1985] M. Sano and Y. Sawada. *Measurement of the Lyapunov Spectrum from a Chaotic Time Series*, Physical Review Letters 55, 10, 1082-1085, 1985.

## CHAPTER IV

### EMBEDDING TECHNIQUES

---

#### 4.1 Introduction

We have seen that chaotic systems relax to regions of the state space which have very complex structure and zero measure. Often, such objects are fractal, and have structure on ever smaller length scales. Strange attractors are characterised by metric invariants (which do not change under smooth transformations), such as fractal dimension, and Lyapunov exponents. However, such measures do not yield enough information on how to model the dynamics. In real applications, mathematical models of the systems are rarely known. In such situations, the idea of *embedding*, using successive values of a time series to construct a vector whose evolution through time better reflects the high dimension dynamics of the system as a whole, was first developed in 1980, and is extremely useful.

The use of successive samples of a single variable (or few variables) to generate an embedding with a view to reconstructing the details of an attractor for a higher dimensional dynamic system was suggested in [Packard 1980] and a frequently quoted embedding theorem [Takens 1980] establishes the existence of such models for homogeneous systems: if the underlying state space of a system has  $d$  dimensions then the embedding space needs to have at most  $2d + 1$  dimensions to capture the dynamics of the system completely. These results were later generalised and improved by [Levin 1993]. It is a remarkable fact that much of the dynamics of a high dimensional system can be recovered from a suitable embedding of a *single* variable, but in practice a critical factor in the accuracy of such reconstructions is the sampling delay. A comprehensive survey of various methods to estimate the optimum time delay can be found in [Casdagli 1991], see also [Buzung 1992] and [Rosenstein 1994]. Practical examples of constructing one-step predictive neural networks based on these ideas can be found in [Dracopoulos 1993].

Methods employing this technique are often referred to as *time delay*, *delay coordinates*, *embedded time series* or *embedding techniques*.

We shall show how to extract a multi-dimensional description of state space dynamics from the time series data of a single dynamical variable. The embedding techniques, which enables this process, is one of the most important technical contributions to the study of nonlinear dynamics. This technique is ideal to use when a mathematical model of the dynamic system under study is not available, as is the case in most real

world applications. The idea is to use the time series data of a single variable to create a multi-dimensional *embedding space*, although G. P. King and I. Stewart [King 1992] proposed a technique which makes the use of multiple variables for better attractor reconstruction. The idea behind Takens' theorem is that if the dynamics of the system is governed by *dth*-order differential equations then to numerically calculate the derivatives with respect to a single variable, we need two time samples for each derivative. In addition, we need the current value of the variable. Hence, we need a total of  $2d + 1$  values. This is an upper limit for the dimension of the required embedding space.

If the embedding space is generated properly, the behaviour of trajectories in it will have the same geometric and dynamical properties which characterise the actual trajectories in the full multi-dimensional state space, so that the evolution of the trajectories in the embedding space mimics the behaviour of the actual trajectories. As we have observed, it is remarkable that the original attractor can be reconstructed from observing a single coordinate of a dynamic system. However, there are a number of pitfalls. For a start we do not know the optimal sampling time to used for the time series. Also we do not know the optimal dimension to be used for the embedding space. These issues are addressed in later sections.

Once a suitable model is created by the embedding techniques, it is possible to use it to estimate the average Lyapunov exponents, the fractal dimension, locate fixed points, and study questions such as stability.

#### **4.2 Delay coordinates method**

For a multi-dimensional system, as the number of state space dimensions increases so does the number of values to be recorded. However, for many systems we may not know the required number of variables in advance. Also in practical terms, some variables are much easier to measure accurately than others. Both of these difficulties are bypassed by the delay coordinates method as the time series record of a single variable is often sufficient to determine many of the properties of the full dynamics of the system. If data is gathered from measurements of a physical system, only one state variable needs to be measured, thereby cutting instrumental and data storage costs. It is interesting to note that even when most of the sensors used to read measurements are not working, a faithful system behaviour might be reconstructed using only one working sensor reading.

The variable used to reconstruct the attractor should be easily accessible and as accurate as possible. In any experiment, there is a certain amount of noise. G. Pfister [Pfister 1992] suggests a method of reducing the effect of noise in experimental data to improve the accuracy of the estimation of dynamical variables.

## Chapter 4 - Embedding techniques

Generally, we wish to have the time between successive samples to be much less than the time to go around the attractor once, so as to have samples over nearly the complete range of the attractor. However, in some cases, the sampling time has been fixed by some experimental or computational criterion. Let us denote the minimum sampling interval between successive samples by  $\tau$ .

A state space attractor is reconstructed by using the experimental data consisting of a scalar time series of values  $x_\tau, x_{2\tau}, x_{3\tau}, \dots$ . This is done by grouping the values to form a set of vectors. For example, suppose we decide to use an  $m$ -dimensional reconstruction, that is to use an *embedding dimension* of  $d_E$ . We then group together  $d_E$  values. Such a vector gives the coordinates of a single point in the  $d_E$ -dimensional space.

A  $d_E$ -dimensional *embedding space vector* has the form

$$\xi_i = (x_{it_j}, x_{it_j + t_D}, \dots, x_{it_j + (d_E - 1)t_D}) \quad (\text{IV.1})$$

where  $t_D$  is the *delay time* and  $t_j$  is the *jump time*. The reconstructed attractor is then described by the set of vectors in the form (IV.1).

The method has a nice property that the signal to noise ratio on each component is the same. However, in practice it has the unpleasant property that in order to use it, it is first necessary to choose the correct embedding dimension, the delay time, and the jump time all of which can be difficult and time consuming.

### 4.3 Delay time

Delay time is the time period between successive components of each of the embedding space vectors. It is written as a multiple of the sampling time,  $t_D = n\tau$  where  $n \in \mathbb{N}$ . This time is also known as *time lag*, *time delay* and *lag*. There are various methods to find a suitable value of  $t_D$ , none of which are universal.

The problem of choosing an appropriate time between samples is a delicate one. If an infinite amount of noise free data is available, then almost any set of time intervals will do. However, with a finite amount of data contaminated by some noise, we must proceed very cautiously.

Although, Takens' theorem [Takens 1981] is important, as it gives a rigorous justification for state space reconstruction, the assumptions are that we have an infinite amount of noise free data. There is no guidance about practical considerations for choosing the right delay time. In practice, there is always some noise in the data. Also with a finite amount of data the approximation of the dynamics in the reconstructed

state space is never perfect. Therefore, it is important to choose a suitable delay time, preferably with a minimum computational cost. However, it is more important to choose the delay time which will reconstruct the original state space faithfully, as it is clear through experiments that the choice of delay time can make a big difference to the quality of the reconstructed attractor. Thus it is often necessary to compromise between the computation time and the quality of the reconstruction.

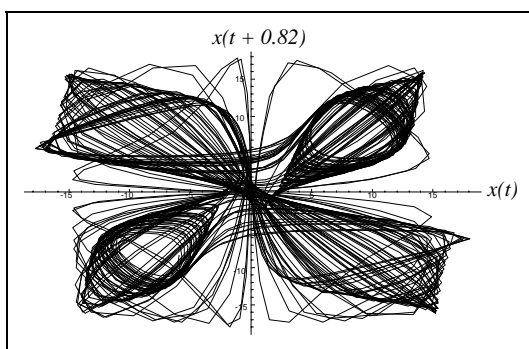


**Figure 4.1** Irrelevance,  $t_D = 0.82$ .

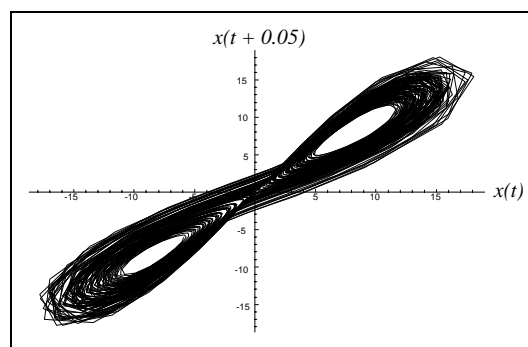


**Figure 4.2** Redundance,  $t_D = 0.05$ .

If  $t_D$  is too large, in the presence of chaos and noise, the dynamics at one time can become effectively causally disconnected from the dynamics at a later time, so that even simple geometric objects look extremely complicated. This is called *irrelevance* [Casdagli 1991]. The component of the embedding space vectors may be completely decorrelated, resulting in an essentially random distribution of points in the embedding space, leading to an attractor dimension close to the dimension of the embedding space [Albano 1988]. Also, if  $t_D$  is close to some periodicity in the system, the component at that period will be under represented in the reconstruction.

On the other hand if delay time is too small, each component in the embedding space vector will be indistinguishable and all trajectories will lie near the main diagonal line of the embedding space, leading to a reconstructed attractor with a dimension close to one. This is called *redundance*. To avoid this,  $t_D$  should make each component in the vector independent.

The algorithms for estimating the dimension of an attractor, which are described in next section, usually require a large number of data points as input, typically a few thousand for systems exhibiting low dimensional dynamics, but the number increases exponentially with the embedding dimension. However, the number of points can be reduced if the set of data points is chosen to maximise the amount of information it contains. This idea leads to algorithms which estimates  $t_D$  in a variety of ways.

Irrelevance and redundancy are illustrated using the Lorenz model in the previous chapter. In Figure 4.2, the delay time ( $t_D = 0.05$ ) is taken to be too small, so that the reconstructed attractor is squashed near to

the line of identity. In Figure 4.1, the delay time is taken to be much larger ( $t_D = 0.82$ ). This has caused the reconstructed attractor to bear little resemblance to the original attractor, by introducing irrelevant information, see section 3.3.1 for detail. There must be an optimum delay time to use for the system reconstruction lying between  $t_D = 0.05$  and  $t_D = 0.82$ . An important question is how to find such a delay time.

Practical criteria for selecting a method to estimate the delay time are that it should be computationally efficient, work well with noisy data and lead to consistent, accurate estimates of key descriptors of the original attractor.

It is also important to choose the right overall *time span*, or *reconstruction window*, covered by the  $m$ -dimensional embedding space vector which is given by  $t_w = (m - 1)t_D$  [Broomhead 1986]. This is the length of the interval spanned by the first and last delay coordinates.

An embedding space vector is a point in the reconstruction space, therefore we wish a set of such vectors to represent a reconstructed attractor which exhibits a similar behaviour to the original attractor. If the delay time is fixed for any embedding dimension, we expect the time span to increase with the dimension. As an embedding space vector is a vector of points on a trajectory of a chosen dynamic variable, an increase in the time span means an increase in the length of the trajectory covered by each vector. This could cause an excessive expansion of the attractor (irrelevance) if the dimension is high. However, if we fix the time span with an appropriate delay time, we could limit the rate of expansion of the attractor.

A number of techniques have been developed with this goal in mind. The key techniques are described in subsequent sections.

### 4.3.1 Autocorrelation based methods

Recall from chapter two that the autocorrelation function measures the similarity between a variable  $x_t$  and  $x_{t+l}$ . It was defined as  $g(l)$  in (II.18), page 26.

A common choice for  $t_D$  is to use the autocorrelation function, which should provide a reasonable measure of the transition from redundancy to irrelevance. The autocorrelation based methods have the advantage of short computation times. However, these methods tend to produce inconsistent results, although there is some evidence [Albano 1991] that autocorrelation methods can provide a good initial estimate for the delay time.

In [Zeng 1991]  $t_D$  was chosen as the time at which the autocorrelation function first falls to  $e^{-1}$ . Similarly, S. J. Schiff and T. Chang [Schiff 1992] have chosen  $t_D$  when  $g(l)$  was not significantly different from zero for the first time. Yet another method [King 1987] is to choose  $t_D$  by locating the first inflection point of  $g(l)$ . Similarly in [Holzfuss 1986],  $t_D$  is chosen to be the time taken for  $g(l)$  to reach the local minimum.

Using the method suggested by [Holzfuss 1986] and [King 1987], 0.82 was calculated to be the time to reach the first local minimum of autocorrelation function for the Lorenz model. As illustrated in Figure 4.1, this choice of  $t_D$  was found to be inadequate.

Most of the autocorrelation based methods do not make use of the reconstruction window, so that once found the delay time is fixed. This may cause the reconstructed attractor to be inaccurate in a multi-dimensional reconstruction. Therefore we must search for more satisfactory techniques.

#### 4.3.2 Mutual information

Another more theoretically sound method to estimate the optimal value of  $t_D$  for state space reconstruction has been proposed by A. M. Fraser and H. L. Swinney [Fraser 1986]. They have developed a recursive algorithm to calculate the *mutual information*, which measures the general dependence of two variables, rather than the linear dependence calculated by the autocorrelation function. This in practical terms estimates the accuracy of predicting  $x_{t+1}$  given a measure of  $x_t$ . Successive delay coordinates are relatively independent when the mutual information is small. Fraser and Swinney suggested that the value of  $t_D$  which produces the first local minimum of mutual information should be used for state space reconstruction, as this leads to the least redundancy.

The major drawback of this method is that it requires an enormous computational cost to estimate the first minimum of mutual information. For each value of  $t_D$ , the method requires four to five orders of magnitude more computation than the autocorrelation method [Rosenstein 1994]. Furthermore, this method was found to give inconsistent results in identifying the optimal value of delay time in some cases [Martinerie 1992].

#### 4.3.3 Average displacement

One recent technique to estimate the optimal time delay has been proposed by M. T. Rosenstein and his colleagues [Rosenstein 1994]. The method is known as the *average displacement method* and it estimates the optimal expansion of the reconstructed attractor from the line of identity in the reconstruction space. This is achieved by an appropriate reduction in *redundance error*.

For small delays, redundancy is high as the measurement error is comparatively large. That is in the presence of noise, the coordinates are almost indistinguishable. The measurement error in reconstruction is referred to as the *redundance error*. As the delay increases, the relative impact of the redundancy error decreases, since the signal to noise ratio is assumed to remain constant.

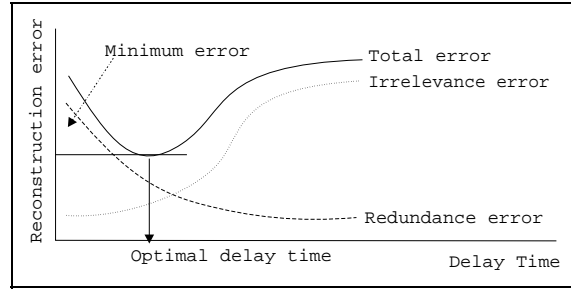


Figure 4.3 Reconstruction error.

*Irrelevance error* is a term used for the error that grows exponentially due to small differences in location of the trajectory due to noise. This error starts off low but increases due to the exponential growth of error as a function of delay time. The total error is calculated to be the sum of the two errors.

The idea is illustrated in Figure 4.3. Both redundancy and irrelevance errors reach plateaus as the attractors are bounded. When redundancy error reaches a plateau, we cannot hope to find a better time delay by increasing the delay any further. The optimal delay time is estimated to be the time when the total error is at its minimum.

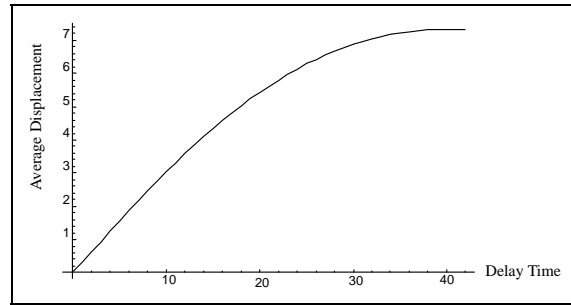


Figure 4.4 Average displacement.

The average displacement function is a measure of an attractor's expansion as a function of delay in  $m$ -dimensional space. Using the scalar time series it is defined as

$$S_m(n\tau) = \frac{1}{N} \sum_{i=1}^N \sqrt{\sum_{j=1}^{m-1} (x_{i+jn} - x_i)^2} \quad (\text{IV.2})$$

where  $N$  is the number of data points used for the estimate and  $t_D = n\tau$ . Maximising the average displacement is equivalent to minimising the redundancy error. As the delay time increases from zero, the reconstructed trajectory expands from the diagonal and the average displacement increases accordingly until it reaches a plateau. With larger values of  $m$ , reconstruction expansion reaches a plateau at a smaller value of the delay time. This maintains the time span  $t_w = (m - 1)t_D$  approximately constant.

In Figure 4.4, the Lorenz model with embedding dimension of 5 was used. The graph of average displacement versus delay time was created using the  $x$ -coordinate and 500 data points. The point where the slope first decreased to less than 40% of its initial value was found to yield a satisfactory delay time [Rosenstein 1994]. Using such a method the optimal delay time was found to be 0.09. When  $m = 2$ ,  $t_D$  was found to be 0.28. The reconstructed attractor using this value is shown in Figure 4.5. This resembles

the original attractor of the Lorenz model in chapter three more closely than those depicted in Figure 4.1 or Figure 4.2.

#### 4.3.4 Other methods

Delay time is usually fixed once an appropriate value is found but J. L. Breedon and N. H. Packard [Breedon 1992] have developed a so called *fuzzy delay coordinate reconstruction technique* which employs variable time sampling to improve the quality of the reconstructed attractor.

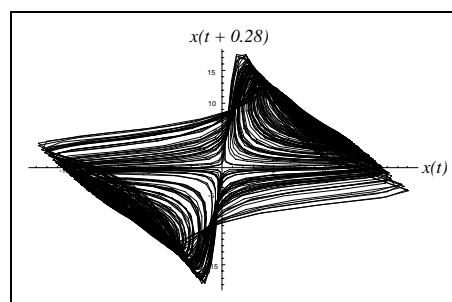


**Figure 4.5** Reconstruction by average displacement,  $t_D = 0.28$ .

The *fill factor* method [Buzug 1992] quantifies an attractor's utilisation of embedding space as a function of delay time. The optimal  $t_D$  is chosen as the one that leads to the most voluminous reconstruction. The essence of this method is to estimate the value of delay time when it yields the most space filling reconstruction. A drawback is that it cannot account for the over folding of the attractor once the reconstruction has expanded from the main diagonal.

J. C. Roux [Roux 1993] has suggested that there is an optimum choice of  $t_D$ , typically one tenth to a half of the mean orbital period over the entire recorded data.

Strategies for the choice of  $t_D$  have also been discussed in [Pi 1994]. The method establishes functional dependencies given a sequence of measurements. These dependencies are used to choose an optimal  $t_D$ .

#### 4.3.5 Summary of methods for delay time

A comprehensive survey of various methods to estimate the optimum time delay can be cited in [Casdagli 1991], [Buzung 1992], [Rosenstein 1994]. It should be noted that none of the algorithms mentioned above or elsewhere are universal, and the estimated  $t_D$  usually requires some refinements which are proceeded by trial and error.

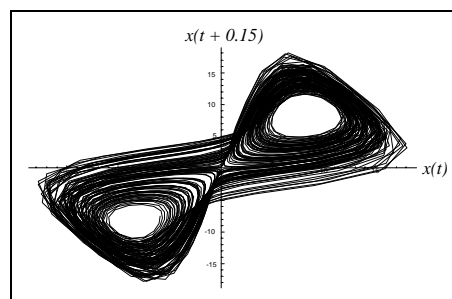


**Figure 4.6** Reconstruction by trial and error,  $t_D = 0.15$ .

When we know the original attractor it is fairly easy to search for a delay time which can be used to reconstruct the attractor by using the delay time estimate obtained by one of the methods described. Figure 4.6 illustrates the reconstructed Lorenz attractor using a delay time of 0.15. This time was found by trial and error. By

comparing the reconstructed attractor to that of the original  $xy$  attractor of the Lorenz model in Figure 3.1 (page 37), we can see a very good resemblance. It is ideal to recalculate the delay time once the embedding dimension is decided, as the embedding works better if we consider the time span of the vectors rather than just the delay time.

Model	$\tau$	Average displacement	Autocorrelation to reach zero	Autocorrelation to reach local minimum point
Lorenz	0.01	dim = 2, 0.28 dim = 3, 0.14 dim = 4, 0.11 dim = 5, 0.09 dim = 6, 0.07 dim = 7, 0.06	0.48	0.82
Rössler	0.1	dim = 2, 2.2 dim = 3, 1.4 dim = 4, 1.0 dim = 5, 0.8 dim = 6, 0.7 dim = 7, 0.6	1.4	2.9
Duffing oscillator	0.1	dim = 2, 0.7 dim = 3, 0.5 dim = 4, 0.4 dim = 5, 0.3	2.3	4.7

**Table 4.1** The delay times estimated by the average displacement and the autocorrelation based methods for the three continuous time chaotic systems.

Table 4.1 contains different delay times calculated by three different methods for the three chaotic models studied in chapter three.  $\tau$  is the sampling time as before. The average displacement method were calculated for a number of different dimensions.

#### 4.4 Jump time

The jump time  $t_j$ , is the time interval between successive vectors. We want to have it small enough so that we map out the trajectory as it proceeds around the attractor, but if we make it too small the total number of data points required becomes very large. Furthermore, if the vectors used are closer in time than roughly the time for which the autocorrelation function first drops to zero, say  $\beta$ , then we learn nothing new by comparing the vectors, as they are nearly identical. Thus, we generally choose  $t_j$  to be several times larger than  $\beta$ . The topology of the reconstructed attractor is independent of  $t_j$ , however the sequence of points generated for the attractor and the number of embedding space vectors required to obtain the

attractor plot are affected by the choice of  $t_J$ . For smaller value of  $t_J$  we expect the sequence of points to define the trajectory well, but the number of the vectors required to cover the attractor increases with respect to the reduction in  $t_J$ .

If we wish to use the embedded space vectors to reconstruct attractor with a reasonable number of ‘almost’ periodic points, it is ideal to set the jump time as the average time for the system to go around the original state space once. When we try to reconstruct the attractor from a time series of a physical experiment, in most cases we do not know if there is a forcing frequency or the average time for the system to go around the original state space once. In such a situation, estimation of the jump time can be difficult. Our approach to find a suitable value of  $t_J$  to reconstruct such an attractor is described in section 4.7.

When the system is driven by an external periodic force, the period of the external drive establishes a natural period for sampling the dynamics of the system. In such a case, we sample some variable of the system at a particular phase of the external force to form a surface of section. In this case the sampling time  $\tau$  is the period of the external force. It is then reasonable to use  $\tau$  as both the delay time and jump time since the variable samples are already reasonably separated in time.

#### **4.5 Embedding dimension**

Another difficulty with the reconstruction is the estimation of the dimension to use for the embedding space vectors. For many systems, we have a little knowledge of the fractal dimension.

In order to successfully implement the delay coordinates method, we must choose the number of dimensions  $d_E$ , to use in the embedding space. This dimension is called the embedding dimension.

As mentioned before, it has been shown by Takens [Takens 1981] that a faithful reconstruction can be achieved by at most  $2d + 1$  embedding dimension for a  $d$ -dimensional system. However, for a dissipative system the effective dimensionality for the long term behaviour is that of the attractor. This dimensionality may be considerably smaller than that of the original state space. Thus, we could use the dimension of the attractor, say  $D$ , instead of  $d$  to reconstruct the original dynamics of the attractor by the delay coordinates method.

Once the dimension of the attractor is estimated, the minimal requirement for the embedding dimension is  $d_E \geq D$  [Farmer 1987]. Combining this result with that of Takens’ theorem, we have

$$D \leq d_E \leq 2D + 1 \quad (\text{IV.3})$$

Almost all strange attractors have fractal dimension and we may need to estimate this in order to choose the embedding dimension.

#### 4.5.1 Correlation dimension

The correlation dimension was introduced in section 2.7.3.

The discrete correlation integral is defined as

$$C^{(m)}(R) = \lim_{N \rightarrow \infty} \frac{1}{N^2} \sum_{i,j=1}^N \theta(R - |X_i - X_j|) \quad (\text{IV.4})$$

where  $\theta(y)$  is the Heaviside function, defined as  $\theta(y) = 1$  for  $y > 0$  and  $\theta(y) = 0$  for  $y \leq 0$ . The correlation integral is obtained by considering correlations between points of a time series on the attractor. It tells us the relative number of pairs of points that are located within the distance  $R$  of each other in the space. In (IV.4) the superscript to  $C$  indicates that the correlation integral may depend on  $m$ , and  $X$  are the embedding space vectors.

The length of the difference between two vectors is usually taken to be the *Euclidean* length

$$|X_i - X_j| = \sqrt{\sum_{k=0}^{d-1} (x_{i+kt_D} - x_{j+kt_D})^2} \quad (\text{IV.5})$$

However, to save some computation time (IV.5) could be replaced by the *max-norm* in which the distance between two points is the largest of all the component differences

$$|X_i - X_j| = \text{Max}_{0 \leq k \leq d-1} |x_{i+kt_D} - x_{j+kt_D}| \quad (\text{IV.6})$$

We define  $D_C(m)$  to be the number which satisfies

$$C^{(m)}(R) = kR^{-D_C(m)} \quad (\text{IV.7})$$

for some range of  $R$ , which we call the *scaling region*, where  $m$  indicates that  $D_C$  may also depend upon the embedding dimension and  $k$  is a constant.

We should choose the total number of data points to be used in calculating the correlation dimension. Usually more data points we have the better, but the computation time increases rapidly. Therefore we

may need to compromise. We want to have enough data so that in the neighbourhood of each vector in an  $m$ -dimensional embedding space, there will be a sufficient number of vectors to get an accurate estimate of the correlation dimension. We also want those vectors to consist of data points reasonably separated in time so as to compare trajectory points which have passed through a particular section of state space at different times.

In practice, data sets of a few thousand data points seem to be sufficient for reasonable estimates of the correlation dimension [Abraham 1986] for systems exhibiting low-dimensional dynamics.

If there are  $N$  scalar time series values,  $d_E$  is used with delay time  $t_D$  and jump time  $t_J$  to reconstruct the dynamics by  $(N\tau/t_J)$   $d_E$ -dimensional embedding space vectors.

What we do in practice is to compute  $D_C(m)$  for  $m = 1, 2, 3, \dots$ . In order to estimate the correlation dimension, we need to examine the graph of  $\ln C(R)$  versus  $\ln R$  for each  $m$ . For each graph, we locate the scaling region where the gradient is almost constant for the range of  $R$ . The gradient is then taken to be  $D_C(m)$ . This is illustrated in Figure 4.7.

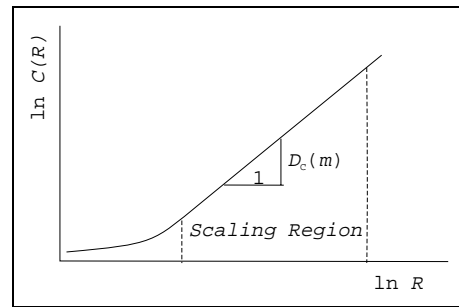


**Figure 4.7** Natural logarithms of the correlation integral versus  $R$ .

Estimated values of the correlation dimension in embedding space typically increase with the embedding dimension and eventually reach a plateau, on which the correlation dimension estimate is relatively constant, whose value is commonly taken as an estimate of the correlation dimension of the underlying chaotic attractor. [Ding 1993] reports a rigorous result which implies that, for long enough data sets, the plateau begins when  $m$  first exceeds  $D_C$ . They have also discussed how lack of sufficient data delays the plateau onset.

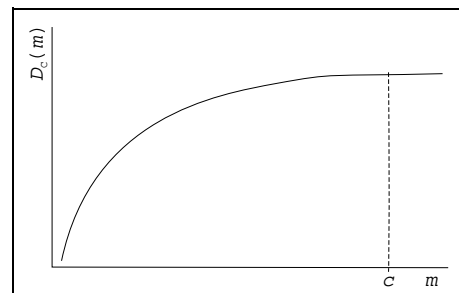


**Figure 4.8** Correlation dimension versus  $m$ .

A plot of  $D_C$  as a function of  $m$  is illustrated in Figure 4.8. We expect  $D_C$  to vary with  $m$  until  $m \geq c$ . The correlation dimension is taken as the value of  $D_C$  at  $c$ , and  $c$  can be used as the embedding dimension.

#### 4.5.2 Lyapunov dimension

Estimates of average Lyapunov exponents from a time series have been demonstrated by [Sano 1985], [Auerbach 1987], [Lathrop 1989], [Zeng 1991]. X. Zeng and his colleagues [Zeng 1991] have suggested a method to estimate the Lyapunov exponents from limited experimental data of only 5,000 data points with a precision of  $10^{-1}$  or  $10^{-2}$  in three or four dimensional state space, and 10,000 data points in five dimensional state space.

Once the Lyapunov exponents are found, the computation required to estimate the dimension of the attractor by the Lyapunov dimension described in section 2.7.2 is minimal as can be seen from the calculations in sections 3.3.1, 3.3.2 and 3.3.3.

### 4.5.3 $\Gamma$ -test

Another recently developed method called the  $\Gamma$ -test [Stefánsson 1995] can also be used to find the embedding dimension, but without estimating the dimension of the attractor. It can be very effective and less computationally expensive when compared to the use of correlation dimension. The algorithm runs in  $O(M \log M)$ , where  $M$  is the number of sample data points.

Using the condition in (IV.3), we could limit the range of the embedding dimension once the fractal dimension is estimated. A problem arise as the search area increases with the fractal dimension. For example, if a given model has a fractal dimension of say 3.6, (IV.3) predicts that there is an optimal embedding dimension in the range,  $3.6 \leq d_E \leq 2(3.6) + 1$ . As  $d_E$  must be a natural number, the range can be interpreted as  $4 \leq d_E \leq 9$ . Once this range is known, we must examine the set of embedding space vectors for each embedding dimension within the range which yields the best result. This is a time consuming process. Using the  $\Gamma$ -test, we can predict the embedding dimension without defining the search area.

On the assumption of a continuous or smooth underlying input/output model, given the input/output data set, the  $\Gamma$ -test estimates the best mean squared output error that can be achieved without overfitting. Applied in the correct context, in effect the  $\Gamma$ -test estimates that part of the output variance which cannot be attributed to variations due to a continuous or smooth model, i.e. it estimates that part of the output variance due to noise. If the  $\Gamma$ -test result is close to zero, this signifies that the model is deterministic. We denote the input vector by  $\mathbf{x} = (x_1, \dots, x_n)$  and the scalar output by  $y$ . In cases where there is more than one output the  $\Gamma$ -test can be applied to each separately with very little extra computational cost.

Suppose the samples are generated by a continuous function  $f: \mathbb{R}^m \rightarrow \mathbb{R}$  and let  $y$  be defined as where  $r$  represents an indeterminable part, which may be due to noise or lack of functional determination

$$y = f(x_1, \dots, x_m) + r \quad (\text{IV.8})$$

in the input/output relationship.

The variance of  $r$ ,  $\text{Var}(r)$  provides a lower bound for the mean squared error of the output  $y$ . If  $f$  is continuous and there is no noise then  $\text{Var}(r)$  is zero. The  $\Gamma$ -test is a method for estimating  $\text{Var}(r)$ .

Suppose  $(\mathbf{x}, y)$  is a data sample. Let  $(\mathbf{x}', y')$  be a data sample such that  $|\mathbf{x}' - \mathbf{x}| > 0$  is minimal. Here  $|\cdot|$  denotes Euclidean distance and the minimum is taken over the set of all sample points different from  $(\mathbf{x}, y)$ . Thus  $\mathbf{x}'$  is the nearest neighbour to  $\mathbf{x}$  (in any ambiguous case we just pick one of the several equidistant points arbitrarily).

It is well to observe that  $y'$  may well *not* be the nearest neighbour of  $y$  in output space. The dash notation is not ideal but it leads to less complicated expressions than many alternatives.

The  $\Gamma$ -test is based on the statistic

$$\gamma = \frac{1}{2M} \sum_{i=1}^M (y'(i) - y(i))^2 = \frac{1}{2} \langle (y' - y)^2 \rangle \quad (\text{IV.9})$$

Given data samples  $(\mathbf{x}(i), y(i))$ , where  $\mathbf{x}(i) = (x_1(i), \dots, x_n(i))$ ,  $1 \leq i \leq M$ , let  $\mathbf{x}(N(i, p))$  be the  $p$  th nearest neighbour to  $\mathbf{x}(i)$ . It can be shown that  $\lim \gamma = \text{Var}(r)$  as nearest neighbours tend to zero, and even the crude measure provided by (IV.9) often proves useful. However, if one is prepared to assume that  $f$  is smooth with bounded first partial derivatives we can improve this estimate by making a first order approximation to  $f(\mathbf{x}')$  based on Taylor's theorem. By computing a regression line based on some 20 or 30 nearest neighbours one can estimate the intercept  $\bar{\Gamma} = \lim \Gamma$  by extrapolating the regression line to  $\Delta = 0$ .

Thus we write

$$\delta(p) = \frac{1}{M} \sum_{i=1}^M |\mathbf{x}(N(i, p)) - \mathbf{x}(i)|^2 \quad (\text{IV.10})$$

and

$$\gamma(p) = \frac{1}{2M} \sum_{i=1}^M (y(N(i, p)) - y(i))^2 \quad (\text{IV.11})$$

and form the cumulative averages

$$\Delta(p) = \frac{1}{p} \sum_{h=1}^p \delta(h) \quad (\text{IV.12})$$

and

$$\Gamma(p) = \frac{1}{p} \sum_{h=1}^p \gamma(h) \quad (\text{IV.13})$$

Then  $\Delta(p)$  is the mean square distance of the  $h \leq p$  nearest neighbours and  $\Gamma(p)$  is an estimate for the statistic  $\gamma$  (defined in (IV.9)) based on the  $h \leq p$  nearest neighbours. We perform least squares fit on coordinates  $(\Delta(p), \Gamma(p))$  to obtain a regression line in the form of  $y = Ax + \bar{\Gamma}$ . A simple implementation of the  $\Gamma$ -test is given in Algorithm 4.1.

If the inputs used, say  $x_t$ , are the past history values of an observable system output sampled with the delay time  $t_D$  we can apply the  $\Gamma$ -test to the problem of estimating the embedding dimension.

Let an input vector be defined as

$$X = (x_{t_D}, \dots, x_{nt_D}) \quad (\text{IV.14})$$

Typically as the embedding dimension is increased,  $\bar{\Gamma}$  first decreases, reaches a minimum, and then increases. To find the optimal embedding dimension, we start with  $n = 2$  in (IV.14).  $n$  is increased by one until the minimum of  $\bar{\Gamma}$  is attained, say at  $n = n_m$ . The embedding dimension is estimated as  $n_m$ .

Figure 4.9 illustrates a plot of  $\bar{\Gamma}$  versus the number of past values in (IV.14), i.e. the embedding dimension. Figure 4.9 was obtained by using a time series of the  $x$ -coordinate for the Lorenz model, with the delay times calculated by the average displacement method.  $n_m$  was found to be five with  $\bar{\Gamma} \approx 0.021$ .

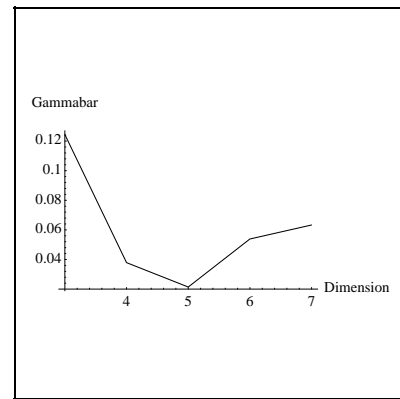


**Figure 4.9**  $\bar{\Gamma}$  versus embedding dimension using the average displacement method.

If  $\bar{\Gamma}$  is not close to zero, the data set is non-deterministic, therefore we cannot hope to reconstruct the attractor accurately. This may happen if the signal-to-noise ratio is high, or the choice of delay time is poor. It is interesting to note that smaller the signal-to-noise ratio the less embedding dimension is required. However, the reduction of noise is less when compared to a model with a higher signal-to-noise ratio requiring a higher embedding dimension.

It is very important to use a suitable value of delay time, as the test is sensitive to the delay time. For a deterministic continuous time system, a poor choice of delay time could mean very high values of  $\bar{\Gamma}$ . With a suitable choice of delay time we would expect  $\bar{\Gamma}$  to be small and initially decrease with increasing dimension. For the Lorenz model, the smallest  $\bar{\Gamma}$  was found to be approximately 21.52 when the delay time was estimated as the time for the autocorrelation function to reach zero, which was 0.48. Furthermore,  $\bar{\Gamma}$  did not decrease at all. This is illustrated in Figure 4.10. This figure of 21.52 should be contrasted with the significantly improved  $\bar{\Gamma}$  of 0.021. The large difference between the numbers highlights the importance of choosing a correct delay time.

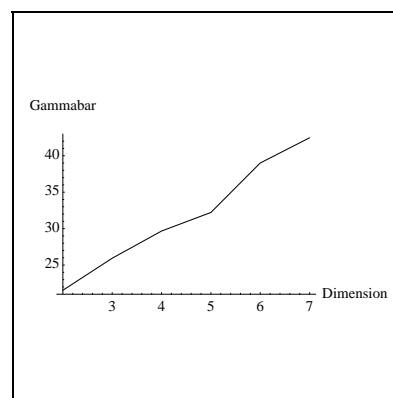


**Figure 4.10**  $\bar{\Gamma}$  versus embedding dimension using the autocorrelation method.

Using an estimation of the embedding dimension provided by the  $\Gamma$ -test for the Lorenz model, the Rössler model and the Duffing oscillator, the delay times found by the autocorrelation method always performed poorly when compared to ones found by the average displacement method. A reason for this is that the delay time is independent of the dimension, i.e. the delay time is fixed, for the autocorrelation method. Using the average displacement method, delay times were calculated for each dimension as the delay times depended on the dimension.

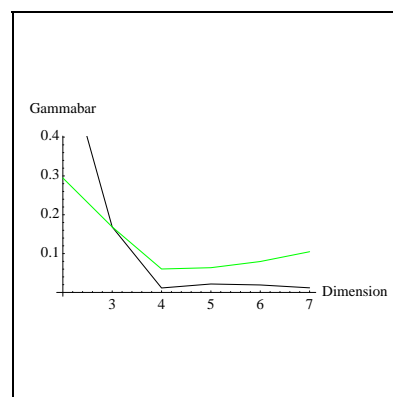


**Figure 4.11**  $\bar{\Gamma}$  versus the dimension for the Rössler model.

The embedding dimensions estimated by the  $\Gamma$ -test using the delay times calculated by the average displacement method, satisfy the condition of (IV.3), i.e. for the Lorenz model,  $2.06 \leq 5 \leq 5.12$  and for the Rössler model,  $2.01 \leq 4 \leq 5.02$ .

For smaller values of  $a$ , we expect to require fewer data points to reconstruct the state space. For the Rössler model, the same embedding dimension was predicted by the autocorrelation and the average displacement methods. This is illustrated in Figure 4.11. The plot obtained for the average displacement

method is in black and the autocorrelation in grey. Notice that  $\bar{\Gamma}$  values are consistently lower for the average displacement method for dimensions of greater than three.

The plot of the slope versus the dimension reveals that the slopes are also consistently lower for the average displacement method for the dimensions. This is illustrated in Figure 4.12. This means that the choice of delay time chosen by the average displacement method is superior to that found by the autocorrelation method.

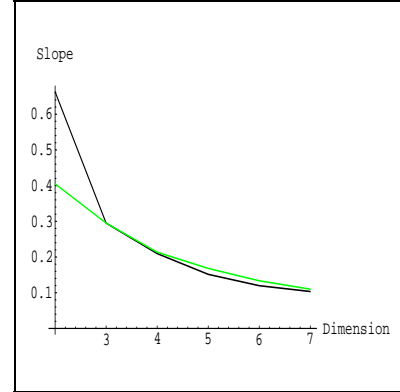


**Figure 4.12** The slope versus the dimension for the Rössler model.

We could also use the  $\Gamma$ -test to validate the delay time. If  $\bar{\Gamma}$  never reaches zero, or does not decrease for increasing dimension initially for a deterministic system, the choice of delay time must be changed. For continuous time systems with no noise, we expect  $\bar{\Gamma}$  to be close to zero if a suitable dimension is used and the delay

time is very small. Therefore decreasing the delay time may assist  $\bar{\Gamma}$  to be smaller. Of course, we should be careful not to make the delay time too small as this may introduce a high redundancy error.

Procedure  $\Gamma$ -test (data)

(\* data is an array of points  $(\mathbf{x}(i), y(i))$ ,  $(1 \leq i \leq M)$ , in which  $\mathbf{x}$  is a real vector of dimension  $m$  and  $y$  is a real scalar \*)

For  $i = 1$  to  $M$  (\* compute  $\mathbf{x}$ -nearest neighbour list for each data point \*)

For  $p = 1$  to  $p_{\max}$

$N(i, p) = t$  where  $\mathbf{x}(t)$  is the  $p$  th nearest neighbour to  $\mathbf{x}(i)$ .

endfor  $p$

endfor  $i$

For  $p = 1$  to  $p_{\max}$

compute  $\delta(p)$  as in (IV.10)

compute  $\gamma(p)$  as in (IV.11)

endfor  $p$

For  $p = 1$  to  $p_{\max}$

compute  $\Delta(p)$  as in (IV.12)

compute  $\Gamma(p)$  as in (IV.13)

endfor  $p$

Perform least squares fit on coordinates  $(\Delta(p), \Gamma(p))$  ( $4 \leq p \leq p_{\max}$ ) obtaining (say)  $y = Ax + \bar{\Gamma}$

Return  $(\bar{\Gamma}, A)$

**Algorithm 4.1** The  $\Gamma$ -test.

If the time series is obtained from a physical experiment where the underlying mathematical model is not known, we should at first check if the system is chaotic by the tests described in section 2.10. A chaotic dissipative system has an attractor and thus the  $\Gamma$ -test should yield  $\bar{\Gamma}$  close to zero.

#### 4.5.4 Conclusion

If the reason for finding the dimension of the attractor is to estimate the minimum number of elements in the embedding space vectors, there seems no theoretical reason for choosing one type of fractal dimension over another.

Criteria are the ease of implementation and computation. The capacity dimension is the one we should avoid as it is computationally intensive. The Lyapunov dimension is good to use if the average Lyapunov exponents can be computed easily. The correlation dimension has an advantage over the other dimensions, as the embedding dimension can be estimated at the same time as the fractal dimension.

The  $\Gamma$ -test utilises a quite different approach to estimate the embedding dimension. This technique does not require an estimate of the fractal dimension but finds the embedding dimension by locating the least variance of an unknown stochastic variable  $r$ .

When we try to estimate the embedding dimension by any of the above methods, it is necessary to first choose a reasonable estimate of the delay time.

In a graph of two-dimensional embedding space, the value of  $x_{tj}$  is plotted as a function of  $x_{tj + \tau D}$ . In a graph of embedding space of dimension three,  $x_{tj}$  is plotted along one axis,  $x_{tj + \tau D}$  along the second and  $x_{tj + 2\tau D}$  along the third. These plots illustrate how a multidimensional state space can be constructed from a single time series without the necessity of taking derivatives of the data. A periodic system will exhibit a closed loop. A fuzzy loop signifies the system is quasiperiodic. For a dimension of more than three, we have difficulties in representing the models graphically. In such a case, we could plot  $(d - 1)$  two dimensional graphs of  $x_{tj}$  versus  $x_{tj + k\tau D}$ , where  $d$  is the embedding dimension and  $k = 2, 3, \dots, d$ . We expect the plot of the attractor to expand with increasing  $d$ . Note that we need to plot only  $(d - 1)$  graphs as for example plots of  $x_{tj}$  versus  $x_{tj + 2\tau D}$ ,  $x_{tj + 2\tau D}$  versus  $x_{tj + 3\tau D}$ ,  $x_{tj + (d - 1)\tau D}$  versus  $x_{tj + d\tau D}$  etc are the same.

#### 4.6 Automated embedding method

As we have discussed throughout this chapter, implementations of the delay coordinates method can be

## Chapter 4 - Embedding techniques

difficult due to uncertainties involved with the choices of delay and jump times, and embedding dimension. In studying various techniques, we have devised an *automated embedding method*, to obtain a reasonable set of embedding space vectors for the state space reconstruction.

The preferred method uses a single coordinate time series of the model to be reconstructed. We set the initial embedding dimension to one. The dimension is increased by one and the delay time is estimated by the average displacement method for that dimension. The time series of a few hundred data points is usually sufficient for the average displacement method, typically 500 data points for a low dimensional models. We then create the set of input pairs using the dimension and the delay time. The statistic  $\bar{\Gamma}$  is estimated by the  $\Gamma$ -test using the input pairs. The estimations of the delay time and the statistic  $\bar{\Gamma}$  are repeated for a number of dimensions until a local minima of  $\bar{\Gamma}$  (which hopefully is close to zero) is found. We choose the optimal embedding dimension  $d_E$ , and delay time  $t_D$ , as the dimension and the corresponding delay time which gave the local minima of  $\bar{\Gamma}$ , respectively.

Procedure *Automated embedding* ( $X$ )

(\*  $X$  is a set of successive real vectors of the dynamic variable \*)

$dim = 1$

Repeat

$dim = dim + 1$

Create a set of  $dim$ -dimensional vectors  $\xi$  from  $X$

$delay_{dim} =$  Estimate the delay time by the average displacement method (IV.1), using  $\xi$

Create a time series  $DTS$  sampled at  $delay_{dim}$ , using  $X$

Create an input data set  $GammaData$  for the  $\Gamma$ -test, using  $DTS$

$GammaValue_{dim} =$  Estimate  $\bar{\Gamma}$  by the  $\Gamma$ -test (Algorithm 4.1), using  $GammaData$

Until  $GammaValue_{dim-1} < GammaValue_{dim}$  AND  $GammaValue_{dim-1} \approx 0$

$t_D = delay_{dim-1}$

$t_J = t_D$

$d_E = dim - 1$

Return ( $t_D, t_J, d_E$ )

**Algorithm 4.2** The automated embedding method.

In order to reconstruct the state space we could set the jump time to almost any value. The effect of jump time is such that for small values, typically the jump time several times smaller than the delay time, the successive embedding space vectors will be similar and thus the trajectory is well defined. The disadvantage in taking the jump time small is that we need to make significantly more embedding space

vectors to construct the attractor. If the jump time is large, typically several times larger than the delay time, we need fewer embedding space vectors to reconstruct the attractor, but it will not be well defined.

Also the time taken to obtain each embedding space vector increases proportionally to the jump time in a physical experiment. We have chosen the jump time to be same as the delay time for the reconstruction, i.e.  $t_J = t_D$ . The automated embedding procedure is summarised in Algorithm 4.2.

Model	Delay time	Embedding dimension	$\bar{\Gamma}$	A	Fractal dimension $D$
Lorenz	0.09	5	0.021393	0.283369	2.06
Rössler	1.00	4	0.011508	0.209624	2.01
Duffing's oscillator	0.40	4	0.010151	0.410428	-

**Table 4.2** The delay times and the embedding dimensions estimated for the three chaotic models.

Table 4.2 contains the delay times and the embedding dimensions found to be suitable by automated embedding method for the three chaotic systems.

#### 4.7 Unstable periodic orbits

A strange attractor is the set of points of the state space visited by the orbit after the transients have settled down. This means that the motion on it is ergodic, thus the orbit of any point  $p$  on the strange attractor will make arbitrarily close returns to  $p$ . It has been suggested [Gunaratne 1989] that nearly periodic orbits are dense on the strange attractor and that since the motion on the attractor is chaotic, these orbits must be unstable. As a periodic behaviour can be interpreted as a regular behaviour, a chaotic system can be thought as a collection of many different regular behaviours. On the surface of section, an *unstable orbit of period  $k$*  (nearly periodic orbit of period  $k$ ) appears as  $k$  points. A point belonging to such a set is referred to as an *unstable periodic point of period  $k$* .

##### 4.7.1 Extraction of unstable periodic points and orbits

We are interested in extracting the sets of points of the unstable periodic orbits of a strange attractor.

Unstable periodic orbits have been successfully extracted from experimental time series [Auerbach 1987], [Belmonte 1988], [Lathrop 1989], [Gunaratne 1989]. It is important to extract many unstable periodic

```

Procedure Locate close returns ( $\xi$ )

(*  $\xi$  is a set of embedding space vectors *)
Set  $N = \text{Length of } \xi$ 
Set  $N_1 = 50$  (* the maximum periodicity *)
Set  $r_1 = \text{two to three orders of magnitude smaller than the signal}$ 

(* Locate all close returning points of periods up to  $N_1$  *)
 $M = \{ \}$  (* Create a new list. Stores the sets of close return points and their periodicities *)
For  $i = 1$  to  $N - N_1$ 
   $k = 1$ 
  Repeat
    If  $|\xi_i - \xi_{i+k}| < r_1$ 
      then
         $vec1 = \xi_i$ 
         $vec2 = \xi_{i+1}$ 
        :
        :
         $veck = \xi_{i+k-1}$ 
        Append ( $k, vec1, vec2, \dots, veck$ ) to  $M$ 
         $k = k + 1$ 
      endif
    Until  $k > N_1$  OR  $|\xi_i - \xi_{i+k}| < r_1$ 
  endfor  $i$ 
(*  $M = \{(k, vec1, vec2, \dots, veck)_1, (k, vec1, vec2, \dots, veck)_2, \dots\}$  *)

(* Group the points collected in  $M$  by the period *)
 $L = \{ \}$  (* Create a new list *)
For  $n = 1$  to  $N_1$ 
   $TL = \{ \}$  (* Create a new list  $TL$  *)
  For  $m = 1$  to Length of  $M$ 
    If  $n = (k_m \text{ in } M)$ 
      then Append ( $vec1_m, vec2_m, \dots, veck_m$ ) to  $TL$  (* Append (Take[ $M[m]$ ,  $-n$ ) to  $TL$  *)
    endif
  endfor  $m$ 
  Append  $TL$  to  $L$ 
endfor  $n$ 
(*  $L = \{TL_1, TL_2, TL_3, \dots\}$  *)
(*  $TL_k = \{(vec1, vec2, \dots, veck)_1, (vec1, vec2, \dots, veck)_2, \dots\}$  *)

Return ( $L, N_1, r_1$ )

```

**Algorithm 4.3** Locate close returning points.

orbits, including the orbits of sufficiently high periods, so as to have a variety of behaviours which can be used to study the system. An experimental point is nearly a  $k$ -cycle (periodic) if it makes a close return

after  $k$  time steps. A close return implies the existence of a nearby cycle. This means there is an unstable periodic point of the underlying map in the neighbourhood of any close return of the experimental data. The unstable periodic orbits are estimated from a time series as follows. Let  $r_1$  and  $r_2 > 0$ ,  $\xi_i$  be a point on the reconstructed attractor in the form of an embedding space vector,  $N_1$  is the maximum period of the orbits we wish to extract and  $N$  is the total number of embedding space vectors.

Starting with  $i = 1$ , we follow the observed images  $\xi_{i+1}, \xi_{i+2}, \dots$  until we find the smallest index  $k$ ,  $1 \leq k \leq N_1$  such that  $|\xi_{i+k} - \xi_i| < r_1$ . If such a  $k$  exists, the orbit represented by  $(k, \xi_i, \xi_{i+1}, \dots, \xi_{i+k-1})$  is stored in a list. We repeat the process for each  $i < N - N_1$ . We have typically set  $N_1$  to 50. When the run is completed, we locate all orbits in the list with the same value of  $k$  and group them into a set of unstable orbits of period  $k$ . A procedure to locate and group the close returning orbits by the period is in Algorithm 4.2.

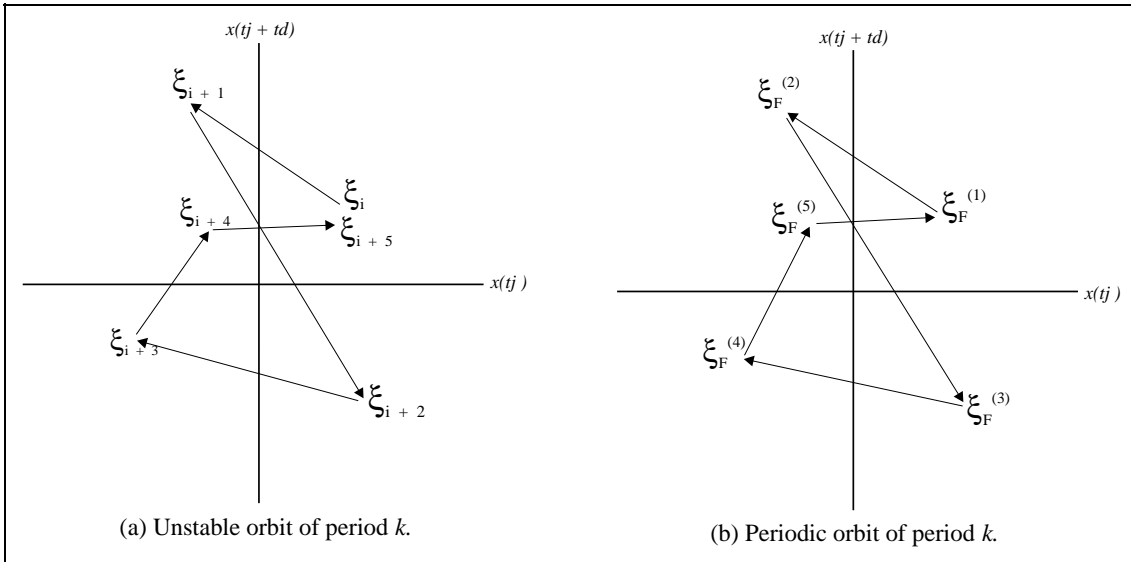


**Figure 4.13** Unstable periodic and periodic orbits.

In practice, it is impossible to locate an exact periodic orbits in a chaotic attractor so instead, we find nearly periodic orbit (unstable periodic orbit) and then represent it by a corresponding periodic orbit. In Figure 4.13 (a), an unstable orbit of period 5 is illustrated. In (b), a corresponding periodic orbit of period 5 is illustrated.

Throughout the length of the run of Algorithm 4.2., the vicinity of a particular unstable periodic orbit may have been visited many times. Therefore we must distinguish each orbit, remove any cyclic permutations and average the orbits extracted for improved approximations. In order to decide whether two sets of points of length  $k$  correspond to same unstable orbit of period  $k$ , their positions relative to each other are checked. The method we use is to sort each set into an ascending order to obtain two new sets and use

```

Procedure Distinguish clusters ( $L, N_1, r_1$ )

(*  $L$  is a list of lists containing the sets of points of orbits sorted in order of periodicity *)
(*  $L = \{TL_1, TL_2, TL_3, \dots\}$  *)
(*  $TL_k = \{(vec1, vec2, \dots, veck)_1, (vec1, vec2, \dots, veck)_2, \dots\}$  *)
(*  $N_1$  and  $r_1$  as in Algorithm 4.2 *)

Set  $r_2 = 2r_1$ 
 $UPO = \{\}$  (* Create a new list. Stores the distinguished and averaged unstable periodic orbits *)
For  $k = 1$  to  $N_1$ 
  While  $TL_n$  is NOT empty
     $TempTL = \{\}$  (* Create a new list *)
     $anupo = (vec1, vec2, \dots, veck)_1$  in  $TL_k$  (*  $anupo = TL_k[1]$  *)
     $theupo = \text{Sort}(anupo)$  (* in ascending order of first element of  $vecs$  *)
    Append  $(vec1, vec2, \dots, veck)_1$  in  $TL_k$  to  $TempTL$  (* Append  $TL_k[1]$  to  $TempTL$  *)
    Remove  $(vec1, vec2, \dots, veck)_1$  from  $TL_k$  (* Remove first element from  $TL_k$  *)
    For  $m = 1$  to Length of  $TL_k$ 
       $currentupo = (vec1, vec2, \dots, veck)_m$  in  $TL_k$  (*  $currentupo = TL_k[m]$  *)
       $currentupo = \text{Sort}(currentupo)$  (* in ascending order of first element of  $vecs$  *)
      For  $i = 1$  to  $k$ 
        If  $|theupo_i - currentupo_i| < r_2$  for all  $i$ 
          then
            Append  $currentupo$  to  $TempTL$ 
            Remove  $(vec1, vec2, \dots, veck)_m$  from  $TL_k$  (* Remove  $m$ th element from  $TL_k$  *)
             $m = m - 1$ 
          endif
        endifor  $m$ 
      endwhile
       $averagedupo = \text{Average of } TempTL$ 
       $(\xi_F^{(1)}, \xi_F^{(2)}, \dots, \xi_F^{(k)}) = \text{Sort}(averagedupo)$  in the same order as  $upo$ 
      Append  $(k, (\xi_F^{(1)}, \xi_F^{(2)}, \dots, \xi_F^{(k)}))$  to  $UPO$ 
    endifor  $n$ 
  (*  $UPO = \{(k, (\xi_F^{(1)}, \xi_F^{(2)}, \dots, \xi_F^{(k)}))_1, (k, (\xi_F^{(1)}, \xi_F^{(2)}, \dots, \xi_F^{(k)}))_2, \dots\}$  *)

Return ( $UPO$ )

```

**Algorithm 4.4** Distinguish and average the unstable periodic points.

them for the comparison. If the distances of all the corresponding points of the two new sets are less than  $r_2$ , then they are grouped into the same unstable periodic orbit cluster. Otherwise, they are considered to be distinct clusters. The centres of the each sets of points in the cluster are then used as estimations of an unstable orbit of period  $k$ . It follows from the central limit theorem that such averaging reduces the effective noise by a factor  $\sqrt{N_b}$  where  $N_b$  is the number of sets in a cluster [Belmonte 1988]. A procedure

to distinguish and average the close returning points to estimate the unstable periodic orbits is in Algorithm 4.3.

The two parameters  $r_1$  and  $r_2$  are chosen by the following criteria [Lathrop 1989].  $r_1$  is chosen large enough to include several sequences corresponding to a particular periodic point, typically two to three orders of magnitude smaller than the signal. The distance between the points,  $r_2$ , is set small enough to distinguish between distinct periodic points under the condition that  $r_2 > r_1$ , typically  $r_2 = 2r_1$ .

```

Procedure Remove repeated orbits (UPO, r1)

(* UPO is a list of lists containing the distinguished and averaged unstable periodic orbits*)
(* UPO = { (k, (ξF(1), ξF(2), ..., ξF(k)))1, (k, (ξF(1), ξF(2), ..., ξF(k)))2, ... } *)
(* r1 as in Algorithm 4.2 *)

Set r2 = 2r1
For i = 1 to Length of UPO
  A = (k, (ξF(1), ξF(2), ..., ξF(k)))i (* A = UPO[i] *)
  k1 = k in A (* k1 = A[1] *)
  A' = {} (* Create a new list *)
  For j = 1 to Length of UPO
    k1 = kj in UPO (* k1 = UPO[j, 1] *)
    If (k2 < k1) AND (k1 MOD k2) = 0
      then
        Append (k, (ξF(1), ξF(2), ..., ξF(k)))j to A' (* Append UPO[j] to A' *)
    endifor j
  l = 1
  While (l ≤ k1) AND (stop = FALSE)
    ξa = ξF(1) in A (* ξa = A[2,1] *)
    For m = 1 to Length of A'
      B = (k, (ξF(1), ξF(2), ..., ξF(k)))m in A' (* B = A'[m] *)
      ξb = ξF(1) in B (* ξb = B[2,1] *)
      If | ξa - ξb | < r2
        then
          Remove (k, (ξF(1), ξF(2), ..., ξF(k)))i from UPO (* Remove ith element from UPO *)
          stop = TRUE
          i = i - 1
        endif
      endifor m
    l = l + 1
  endwhile
endifor i

Return (UPO)

```

**Algorithm 4.5** Remove repeated unstable periodic orbits.

Finally we have to remove orbits made of repetitions of lower orbits. For example a period four orbit may

be made up of two iterations of a period two orbit. For each unstable orbit of period  $k$  located, say  $A$ , we select the set of unstable orbits of periods less than  $k$ , say  $A'$ . For each orbit in  $A'$ , say  $B$ , we compare the distances between the points in  $A$  and  $B$ . If  $\exists (a, b)$  such that  $|\xi_a - \xi_b| < r_2$ , where  $\xi_a \in A$  and  $\xi_b \in B$ , and the periodicity of  $B$  is a factor of  $k$ , the orbit  $A$  is removed. A procedure to remove orbits made of repeated lower orbit is in Algorithm 4.5.

In order to increase the accuracy of the unstable periodic orbits, we increase the number of embedding space vectors used for the estimation. This has two effects. The first is to increase the number of unstable periodic orbits collected before the averaging process. The second is to locate orbits which were not included in the smaller set of vectors. Another approach to increase the accuracy is to decrease the sizes of  $r_1$  and  $r_2$ . We must be careful not to decrease the sizes too excessively as doing so will reduce the number of orbits extracted significantly. Generally we need to increase the number of vectors and decrease the sizes of  $r_1$  and  $r_2$  and hit a right balance by trial and error.

#### 4.7.2 Stability of an unstable periodic point

An unstable periodic point of period  $k$  can be extracted from an unstable orbit of period  $k$ . The stability of each unstable periodic point in units of  $k$  iterations is estimated from a linear approximation of the dynamics at points on nearby trajectories. Let  $\xi_F$  be an unstable periodic point of period  $k$ , and let  $(\xi_j, \xi_{j+k})$  be a collection of pairs of points in a circle with radius of  $nr_1$  centred at  $\xi_F$ , where  $n$  is typically set to be 6. We assume that the dynamics in this neighbourhood is nearly linear, so we write the map  $f$  which takes  $\xi_j$  to  $\xi_{j+k}$  as  $f(\xi) = J\xi + b$  for some  $d_E \times d_E$  Jacobian matrix  $J$  and a  $d_E$ -dimensional vector  $b$ .  $b$  is almost a null vector when the points are very close to  $\xi_F$ . A least squares fit method is used to calculate  $J$  and  $b$ . The absolute value of the largest eigenvalue of  $J$  provides an estimate of the stability of the unstable periodic point near  $\xi_F$ . The accuracy of the eigenvalues associated with a given unstable periodic point depends on the number of trajectories that lie nearby. Therefore, unstable periodic orbits in densely populated regions of the attractor are easier to characterise than those in regions which are rarely visited.

Recent developments suggest that the dimension of a chaotic attractor can be estimated by extracting enough unstable periodic orbits. In [Grebogi 1988], the relationship between the fractal dimension and the unstable orbits is discussed in detail.

#### 4.7.3 Choice of the jump time : The creep phenomenon

When using embedding techniques to model a chaotic system, we must be careful in choosing a suitable

value of the jump time  $t_j$ , so that there are a reasonable proportion of successive vectors which are close to each other.

One could estimate a reasonable jump time by comparing successive embedding space vectors, say  $\xi_i$  and  $\xi_{i+1}$ , for increasing values of  $t_j$  (in steps of  $\tau$ , the sampling period) for  $t_j > t_W$ , where  $t_W$  is the time span as described in section 4.3. If there are many vectors such that  $|\xi_i - \xi_{i+1}| < r_1$ , the jump time used to create the set of embedding space vectors should be used. This is because any faithful reconstruction of the attractor should contain many close returning orbits. In the attractor, the embedding space vectors near an unstable periodic point of period one should stay nearby for a number of iterations. Therefore we should observe a good proportion of vectors say 10%, satisfying the condition  $|\xi_i - \xi_{i+1}| < r_1$ , assuming the set of the vectors used is large. We have typically used 500 vectors for this estimation. If the system has a natural forcing frequency, we should be able to estimate it by the method explained above and successive vectors should remain nearby.

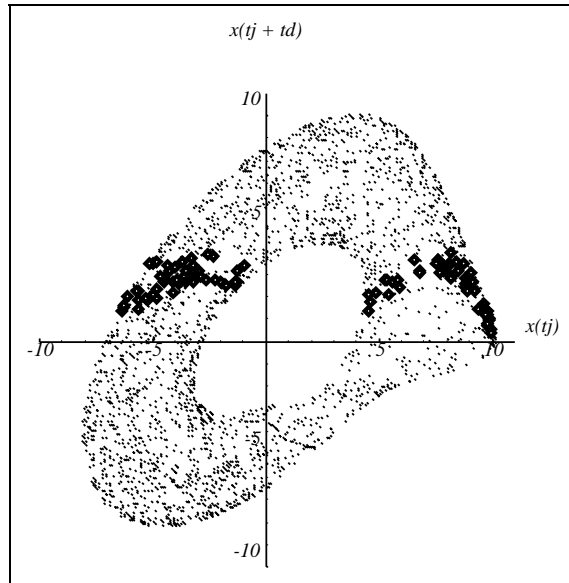


Figure 4.14 Reconstructed Rössler attractor with a set of suitable embedding parameters.

In Figure 4.14 the Rössler attractor is reconstructed by a set of 2,500 embedding space vectors with embedding dimension of 4, the delay time of 1.00 (as found suitable by the automated embedding method in section 4.6) and the jump time of 17.9. The plot is a two-dimensional representation of the four-dimensional state space ( $x_{tj}$  versus  $x_{tj + td}$ ). The dark region in the forth quadrant of the plot represents 50 successive points falling on the attractor. The iterates of points move clockwise and after 500 points, reach the dark region in the first quadrant of the plot, represented by another 50 successive points. As can be seen, the successive points remain nearby. We have named this effect the *creep phenomenon*.

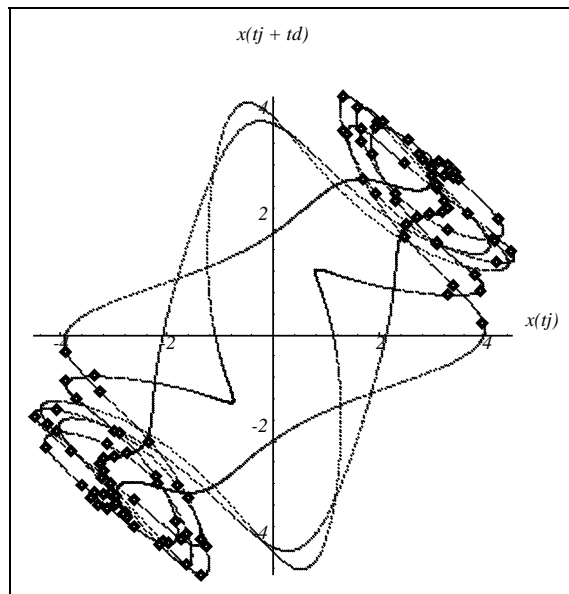


Figure 4.15 Reconstructed Duffing attractor with a set of suitable embedding parameters.

In Figure 4.15, the Duffing attractor is reconstructed by a set of 5,000 embedding space vectors with embedding dimension of 2, the delay time of 0.7 and the jump time of 9.4. As mentioned in section 3.3.4, the model has natural oscillations in units of  $2\pi/\omega$ . Using the set of parameters as in Table 3.1, Table 4.2, the forcing frequency occurs at every 9.449. units. Our method successfully predicted the jump time very close to this time. The method could have estimated a more accurate jump time if we had used a smaller sampling time, for example 0.01 instead of 0.1. The same can be said for the case of the Rössler attractor. The creep phenomenon is also observed in Figure 4.15. Here, the first 50 successive points are in the third quadrant. After 100 points, the second set of 50 points moved to the first quadrant of the plot.

These are particularly interesting observations in that a relatively long term prediction, 17.9 for the Rössler model and 9.4 for the Duffing oscillator, can be made quite accurately with a good choice of the jump time. Generally, with a poor choice we cannot predict where the next point falls. Furthermore, we may not be able to locate any unstable periodic points.

```

Procedure Jump time ( $X, t_D, d_E$ )

(*  $X$  is a real vectors of the dynamic variable *)
(*  $t_D$  and  $d_E$  are estimated by the automated embedding - Algorithm 4.2 *)

Choose  $r =$  two to three orders of magnitude smaller than the values in  $X$ 
 $t_W = (d_E - 1)t_D$ 
 $t_J = t_W - \tau$ 

Repeat
   $t_J = t_J + \tau$ 
  Create a set of embedding space vectors  $\xi$  from  $X$  using  $t_D, t_J$  and  $d_E$  as in (IV.1)
   $counter = 0$ 
   $N =$  Length of  $\xi$ 
  For  $n = 1$  to  $N-1$ 
    If  $|\xi_n - \xi_{n+1}| < r$ 
      then  $counter = counter + 1$ 
  endfor  $n$ 
Until  $counter/N > 0.1$ 
(* at least 10% of the successive embedding space vectors are close returns *)

Return ( $t_J$ )

```

**Algorithm 4.6** The jump time for close returns.

A procedure to estimate a value of jump time which yields sufficient number of close returns is summarised in Algorithm 4.6.

Using the Rössler model we have created two sets of 10,000 and 2,500 embedding space vectors with the embedding dimension of 4, the delay time of 1.00 and the jump time of 17.9 to extract unstable periodic orbits of periods up to 10.  $r_1$  was set to be 0.1 and  $r_2 = 2r_1$ . The number of distinct unstable periodic orbits extracted are given in Table 4.3.

Period	Number of orbits extracted using 10,000 embedding space vectors	Number of orbits extracted using 2,500 embedding space vectors
1	0	0
2	36	9
3	44	11
4	46	14
5	16	6
6	13	5
7	14	3
8	6	3
9	4	4
10	3	1
Total	182	56

**Table 4.3** Distinct unstable periodic orbits of orders up to 10 extracted - the Rössler model.

#### 4.8 Chapter summary

In this chapter we have described the delay coordinates method, which is one of the most important and useful development of chaos theory. The technique is widely used to model a physical system where the mathematical description is unknown.

We have seen that it is possible to reconstruct the original attractor from a time series of one observable system output, if the choices of embedding dimension, delay time and jump time are appropriate. It is not an easy task to estimate these values, therefore a number of techniques were explored.

Delay time is the time between successive components of the embedding space vector. If the amount of data is infinite and is noise free, then any choice of the delay time could reproduce the dynamics. However, in real applications we are limited both in the amount and accuracy of the data. The choice of

## Chapter 4 - Embedding techniques

delay time is important, as a good choice can reduce both the amount of data needed and the effect of noise. Different techniques described were autocorrelation based methods, mutual information and average displacement.

Jump time is the time difference between successive embedding vectors. The trajectory of the reconstructed attractor is well defined for a small jump time but more vectors are required for the reconstruction. If the choice of the jump time is such that it equals approximately the average time for the original trajectory to go around the attractor once, the plot of the successive vectors are confined in a small region of the reconstructed space. A method to estimate a reasonable jump time to reconstruct an attractor with a good proportion of close return points was also discussed.

The embedding dimension is also an important parameter to choose, as no matter what delay or jump time we choose, if the embedding dimension is too small we will not be able to reproduce the full system behaviour. Different techniques discussed in estimating the embedding dimension were the use of correlation and Lyapunov dimensions, and the  $\Gamma$ -test.

The automated embedding method we have developed was described as a new approach to estimate a reasonable set of the delay and jump times, and the embedding dimension for a reconstruction of the attractor.

This chapter concluded with discussions on how to locate unstable periodic orbits from a set of embedding space vectors, and a method to study the stability of such points. In order to locate unstable periodic orbits from a set of embedding space vectors, a suitable jump time should be used. This was discussed in detail and studies to estimate a suitable jump time lead to the discovery of the creep phenomenon. The extraction method was used to locate unstable periodic orbits of periods up to 10 of the Rössler model from two sets of embedding space vectors and the result was presented in Table 4.3.

### Chapter references

[Abraham 1986] N. B. Abraham, A. M. Albano, B. Das, G. De Guzman, S. Yong, R. S. Gioggia, G. P. Puccioni, and J. R. Tredicce. *Calculating the Dimension of Attractors from Small Data Sets*, Physics Letters A 114, 217-221, 1986.

[Albano 1988] A. M. Albano, J. Muench, C. Schwartz, A. I. Mees and P. E. Rapp. Singular-Value Decomposition and the Grassberger-Procaccia Algorithm, Physical Review A 38, 3017-3026, 1988.

[Albano 1991] A. M. Albano, A. Passamante and M. E. Farrell. *Using higher-order correlation to define an embedding window*, Physica D 54, 85-97, 1991.

[Auerbach 1987] Ditzia Auerbach, Predrag Cvitanovic, Jean-Pierre Eckmann, Gemunu Gunaratne and

Itamar Procaccia. *Exploring Chaotic Motion Through Periodic Orbits*, Physical Review Letters 58, 23, 2387-2389, 1987.

[Belmonte 1988] A. L. Belmonte, M. J. Vision, J. A. Glazier, G. H. Gunaratne and B. G. Kenny. *Trajectory Scaling Functions at the Onset of Chaos: Experimental Results*, Physics Review letters 61, 5, 539-542, 1988.

[Breedon 1992] J. L. Breedon and N. H. Packard. *Nonlinear analysis of data sampled nonuniform in time*, Physica D 58, 273-283, 1992.

[Broomhead 1986] D. S. Broomhead and G. P. King. *Extracting qualitative dynamics from experimental data*, Physica D 20, 217, 1986.

[Buzung 1992] Th. Buzung and G. Pfister. *Comparison of algorithms calculating optimal embedding parameters for delay time coordinates*, Physica D 58, 127-137, 1992.

[Casdagli 1991] M. Casdagli, S. Eubank, J. D. Farmer and J. Gibson. *State space reconstruction in the presence of noise*, Physica D 51, 52-98, 1991.

[Dracopoulos 1993] D. C. Dracopoulos and Antonia J. Jones. *Neuromodels of analytic Dynamic Systems*. Neural Computing & Applications, 1, 4, 268-279, 1993.

[Ding 1993] Mingzhou Ding, Celso Grebogi, Edward Ott, Tim Sauer and James A. Yorke. *Plateau Onset for Correlation Dimension: When Does it Occur?*, Physical Review Letters 70, 25, 3872 -3875, 1993.

[Farmer 1987] J. D. Farmer and J. J. Sidorowich. *Predicting Chaotic Time Series*, Physical Review Letters 59, 8, 845-848, 1987.

[Fraser 1986] Andrew M. Fraser and Harry L. Swinney, *Independent coordinates for strange attractors from mutual information*, Physical Review A 33, 2, 1134-1140, 1986.

[Grebogi 1988] C. Grebogi, E. Ott, J. A. Yorke. *Unstable periodic orbits and the dimensions of multifractal chaotic attractors*, Physical Review A 37, 1711-1723, 1988.

[Gunaratne 1989] G. H. Gunaratne, P. S. Linsay and M. J. Vision. *Chaos beyond Onset: A Comparison of Theory and Experiment*, Physics Review Letters 63, 1, 1-4, 1989.

[Holzfuss 1986] J. Holzfuss and G. Mayer-Kress. *An approach to error estimation in the application of dimension algorithms*, in Dimensions and Entropies in Chaotic Systems, editor G. Mayer-Kress, Springer-Verlag, New York, 114-122, 1986.

[King 1987] G. P. King, R. Jones, D. S. Broomhead. *Phase portraits from a time series: a singular system approach*, Nuclear Physics B 2, 379, 1987.

[King 1992] G. P. King and I. Stewart. *Phase space reconstruction for symmetric dynamical systems*, Physica D 58, 216-228, 1992.

[Lathrop 1989] Daniel P. Lathrop and Eric J. Kostelich. *Characterization of an experimental strange attractor by periodic orbits*, Physical Review A 40, 7, 4028-4031, 1989.

[Levin 1993] A. U. Levin. *Recursive Identification Using Feedforward networks*. Department of Computer Science and Engineering, Oregon Graduate Institute, 2000 NW Walker Road. PO Box 91000, Portland, Oregon OR 97291-1000.

#### Chapter 4 - Embedding techniques

- [Martinerie 1992] J. M. Martinerie, A. M. Albano, A. I. Mees, P. E. Rapp. *Mutual information, strange attractors, and the optimal estimation of dimension*, Physical Review A 45, 7085, 1992.
- [Packard 1980] N. H. Packard, J. P. Crutchfield, J. D. Farmer and R. S. Shaw. *Geometry from a time series*, Physics Review Letters 45, 9, 712-16, 1980.
- [Pfister 1992] G. Pfister, Th. Buzung and N. Enge. *Characterization of experimental time series from Taylor-Couette flow*, Physica D 58, 441-454, 1992.
- [Pi 1994] H. Pi and C. Peterson. *Finding the embedding dimension and variable dependencies in time series*. Neural Computation 6, 509-520, 1994.
- [Provenzale 1992] A. Provenzale, L. A. Smith, R. Vio and G. Murante. Distinguishing between low-dimensional dynamics and randomness in measured time series, Physica D 58, 31-49, 1992.
- [Rosenstein 1994] M. T. Rosenstein, J. J. Collins, C. J. De Luca. *Reconstruction expansion as a geometry-based framework for choosing proper delay times*, Physica D 73, 82-98, 1994.
- [Roux 1993] J. -C. Roux. *Dynamical Systems Theory Illustrated: Chaotic Behavior in the Belousov-Zhabotinsky Reaction*, in Chaos in Chemistry and Biochemistry, R. J. Field and L. Györgyi eds, 21-46, World Scientific Publishing, 1993.
- [Russell 1980] D. A. Russell, J. D. Hansen, and E. Ott. *Dimensions of Strange Attractors*, Physical Review Letters 45, 1175-1178, 1980.
- [Sano 1985] M. Sano and Y. Sawada. *Measurement of the Lyapunov Spectrum from a Chaotic Time Series*, Physical Review Letters 55, 10, 1082-1085, 1985.
- [Schiff 1992] S. J. Schiff and T. Chang. *Differentiation of linearly correlated noise from chaos in a biologic system using surrogate data*, Biological Cybernetics 67, 387-393, 1992.
- [Stefánsson 1995] Aðalbjörn Stefánsson, N. Koncar and Antonia J. Jones, *The Gamma test: a simple estimate for the best possible performance of a continuous or smooth data model*, report, Dept. Comp. Maths, University of Wales, 1995.
- [Takens 1980] F. Takens. *Detecting strange attractors in turbulence*. In A. Dold and B. Eckmann, editors, Dynamical Systems and Turbulence, pages 366-381. Springer-Verlag, 1980.
- [Takens 1981] F. Takens. *Dynamical Systems and Turbulence*. Lecture Notes in Mathematics 898, D. A. Rand and L. S. Young, eds, Springer-Verlag, 1981.
- [Zeng 1991] X. Zeng, R. Eykholt and R. A. Pielke. *Estimating the Lyapunov-Exponent Spectrum from Short Time Series of Low Precision*, Physical Review Letters 66, 25, 3229-3232, 1991.



## CHAPTER V

# CONTROL OF CHAOTIC SYSTEMS

---

### 5.1 Introduction

The extreme sensitivity to initial conditions displayed by chaotic systems makes them unstable and unpredictable. Yet the same sensitivity also makes them highly susceptible to control, provided that the chaotic system can be analyzed and the analysis is then used to make small effective control interventions. By perturbing the system in the right way, it is possible to encourage it to follow one of its many unstable but natural behaviours. In such situations, it may be possible to use chaos to advantage, as chaotic systems, once under control, are very flexible. Such systems can rapidly switch among many different behaviours. Incorporating chaos deliberately into practical systems therefore offers the possibility of achieving greater flexibility in their performance.

In the context of chaos, control could mean a number of things. It could mean the elimination of multiple basins of attraction, stabilisation of the fixed points or stabilisation of the unstable periodic orbits. Control of chaos is still in its infancy but the potential it offers is enormous.

There are four main categories of chaos control methodologies. They are *low energy*, *high energy*, *non-feedback* and *feedback* methods.

Low energy control methods require very small changes in the control parameter. In contrast, high energy control methods require large changes. It is always desirable to have a control method which is of the low energy type, as in physical systems control parameter may be fixed or can be changed by only a very small amount. When large changes are required, a physical system may need to be redesigned defeating the 'control of chaos' concept, as such an approach is closer to avoiding chaos.

In feedback methods, a control parameter is changed during the control. In non-feedback methods, a control parameter is changed at the beginning of the control only, and untouched during the control phase.

Perhaps the simplest method to control a chaotic system is to avoid the regions of chaos by studying the bifurcation diagram and thereby choosing appropriate control parameter values, for which the desired periodic behaviour is achieved. A control method which involves a detail study of the bifurcation diagrams

is often referred to as a *bifurcation diagram approach*. Such methods are high energy and non-feedback, and require good mathematical descriptions of the models, as the bifurcation behaviour in real physical system is difficult to learn, due to the requirement of large changes in the control parameter.

Another method is to add supplementary dynamical systems whose role is to create stable orbits in the original chaotic attractor. The difficulty here is that creation of an ideal supplementary system may require the whole system to be redesigned and the goal behaviour has to be chosen by trial and error. This method is also non-feedback.

## **5.2 The OGY method**

The control methods mentioned above share a disadvantage, they do not use the chaotic nature of the system to its best advantage. One of the beauties of controlling a chaotic system is the possibility of producing many quite different behaviours from the same system.

The motion on the strange attractor is ergodic, as the attractor is the set of points of the state space visited by the orbit, after the transients have settled down. Thus the orbit of any point  $P$  on the attractor will make arbitrarily close returns to  $P$ . Due to the smoothness and nonlinearity of the dynamics, one should in general be able to move  $P$  by a small amount so that the close return becomes exact. That is, there is a nearly periodic point arbitrarily close to  $P$ . This leads to the key observation that the set of chaotic orbits is the closure of the set of unstable periodic orbits [Grebogi 1988] and is thus dense on the strange attractor [Gunaratne 1989]. Thus the behaviour of a chaotic system can be viewed as a collection of many orderly behaviours, none of which dominate under ordinary circumstances. Since the motion on the attractor is chaotic, these orbits have to be unstable.

In chaotic dissipative systems, the unstable periodic points have associated directions along which the trajectories converge and diverge, the stable and unstable manifolds. The unstable periodic points on the attractor possess at least one stable and one unstable manifold [Kaplan 1979], i.e. they are saddle points. The local dynamics is approximated by the Jacobian matrix, the derivative of the locally linear map. The eigenvalues of the Jacobian give the local scaling amplitudes, and the eigenvectors determine the directions of the manifolds.

If we can extract the unstable periodic points of a chaotic attractor and learn the local dynamics around the corresponding points in the surface of a section, we may be able to stabilise any one of the different orbits. Of course, we are free to choose the point which best achieves the desired system performance. If the attractor is periodic then small control parameter perturbations change the orbit only slightly. In such

a case we cannot hope to improve the system performance by a low energy method. Furthermore, we may wish to use a system for different purposes under different conditions at different times. Thus, depending on the use, different requirements are made of the system. If the system is chaotic, this type of multiple use situation might be possible with a low energy method.

In 1989 Edward Ott, Celso Grebogi and James A. Yorke, abbreviated as *OGY*, at the University of Maryland introduced a general method by which to control a chaotic system [Ott 1990]. The term ‘control’ here is used to describe a means to encourage the system to remain at the fixed point of choice in the surface of section. OGY first demonstrated the method to control a dissipative chaotic system, using a variation of the Hénon map as in chapter 6. The system was forced to follow an unstable periodic orbit of period one, using only small time dependent perturbations in an accessible control parameter. Their work had a significant impact in the society of researchers working with chaotic systems, since the method does not require a mathematical description of the system to be controlled, and it is a low energy feedback method. More importantly the OGY method could be used to control the system at many different fixed points, in the same control parameter range, thereby encouraging the system to behave quite differently.

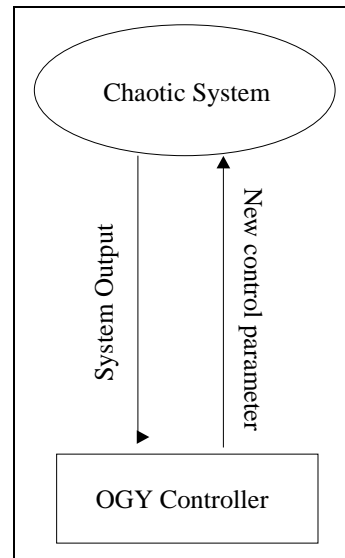


Figure 5.1 OGY control.

The OGY method has two phases the first of which is learning followed by the second, control. The learning phase is broken down into three stages. The first stage is to model the given chaotic system by using embedding techniques.

In the second stage, the embedding space vectors are used to locate the *control point*. A control point is an unstable periodic point which, when controlled, gives the most desirable system behaviour. Once a control point has been selected, a reconstructed surface of section is used to obtain a local linearisation about this point, i.e. construct an approximation to the Jacobian. The OGY method exploits the fact that unstable periodic orbits are dense in a typical strange attractor. The structure of the strange attractor in the neighbourhood of a periodic point, and the motion of points in this neighbourhood, are determined by the tangent space of the periodic point. In particular, the eigenvalues give the local scaling observed in the strange attractor. Thus the nonlinear attractor can be considered as a collection of linear neighbourhoods about the periodic points.

In the third stage a sensitivity analysis is performed, this determines the effects of small perturbations of

the control parameter on the dynamics around the control point.

In the control phase, a perturbation required to control the system is calculated and applied when the system is near the control point. To control chaotic systems, we attempt to confine the iterates of the surface of section to a small neighbourhood of the control point. When an iterate falls nearby, the accessible control parameter  $p$  is changed from its nominal value  $p_0$  by

an amount  $\delta p$ , thereby changing the location of the control point and its stable manifold. The OGY method feeds the new control parameter value to the chaotic system and the output is returned to estimate the next value of the control parameter as illustrated in Figure 5.1. The perturbation  $\delta p$  is chosen such that the next iterate will be forced back toward the stable manifold of the original control point when  $p = p_0$ . The method forces the points to stay in the neighbourhood of an unstable periodic point in the attractor and this makes it quite different from any other previous methods. In Figure 5.2,  $\xi_i$  is the  $i$ th iterates of the surface of section.  $\xi_F$  is the point at which we wish to stabilise the system, i.e. the control point. The circle indicates the region in which the control could be achieved by the OGY method. In (a),  $\xi_n$  falls in the region but the subsequent iterates diverge away from the point in the absence of control. In (b), the iterates are confined within the region due to the effects of perturbations calculated by the OGY control law.

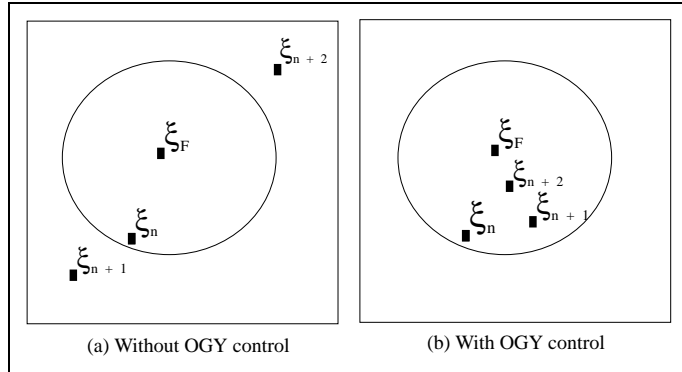


Figure 5.2 Control using a surface of section.

Let the system be described by a function  $f: \mathbb{R}^d \rightarrow \mathbb{R}^d$ . Suppose  $x_\tau$  is some scalar variable which can be experimentally measured. We define an embedding of the system using the delay coordinates method described in Chapter 4 by

$$\xi_i = (x_{it_J}, x_{it_J + t_D}, \dots, x_{it_J + (d_E - 1)t_D}) \quad (\text{V.1})$$

If  $d_E$ ,  $t_J$  and  $t_D$  are chosen suitably the essential features of the system  $f$  can be recovered by studying the embedding space vectors. For  $i \geq 1$ . We are interested in points  $\xi_i$  where  $\xi_i \approx \xi_{i+r}$  for small  $r \geq 1$ . If  $r = 1$  these will be unstable orbits of period 1 in  $\xi(t)$ , if  $r = 2$  period 2, and so on. The aim of the OGY method is to stabilise the system into such a natural (but unstable) orbit. In the case of the Poincaré section we would stabilise  $\xi(t)$  on the section, in the case of equispaced sample points we would stabilise  $\xi(t)$  on a return map.

Suppose  $p$  is some scalar control parameter which is to be varied at times  $t_i$ , say  $p = p_i$  over the interval  $(t_i, t_{i+1})$ , see Figure 5.3. Suppose that the nominal value of  $p$  is  $p_0$ . Our aim is to vary  $p$  by small amounts about  $p_0$  so as to stabilise  $\xi(t)$  about a suitable control point  $\xi_F$ . Discussion on how to locate unstable periodic points can be found in section 4.7.

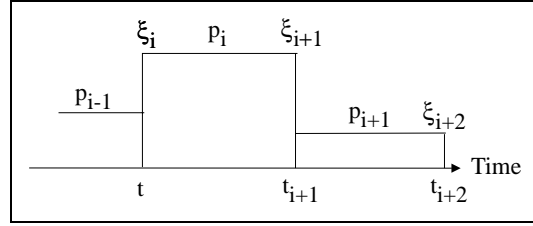


**Figure 5.3** Intervals for which the variables are defined.

The original OGY method considered the successor to  $\xi_i$  and attempted to choose  $\delta p_i$  so that  $\xi_{i+1}$  was close to the control point.

### 5.3 The original OGY control law

For all  $i \geq 1$  let

$$\delta p = p - p_0 \quad \text{and} \quad \delta \xi_{i+1}(p_i) = \xi_{i+1}(p_i) - \xi_F(p_0) \quad (\text{V.2})$$

Suppose that the iteration is described by the map  $\xi_{i+1} = F(\xi_i, p)$ . The locally linear behaviour of  $F$  in the vicinity of a control point  $\xi_F$  is described by the  $d_E \times d_E$  Jacobian matrix

$$J = \left[ D_{\xi} F(\xi, p) \right]_{\xi = \xi_F, p = p_0} \quad (\text{V.3})$$

and in what follows we assume  $\det J \neq 0$ .

This yields the first order approximation

$$\delta \xi_{i+1}(p_i) \approx J \delta \xi_i(p_{i-1}) + u \delta p_i \quad (\text{V.4})$$

where  $u$  is a vector which reflects the direction of the local gradient with respect to  $p$ .

Now suppose that an eigenvector of  $J$ , say  $e_u$ , has a real eigenvalue whose absolute value is greater than 1. This means that points  $\xi_i$  such that  $\delta \xi_i$  lies in the direction of  $e_u$  will, if  $p = p_0$  in the intervening time period, be such that on the next iteration  $\xi_{i+1}$  will lie further away from  $\xi_F(p_0)$ . We refer to this as an *unstable* direction. *Stable* directions are characterised by eigenvectors of  $J$  which have absolute value less than 1.

The basic idea of the OGY method is to choose  $\delta p_i$  so as to eliminate the component of  $\delta \xi_{i+1}$  in the unstable direction(s). We are now almost ready to derive the appropriate control strategy. However, we

first observe the following lemma.

**Lemma 5.1.** Suppose the  $d \times d$  matrix  $J$  has  $d$  linearly independent eigenvectors  $e_1, \dots, e_d$ , with real eigenvalues  $\lambda_1, \dots, \lambda_d$ . Thus we assume the eigenvectors form a basis in  $\mathbb{R}^d$ . Construct the dual basis  $f_1, \dots, f_d$  defined by

$$e_i \cdot f_j = \begin{cases} 1 & \text{if } i = j \\ 0 & \text{if } i \neq j \end{cases} \quad (\text{V.5})$$

Then for any  $x \in \mathbb{R}^d$

$$f_u \cdot Jx = \lambda_u f_u \cdot x \quad (\text{V.6})$$

**Proof.** Express  $x$  in terms of the eigenvectors, writing

$$x = \alpha_1 e_1 + \alpha_2 e_2 + \dots + \alpha_d e_d \quad (\text{V.7})$$

where the  $\alpha_i$  are suitable scalars depending on  $x$ . Thus from (V.5)

$$f_u \cdot x = \alpha_u \quad (\text{V.8})$$

The effect of  $J$  on  $x$  is (from the definition of eigenvectors and eigenvalues)

$$Jx = \alpha_1 \lambda_1 e_1 + \dots + \alpha_d \lambda_d e_d \quad (\text{V.9})$$

Taking the inner product with  $f_u$  yields  $f_u \cdot Jx = \alpha_u \lambda_u$  and the conclusion now follows from (V.8). ■

We can now prove

**Theorem 5.1 (OGY).** The constraint  $f_u \cdot \delta \xi_{i+1} = 0$  leads to the first order control law:

$$\delta p_i \approx - \lambda_u \frac{f_u \cdot \delta \xi_i(p_{i-1})}{f_u \cdot u} \quad (\text{V.10})$$

where for  $\xi_i$  near  $\xi_F$ , the sensitivity vector  $u$  is defined as

$$u = \left[ \frac{\partial}{\partial p_i} (\delta \xi_{i+1}(p_i) - J \delta \xi_i(p_{i-1})) \right]_{p_0} = \lim_{p_i \rightarrow p_0} \frac{\xi_{i+1}(p_i) - J \xi_i(p_{i-1})}{p_i - p_0} \quad (\text{V.11})$$

**Proof.** Dotting (V.4) with  $f_u$  using Lemma 1 we have

$$f_u \cdot \delta \xi_{i+1}(p_i) \approx \lambda_u f_u \cdot \delta \xi_i(p_{i-1}) + f_u \cdot u \delta p_i \quad (\text{V.12})$$

Using the constraint  $f_u \cdot \delta \xi_{i+1} = 0$  we obtain from (V.12)

$$\lambda_u f_u \cdot \delta \xi_i(p_{i-1}) + f_u \cdot u \delta p_i \approx 0 \quad (\text{V.13})$$

which on solving for  $\delta p_i$  yields (V.10). ■

The following conditions are required to control a chaotic system with the original OGY method.

- Experimental time series of some scalar-dependent variable  $x_t$  can be measured and a suitable embedding technique can be applied, or the mathematical model describing the system is available.
- The dynamics of the system can be represented as a low-dimensional surface of section and the system has at least two linearly independent real eigenvectors.
- There is a specific periodic orbit of the map which lies in the attractor and around which one wishes to stabilise and the corresponding unstable periodic point can be located.
- A parameter  $p$  is available for external adjustment which can be used to slightly modify the system dynamics. Let the range in which  $p$  is allowed to vary  $p_{\text{MAX}} > p > p_{\text{MIN}}$ . There is maximum perturbation  $\delta p_*$  in the parameter  $p$  by which it is acceptable to vary  $p$  from the nominal value  $p_0$ .
- The position of the periodic orbit is a function of  $p$ , but the local dynamics about it do not vary much with small changes in  $p$ .

#### 5.4 Variations and use of the OGY method

Before we look at some variations of the OGY method, let us define the advantages and disadvantages. Since the introduction of the method, a number of improvements have been published to overcome some of the disadvantages.

The advantages:

- No mathematical model of the dynamics is required.
- The computations required at each iterate to calculate the perturbation to be applied are minimal.
- The required changes in the control parameter to obtain effective control are small.
- Different control points could be stabilised for the same system in the same parameter range.

- Control can be achieved even with imprecise measurements of the eigenvectors and eigenvalues.
- The method extends to any smooth chaotic system whose dynamics can be characterised by a nonlinear map.
- The method is relatively robust to small noise levels (for control of low period orbits).
- Different control parameters can be used to control a given system.
- If the system is intrinsically chaotic and fulfils these requirements then there is no need to redesign the system in any way. This may be particularly relevant to large natural systems to which high-energy control methods cannot possibly be applied (e.g. the ionosphere and the HARP project).

The disadvantages:

- One needs to locate a control point which gives a satisfactory system behaviour when control is applied.
- Only unstable periodic orbits which exist in the original attractor can be stabilised.
- A long time may be taken for the system to approach the control point.
- There is a requirement for a system wide control parameter which can be readily manipulated.
- Use of different control parameters may give different performances.
- High dimensional control might be difficult, especially when there is more than one unstable manifold.
- Control of high periodicity orbits is difficult.
- The original method does not take previous perturbations into account; arguably these are relevant (refer to next section).
- The method will not work for systems with complex eigenvectors.
- When a mathematical model of the system is not available, choosing a suitable embedding technique may be difficult and time consuming.

One of the practical difficulties of the OGY method using embedding techniques is that the learning phase can take a long time. This means the time taken before any control can be applied to the system may be significant. This could be a major problem if the method were to be applied to a real time control system, especially when adaptive control is required. This appears to be one of the worst disadvantages of the method, and as far as we are aware has not been addressed in the literature.

A number of analyses and surveys of the OGY method have been published including [Romeiras 1992], [Ditto 1993], [Shinbrot 1993], [Ott 1994]. Control of well known mathematical systems using the method includes the Lorenz model [Singer 1991], [Shinbrot 1992b], a variation of the Hénon map [Ott 1990], and the Duffing oscillator [Dressler 1992].

## *Chapter 5 - The OGY method*

Many practical applications have been demonstrated using the OGY method and several different formalisms have been used in the literature to describe the method along with some improvements.

The improvements include control of higher periodic orbits [Hunt 1991], [Roy 1992], [Romeiras 1992], [Lai 1993], control of high dimensional systems [Auerbach 1992], control of Hamiltonian chaotic systems [Lai 1993], use of the previous values of the control parameter [Dressler 1992], creations of nonexisting periodic orbits [Hunt 1991], tracking of unstable orbits [Gills 1992], [Carroll 1992], and control spatiotemporal systems [Schwartz 1994].

First control of a physical system using the OGY method, in the form of chaotically buckling magnetostrictive ribbon, was reported in [Ditto 1990]. Other control of physical systems includes a thermal convection loop [Singer 1991], spin-wave instabilities [Azevedo 1991], a diode resonator with up to 23 drive cycles [Hunt 1991], a chaotic multimode laser [Roy 1992], [Gills 1992], a Duffing like circuit [Carroll 1992] and an oscillatory chemical system: the Belousov-Zhabotinsky reaction [Petrov 1993].

The OGY method has also been used to control biological systems such as the control of cardiac arrhythmias in rabbit ventricle [Garfinkel 1992] and chaos in rat brain [Moss 1994], [Schiff 1994] .

Variations of the OGY method have been used for synchronisation of chaos [Carroll 1993], [Roy 1994], [Lai 1994]. In a similar manner, the method was varied slightly to allow for use of chaos to encode and decode transmitted data [Hayes 1993].

The sensitivity of a chaotic system to small perturbations was used to rapidly direct orbits from an arbitrary initial state to an arbitrary but accessible desired state [Shinbrot 1990], [Shinbrot 1992a], [Shinbrot 1992b]. This technique can be used to significantly reduce the time taken for the trajectory to approach the desired point in the surface of section.

The original OGY procedure for a given dynamic system is summarised in Algorithm 4.31.

```

(* Reconstruction of the attractor - Embedding technique *)
Refer to Algorithm 4.2 and Algorithm 4.6
 $\xi$  = A set of embedding space vectors as in (IV.1)

(* Extraction, grouping and averaging of the unstable periodic points *)
Refer to Algorithm 4.2, Algorithm 4.3 and Algorithm 4.5
UPO = A set of unstable periodic orbits with the periods

(* Study of local dynamics of the control points *)
For each  $(k, (\xi_F^{(1)}, \xi_F^{(2)}, \dots, \xi_F^{(k)}))$  in UPO
    C = {} (* Create a new list C - Stores pairs of points falling near  $\xi_F^{(1)}$  *)
    (* Perform local linearisation *)
    Collect sufficient number of pair points  $(\xi_i, \xi_{i+k})$  near  $\xi_F^{(1)}$  and append them to C
    Using these pair points approximate the Jacobian matrix J by a least squares fit,
    where  $\delta\xi_{i+k} \approx J \delta\xi_i$ 
    Compute eigenvectors and eigenvalues of J
    Note the stable and unstable eigenvectors  $e_s, e_u$  and their associated eigenvalues
     $\lambda_s$  and  $\lambda_u$ 
    (* assume there is only one unstable direction *)
    Compute the dual basis of the eigenvectors and select  $f_u$  as in (V.5)
    (* Perform sensitivity analysis *)
    For each  $(\xi_i, \xi_{i+k})$  in C
        For l = 1 to 50
            Randomly generate  $p' \in [p_{MIN}, p_{MAX}]$ 
            Compute  $\xi'_{i+k} = \xi_{i+k}(p')$ 
             $u_1 = (\delta\xi'_{i+k} - J\delta\xi_i)/\delta p'$  as in (V.11)
        endfor l
        set u equal to the mean of all  $u_1$ 
    endfor
endfor
Choose the desired control point  $\xi_F$  and the associated parameters  $(\lambda_u, f_u, u)$ 
Repeat
    Obtain the current point  $\xi_i$ 
    Set  $\delta p'$  by using the OGY control law as in (V.10)
     $p' = p_0 + \delta p'$ 
    If  $p_{MIN} \leq \delta p' \leq p_{MAX}$ 
        then
            control with  $p'$ 
        else no control
    endif
Until instructed to STOP

```

**Algorithm 5.1** OGY chaos control method.

### 5.5 The Dressler and Nitsche control law

The OGY method has a number of disadvantages, one of which is a lack of use of the previous value of the control parameter. This problem was addressed by U. Dressler and G. Nitsche [Dressler 1992]. Their method is based on the OGY method, but the control law takes the previous value of the control parameter into consideration, thereby theoretically and realistically offering a better possibility of effective control.

Theorem 5.1 differs slightly from the original version of the OGY control law. However, this difference is purely notational as we now show. To see that (V.10) is equivalent to the original control law proposed by OGY [Ott 1990] we shall need the following trivial.

**Lemma 5.2.** Suppose the  $d \times d$  matrix  $J$  has  $d$  linearly independent eigenvectors  $e_1, \dots, e_d$ , with real eigenvalues  $\lambda_1, \dots, \lambda_d$ , none of which is equal to 1, and that  $f_1, \dots, f_d$  are the contravariant vectors as in (V.5), then the matrix  $I - J$ , where  $I$  is the  $d \times d$  identity matrix, has eigenvalues  $(1 - \lambda_1), \dots, (1 - \lambda_d)$  and the dual bases for the eigenvectors are the same for both  $J$  and  $I - J$ .

**Proof.** Let  $e$  be an eigenvector of  $J$  and  $\lambda$  its eigenvalue, hence  $Je = \lambda e$ , so that

$$(I - J)e = (1 - \lambda)e \quad (\text{V.14})$$

Thus, provided  $\lambda \neq 1$ ,  $e$  is also an eigenvector of  $I - J$  and  $1 - \lambda$  is its eigenvalue. Moreover, the dual basis is the same in both cases. ■

The original formulation of Theorem 5.1 was

**Theorem 5.2 (OGY).** The constraint  $f_u \cdot \delta \xi_{i+1} = 0$  leads to the first order control law

$$\delta p_i = \frac{\lambda_u}{\lambda_u - 1} \frac{f_u \cdot \delta \xi_i(p)}{f_u \cdot g} \quad (\text{V.15})$$

where the sensitivity vector  $g$  is defined by

$$g = \left[ \frac{\partial \xi_F}{\partial p} \right]_{p_0} = \lim_{p \rightarrow p_0} \frac{\xi_F(p) - \xi_F(p_0)}{p - p_0} \quad (\text{V.16})$$

*Note.* The sensitivity vector  $g$  is defined in terms of the shift of the fixed point  $\xi_F$  with respect to a change in  $p$ , whereas in the Dressler and Nitsche paper,  $u$  is defined as the shift in  $\xi_{i+1}$  with respect to a change in  $p$ . When a sensitivity vector is estimated from real data,  $u$  requires far less data than  $g$ . The estimation

of  $g$  requires us to observe the system for a long enough time after changing the control parameter for the transient to vanish and then to locate the newly shifted fixed point. However, we only need to estimate the changes in the positions of next iterates to estimate  $u$ .

To show that (V.10) is equivalent to (V.15) we must examine the relationship between the sensitivity vectors  $g$  and  $u$ , see Figure 5.4.

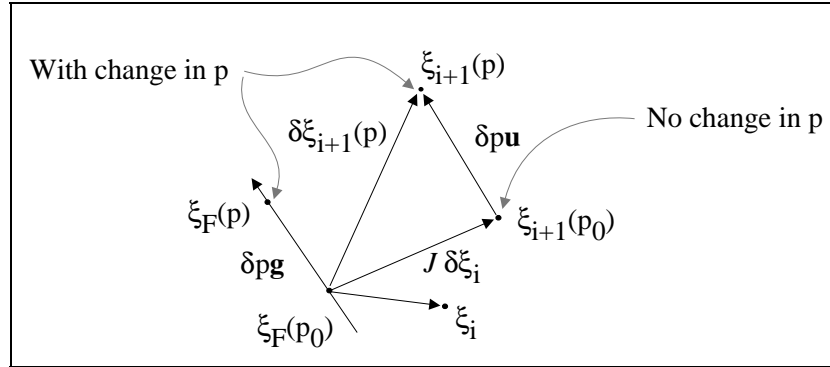


**Figure 5.4** Comparison of the sensitivity vectors  $g$  and  $u$ .

The OGY paper also uses the Jacobian matrix  $J$  but applied to changes in  $\xi_i$  relative to the *shifted* fixed point, i.e.

$$\xi_{i+1}(p) - \xi_F(p) \approx J (\xi_i(p) - \xi_F(p)) \quad (\text{V.17})$$

where from (V.16)

$$\xi_F(p) \approx \xi_F(p_0) + (p - p_0)g \quad (\text{V.18})$$

We note

**Lemma 5.3.** From (V.17) and (V.18) it follows that

$$u = (I - J)g \quad (\text{V.19})$$

**Proof.** From (V.17) and (V.18) we have in the OGY notation

$$\xi_{i+1}(p) - \xi_F(p_0) \approx J (\xi_i(p) - \xi_F(p_0)) + (p - p_0) (I - J) g \quad (\text{V.20})$$

The corresponding equation in the Dressler and Nitsche notation is

$$\xi_{i+1}(p) - \xi_F(p_0) \approx J(\xi_i(p) - \xi_F(p_0)) + (p - p_0)u \quad (\text{V.21})$$

Direct comparison of the two equations (which are first order identities in  $p$ ) yields the result. ■

**Proof of Theorem 5.2.** From Theorem 5.1 and Lemmas 5.3, 5.2 and 5.1 we have

$$\delta p_i = -\lambda_u \frac{f_u \cdot \delta \xi_i(p)}{f_{u,u}} = -\lambda_u \frac{f_u \cdot \delta \xi_i(p)}{f_u \cdot (I - J)g} = \frac{\lambda_u}{(\lambda_u - 1)} \frac{f_u \cdot \delta \xi_i}{f_u \cdot g} \quad (\text{V.22})$$

which is the original OGY control law. ■

### 5.6 Derivation of the Dressler and Nitsche control law.

Here we consider an extension of the OGY method, due to Dressler and Nitsche [Dressler 1992], which considers  $\xi_{i+1}$  and  $\xi_{i+2}$  and defines a control strategy with the goal of making  $\xi_{i+2}$  close to the fixed point and returning  $p_{i+1}$  to its nominal value. This generalisation contains the original method as a special case.

We replace (V.2) by

$$\delta p = p - p_0 \quad \text{and} \quad \delta \xi_{i+1}(p_{i-1}, p_i) = \xi_{i+1}(p_{i-1}, p_i) - \xi_F(p_0, p_0) \quad (\text{V.23})$$

If  $\xi_i$  is given then we can model the effects on  $\xi_{i+1}$  of two successive parameter choices  $p_{i-1}, p_i$  by considering them as independent variables. We first calculate the directional derivatives:

$$v = \left[ \frac{\partial}{\partial p_{i-1}} (\delta \xi_{i+1}(p_{i-1}, p_i) - J \delta \xi_i(p_{i-2}, p_{i-1})) \right]_{(p_0, p_0)} \quad (\text{V.24})$$

$$u = \left[ \frac{\partial}{\partial p_i} (\delta \xi_{i+1}(p_{i-1}, p_i) - J \delta \xi_i(p_{i-2}, p_{i-1})) \right]_{(p_0, p_0)}$$

Next, using Taylor's theorem to obtain a first order approximation, we can write

$$\delta \xi_{i+1}(p_{i-1}, p_i) = J \delta \xi_i(p_{i-2}, p_{i-1}) + v \delta p_{i-1} + u \delta p_i + o(\theta) \quad (\text{V.25})$$

as  $\theta \rightarrow 0$ , where  $\theta = \text{Max}\{\sqrt{(\delta p_{i-1}^2 + \delta p_i^2)}, |\delta \xi_i|\}$  and  $o(g(\theta))$  denotes any function  $f(\theta)$  such that  $f(\theta)/g(\theta) \rightarrow 0$  as  $\theta \rightarrow 0$ . Here  $J$  accounts for that part of the transformation when  $p$  is held constant at  $p_0$ . The terms in  $v$  and  $u$  account for that part due to two successive variations in the control parameter,

see Figure 5.5. Numerical approximations to  $v$  and  $u$  can be determined from observations of the effects of independent changes in the control parameters  $p_{i-1}$  and  $p_i$ . From (V.25) we obtain

$$\begin{aligned}\xi_{i+1}(p_{i-1}, p_i) - \xi_F(p_0, p_0) &= J \left( \xi_i(p_{i-2}, p_{i-1}) - \xi_F(p_0, p_0) \right) + v\delta p_{i-1} + u\delta p_i + o(\theta) \\ \xi_{i+2}(p_i, p_{i+1}) - \xi_F(p_0, p_0) &= J \left( \xi_{i+1}(p_{i-1}, p_i) - \xi_F(p_0, p_0) \right) + v\delta p_i + u\delta p_{i+1} + o(\theta)\end{aligned}\tag{V.26}$$

and from these equations we shall derive the recurrence relation which constitutes the control law.

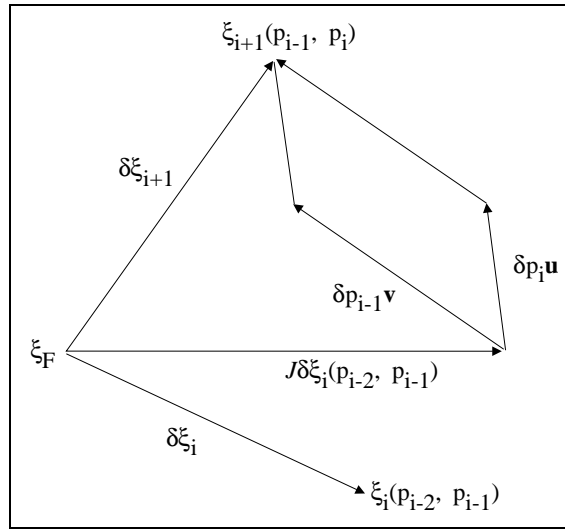


**Figure 5.5** The combined effects of  $J$  in combination with  $\delta p_{i-1}$  and  $\delta p_i$ .

**Theorem 5.3 (Dressler and Nitsche).** The constraints

$$f_u \cdot \delta \xi_{i+2} = 0 \quad \text{and} \quad \delta p_{i+1} = 0\tag{V.27}$$

imply the first order control law

$$\delta p_i \approx - \frac{\lambda_u^2 f_u \delta \xi_i(p_{i-2}, p_{i-1})}{f_u \cdot v + \lambda_u f_u \cdot u} - \frac{\lambda_u f_u \cdot v}{f_u \cdot v + \lambda_u f_u \cdot u} \delta p_{i-1}\tag{V.28}$$

where the sensitivity vectors  $v$  and  $u$  are defined in (V.24).

*Note.* The first condition of (V.27) is designed to place  $\xi_{i+2}$  onto a stable manifold. The second condition is designed to prevent  $\delta p$  from becoming large. Taking the two previous values of  $\delta p$  into account should give better control than the original OGY control law.

**Proof.** From (V.23) and (V.26) we have:

$$\begin{aligned}\delta\xi_{i+1}(p_{i-1}, p_i) &= J\delta\xi_i(p_{i-2}, p_{i-1}) + v\delta p_{i-1} + u\delta p_i + o(\theta) \\ \delta\xi_{i+2}(p_i, p_{i+1}) &= J\delta\xi_{i+1}(p_{i-1}, p_i) + v\delta p_i + u\delta p_{i+1} + o(\theta)\end{aligned}\tag{V.29}$$

Dotting the two equations in (V.29) by  $f_u$  and using Lemma 1 we obtain

$$\begin{aligned}f_u \cdot \delta\xi_{i+1}(p_{i-1}, p_i) &= \lambda_u f_u \cdot \delta\xi_i(p_{i-2}, p_{i-1}) + f_u \cdot v\delta p_{i-1} + f_u \cdot u\delta p_i + o(\theta) \\ f_u \cdot \delta\xi_{i+2}(p_i, p_{i+1}) &= \lambda_u f_u \cdot \delta\xi_{i+1}(p_{i-1}, p_i) + f_u \cdot v\delta p_i + f_u \cdot u\delta p_{i+1} + o(\theta)\end{aligned}\tag{V.30}$$

Using the conditions in (V.27), the second equation in (V.30) reduces to

$$\lambda_u f_u \cdot \delta\xi_{i+1}(p_{i-1}, p_i) + f_u \cdot v\delta p_i \approx 0\tag{V.31}$$

which can be written as

$$f_u \cdot v\delta p_i \approx -\lambda_u f_u \cdot \delta\xi_{i+1}(p_{i-1}, p_i)\tag{V.32}$$

From the first equation in (V.30), and from (V.32), we obtain

$$f_u \cdot v\delta p_i \approx -\lambda_u \left( \lambda_u f_u \cdot \delta\xi_i(p_{i-2}, p_{i-1}) + f_u \cdot v\delta p_{i-1} + f_u \cdot u\delta p_i \right)\tag{V.33}$$

Which, upon collecting terms in  $\delta p_i$  and  $\delta p_{i-1}$ , can be rearranged as

$$(f_u \cdot v + \lambda_u f_u \cdot u)\delta p_i \approx -\lambda_u^2 f_u \cdot \delta\xi_i(p_{i-2}, p_{i-1}) - \lambda_u f_u \cdot v\delta p_{i-1}\tag{V.34}$$

Solving this for  $\delta p_i$  finally yields the Dressler and Nitsche control law in (V.28). ■

Suppose the sensitivity with respect to  $\delta p_{i-1}$  is ignored. Then, on taking  $v$  to be the null vector, (V.28) reduces to (V.10). In this sense the Dressler and Nitsche control law is a generalisation of Theorem 5.1.

## 5.7 High period control strategy

In ordinary periodic systems, the number of different system behaviours is limited. On the other hand, chaotic systems contain an infinite number of nearly regular behaviours which are quite different from each other. Such systems offer an enormous potential if one could select a desired behaviour and persuade the system to behave as desired. As discussed in section 4.7, an unstable periodic orbit of a chaotic system can be thought as a nearly regular system behaviour.

Both the original OGY and the Dressler and Nitsche control laws suffer when confronted with control of unstable orbit of period more than one. Extensions to the OGY method to control unstable orbits of period greater than 1 have been reported in [Hunt 1991], [Roy 1992], [Romeiras 1992], [Auerbach 1992], [Lai 1993].

In the original OGY and the Dressler and Nitsche control laws, control signal is applied to the system at a  $k$ th iterate of the surface of section for control of an unstable orbit of period  $k$ . As  $k$  increases the number of signals applied decreases. Since the orbit is chaotic it diverges from the desired trajectory with time. In  $k$  iterations the orbit may change its behaviour so much that we often cannot reactivate control. In an effort to overcome this hurdle we have developed a new method based on the OGY strategy which is similar to the method independently reported in [Lai 1993], the *high period control strategy*. Here an appropriate signal is applied to the system at *every* iterate of the map independent of  $k$ .

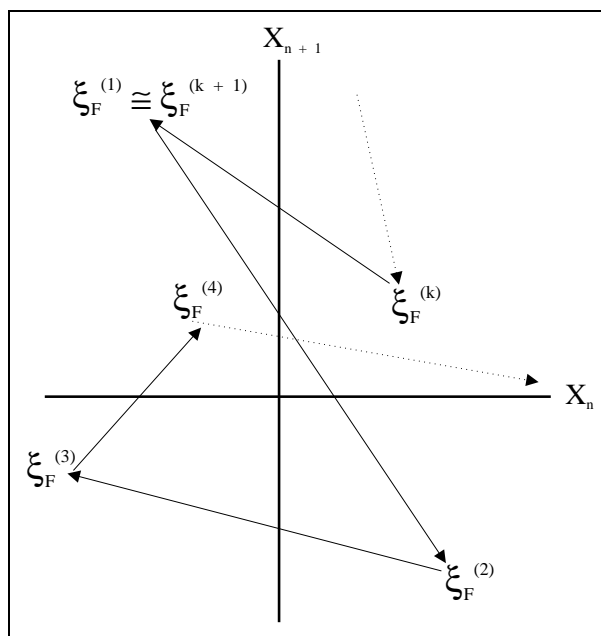


Figure 5.6 A periodic orbit of period  $k$  on the return map.

The effect of noise is thus reduced. The conditions required for our method is same as that of the OGY method stated at the end of section 5.3.

An unstable periodic orbit of a chaotic system can be thought as a periodic behaviour of the system for a short time. Our control method works well with unstable orbits of any period provided that the orbit exists within the original chaotic attractor and can be extracted accurately (refer to section 4.7.1). Let us assume that a periodic orbit of period  $k$ , say  $\Phi$ , is an approximation to an existing unstable orbit of period  $k$  which we wish to control.

On the surface of section,  $\Phi$  consists of  $k$  points. Each point is regarded as the control point at that iterate. Let the sequence of points be denoted as  $\xi_F^{(1)}, \xi_F^{(2)}, \dots, \xi_F^{(k)}$ . Starting at  $\xi_F^{(1)}$ , the next iterate point is  $\xi_F^{(2)}$ , the one after is  $\xi_F^{(3)}$  and so on. When  $\xi_F^{(k)}$  is reached, the next control point returns back to  $\xi_F^{(1)}$ . Such a periodic orbit is illustrated in Figure 5.6.

We seek to derive a general control law for any  $k$ . Given a point  $\xi_i$  near  $\xi_F^{(n)}$  we wish to force the next

iterate point  $\xi_{i+1}$  to be near  $\xi_F^{(n+1)}$ , where  $n \leq k, n \in \mathbb{N}$ . When  $n+1 > k$ , we replace  $(n+1)$  with 1. The method requires  $k$  sets of the transformation matrix  $A^{(n)}$  which translates  $(\xi_i - \xi_F^{(n)})$  to  $(\xi_{i+1} - \xi_F^{(n+1)})$  and the sensitivity vector  $s^{(n)}$ . The matrix  $A^{(n)}$  is described by the  $d_E \times d_E$  transformation matrix and  $s^{(n)}$  as a  $d_E$ -dimensional vector, where  $d_E$  is the dimension of the embedding space vectors. We assume  $\det A^{(n)} \neq 0$ . The linear relation of a map  $\xi_{i+1} = F(\xi_i, p)$  is illustrated in Figure 5.7 (a) and the effect of the sensitivity vector in Figure 5.7 (b). In the diagrams  $\xi'_{i+1}$  are the images of next iterate point relative to  $\xi_F^{(n)}$ .

This yields the first order approximation

$$\xi_{i+1}(p_i) - \xi_F^{(n+1)}(p_0) \approx A^{(n)}(\xi_i(p_{i-1}) - \xi_F^{(n)}(p_0)) + s^{(n)}\delta p_i \quad (\text{V.35})$$

where for  $\xi_i$  near  $\xi_F^{(n)}$ , the sensitivity vector  $s^{(n)}$  is defined as

$$s^{(n)} = \lim_{p' \rightarrow p_0} \frac{(\xi_{i+1}(p') - \xi_F^{(n+1)}(p_0)) - A^{(n)}(\xi_i(p_0) - \xi_F^{(n)}(p_0))}{p' - p_0} \quad (\text{V.36})$$

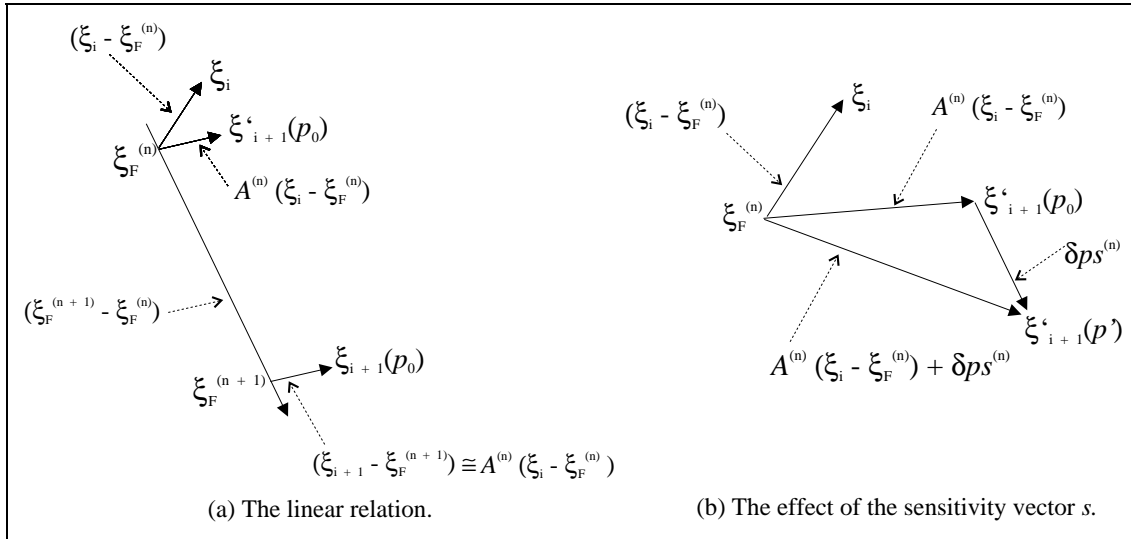


**Figure 5.7** The transformation matrix and the sensitivity vector.

Suppose that an unstable direction (an eigenvector) of  $A^{(n)}$ , say  $e_u^{(n)}$ , has a real length (an eigenvalue), say  $\lambda_u^{(n)}$ , whose absolute value is greater than 1 as in sections 5.3 and 5.6. This means that a point  $\xi_i$  which lies in the direction of  $e_u^{(n)}$  will be such that on the next iteration  $\xi_{i+1}$  will lie further away from  $\xi_F^{(n+1)}$ . As with the OGY method, the idea of our method is to choose  $\delta p_i$  to eliminate the component of  $(\xi_{i+1} - \xi_F^{(n+1)})$  in the unstable direction. This yields a constraint  $f_u^{(n)} \cdot (\xi_{i+1} - \xi_F^{(n+1)}) = 0$ , where  $f_u^{(n)}$  is the dual basis vector of  $e_u^{(n)}$ .

**Theorem 5.4 (High period control).** The constraint  $f_u^{(n)}(\xi_{i+1} - \xi_F^{(n+1)}) = 0$  leads to the first order control law:

$$\delta p_i \approx -\lambda_u^{(n)} \frac{f_u^{(n)}(\xi_i(p_{i-1}) - \xi_F^{(n)}(p_0))}{f_u^{(n)} \cdot s^{(n)}} \quad (\text{V.37})$$

**Proof.** Dotting (V.35) with  $f_u^{(n)}$  and using the constraint  $f_u^{(n)}(\xi_{i+1} - \xi_F^{(n+1)}) = 0$  and Lemma 1 we have

$$\lambda_u^{(n)} f_u^{(n)}(\xi_i(p_{i-1}) - \xi_F^{(n)}(p_0)) + f_u^{(n)} \cdot s^{(n)} \delta p_i \approx 0 \quad (\text{V.38})$$

which on solving for  $\delta p_i$  yields (V.37). ■

We observe that the original OGY control law is a subset of ours. For  $k = 1$ , there is only one control point  $\xi_F$ , where  $\xi_F^{(n)}$  and  $\xi_F^{(n+1)}$  are the same. Starting the control at  $\xi_F^{(n)}$  where  $n = 1$  the next control point is at  $\xi_F^{(n+1)}$ , however  $n + 1 > k$  so  $n$  is set back to 1, i.e.  $\xi_F = \xi_F^{(n)} = \xi_F^{(n+1)}$ . Consequently there is only one transformation matrix  $A$  which is equivalent to  $J$  and the sensitivity vector  $s$  is equivalent to  $u$ . As the result the control law becomes same as (V.10).

During the learning phase of our method, the experimental time series of some scalar variable is used first to create a set of embedding space vectors to reconstruct the attractor. Using the embedding space vectors, a number of unstable periodic orbits of sufficiently high period are extracted. We then select an unstable periodic orbit  $\Phi$  which is similar to the desired system behaviour. Such orbit of order  $k$  consists of a sequence of  $k$  control points on the return map. For each of  $k$  control point, we observe the difference between  $(\xi_i - \xi_F^{(n)})$  and  $(\xi_{i+1} - \xi_F^{(n+1)})$  for a sufficient number of  $(\xi_i, \xi_{i+1})$  where  $|\xi_i - \xi_F^{(n)}| < \epsilon$  and estimate the transformation matrix  $A^{(n)}$  as in (V.35) by the least squares fit method. The sensitivity vector  $s^{(n)}$  is then estimated by the least squares fit method again by fitting  $s^{(n)}$  as in (V.36) for a number of different  $p'$  for  $p_{\text{MAX}} > p' > p_{\text{MIN}}$ .

In practice, it is difficult to extract a true set of control points. It is therefore also difficult to approximate  $A^{(n)}$  accurately. In some situations we may not be able to estimate the matrices which have both unstable and stable eigenvectors. In such cases, we do not attempt control for those successive pairs of control points, i.e. the control for the interval between  $\xi_F^{(n)}$  and  $\xi_F^{(n+1)}$ . There are two ways to increase the accuracy of the transformation matrices. The first is to estimate the unstable periodic orbit more accurately (refer to section 4.7). The second is to increase the number of embedding space vectors and reduce the

distance used in the least squares fit method during the estimation of the matrices.

During the control phase, we wait until  $\xi_i$  is near one of the control points of  $\Phi$ . When applying the control formula (V.37),  $p_1$  must satisfy  $p_{\text{MAX}} > p_1 > p_{\text{MIN}}$ . If the condition is not satisfied  $p_1$  is set to be  $p_0$ . The control parameter is replaced by  $p_1$  to force  $\xi_{i+1}$  to be close to the next control point. As with the original OGY method, the time before realisation of the control increases as the maximum allowed perturbation approaches zero.

A drawback of the method is the necessity to estimate  $k$  sets of the transformation matrices and the sensitivity vectors for control of an unstable orbit of period  $k$ . The estimations are a time consuming part of the learning phase, especially when the set of embedding space vectors is large or the distance used for the least squares fit method small. Another drawback of the method is that it is sensitive to the estimation of the set of control points. When the extraction of  $\Phi$  is poor, the estimation of the matrices and the vectors suffers and the method may not work.

The obvious advantage of our method is the ability to control much higher unstable periodic orbits under the same condition as the OGY method. There is no theoretical limit to the order of the periodicity of the unstable orbit. Using a variation of the Hénon map, we have successfully controlled 205 orbits of periods up to fifty. In contrast, we were only able to control a period one and a period two orbits using either the OGY or the Dressler and Nitsche control methods. The experiments are reported in chapter VI.

A significant difference between our approach compared to that of [Lai 1993] is that, they have estimated the unstable and stable directions (they have used a two dimensional chaotic Hamiltonian system) by applying the Poincaré mapping forward for the stable direction and backward for the unstable directions a number of times. For more detail refer to [Lai 1993], [Shinbrot 1993]. They have devised this method as most of the eigenvectors were found to be complex.

Another approach to estimate the stable and unstable directions when the eigenvectors are complex is to use the singular value decomposition. When a  $d_E$  by  $d_E$  matrix is applied to a  $d_E$ -dimensional sphere, the transformation yields a  $d_E$ -dimensional ellipsoid. The singular value decomposition estimates the direction vectors and the lengths of the principal axes of the ellipsoid. Comparisons of the control method using the principal axes and the eigenvectors are reported in chapter VI for an iterative map (dissipative system).

## 5.8 Chapter summary

In this chapter we have introduced a number of ways in which a chaotic system may be controlled. The

simplest method was to study the bifurcation diagram of the system to be controlled and select the control parameter value which would give desired system behaviour. Another was to add a supplementary dynamic system to the system to be controlled in order to create stable orbits within the existing chaotic attractor.

Both of the above mentioned control methods are far from ideal, as a full mathematical description is not always available. The OGY method was introduced as a better control technique which overcomes many of the problems inherent in the previous control strategies.

The OGY strategy inspired many practitioners in the field. The method and its variants were used to control many physical chaotic systems. The original OGY method had a number of disadvantages and many of these were rectified by the researchers.

The Dressler and Nitsche control law was described in detail, since this is a significant improvement upon the original OGY method. Their method utilises the previous value of the control parameter. Detailed proofs were given for both the OGY and the Dressler and Nitsche methods.

One of the major disadvantage of the OGY and the Dressler and Nitsche methods is the poor performance when confronted with control of unstable orbits of high periods. In an attempt to overcome this problem we have presented our method, the high period control strategy. This is an extension of the OGY method and works under the same condition. A very similar approach has been reported in [Lai 1993]. The difference lies in the way to estimate the stable and unstable direction near the control points.

### Chapter references

[Auerbach 1987] Ditza Auerbach, Predrag Cvitanovic, Jean-Pierre Eckmann, Gemunu Gunaratne and Itamar Procaccia. *Exploring Chaotic Motion Through Periodic Orbits*, Physics Review Letters 58, 23, 2387-2389, 1987.

[Auerbach 1992] D. Auerbach, C. Grebogi, E. Ott and J. A. Yorke. *Controlling Chaos in High Dimensional Systems*, Physical Review Letters 69, 24, 3479-3482, 1992.

[Azevedo 1991] A. Azevedo and S. M. Rezende. *Controlling Chaos in Spin-Wave Instabilities*, Physical Review Letters 66, 10, 1342-1345, 1991.

[Carroll 1992] T. L. Carroll, I. Triandaf, I. Schwartz and L. Pecora. *Tracking unstable orbits in an experiment*, Physical Review A 46, 10, 6189-6192, 1992.

[Carroll 1993] Thomas L. Carroll and Louis M. Pecora. *Using chaos to keep period-multiplied systems in phase*, Physics Review E 48, 4, 2426-2436, 1993.

[Ditto 1990] W. L. Ditto, S. N. Rauseo and M. L. Spano. *Experimental Control of Chaos*, Physical Review

## Chapter 5 - The OGY method

Letters 65, 26, 3211-3214, 1990.

[Ditto 1993] W. L. Ditto and L. M. Pecora. *Mastering Chaos*, SCIENTIFIC AMERICAN, 62-68, August 1993.

[Dressler 1992] U. Dressler and G. Nitsche. *Controlling chaos using time delay coordinates*. Physics Review letters 68, 1, 1-4, 1992.

[Garfinkel 1992] A. Garfinkel, M. L. Spano, W. L. Ditto and J. N. Weiss. *Controlling Cardiac Chaos*, Science 257, 1230-1235, 1992.

[Gills 1992] Z. Gills, C. Iwata, R. Roy, I. B. Schwartz and I. Triandaf. *Tracking Unstable Steady States: Extending the Stability Regime of a Multimode Laser System*, Physical Review Letters 69, 22, 3169-3172, 1992.

[Grebogi 1988] C. Grebogi, E. Ott, J. A. Yorke. *Unstable periodic orbits and the dimensions of multifractal chaotic attractors*, Physical Review A 37, 1711-1723, 1988.

[Gunaratne 1989] G. H. Gunaratne, P. S. Linsay and M. J. Vision. *Chaos beyond Onset: A Comparison of Theory and Experiment*, Physics Review Letters 63, 1, 1-4, 1989.

[Hayes 1993] S. Hayes, C. Grebogi and E. Ott. *Communicating with Chaos*, Physical Review Letters 70, 20, 3031-3034, 1993.

[Hunt 1991] E. R. Hunt. *Stabilizing High-Period Orbits in a Chaotic System: The Diode Resonator*, Physical Review Letters 67, 15, 1953-1955, 1991.

[Lai 1993] Y-C Lai, M. Ding and C. Grebogi. *Controlling Hamiltonian chaos*, Physical Review E 47, 1, 86-92, 1993.

[Lai 1994] Ying-Cheng Lai and Celso Grebogi. *Synchronization of spatiotemporal chaotic systems by feedback control*, Physics Review E 50, 3, 1894-1899, 1994.

[Lathrop 1989] Daniel P. Lathrop and Eric J. Kostelich. *Characterization of an experimental strange attractor by periodic orbits*, Physics Review A 40, 7, 4028-4031, 1989.

[Moss 1994] Frank Moss. *Chaos under control*, NATURE 370, 596-597, 1994.

[Ott 1990] E. Ott, Celso Grebogi and J. A. Yorke. *Controlling chaos*. Physical Review Letters 64, 11, 1196-1199, 1990.

[Ott 1994] E. Ott, T Sauer and J. A. Yorke, *Coping with Chaos*, John Wiley & Sons, Canada, 1994.

[Petrov 1993] Valery Petrov, Vilmos Gaspar, Jonathan Masere and Kenneth Showalter. *Controlling chaos in the Belousov-Zhabotinsky reaction*, NATURE 361, 240-243, 1993.

[Romeiras 1992] F. J. Romeiras, C. Grebogi, E. Ott and W. P. Dayawansa. *Controlling chaotic dynamical systems*, Physica D 58, 165-192, 1992.

[Roy 1992] R. R. Roy, T. W. Murphy, T. D. Maier, Z. Gills and E. R. Hunt. *Dynamical Control of a Chaotic Lazer: Experimental Stabilization of a Globally Coupled System*, Physical Review Letters 68, 9, 1259-1262, 1992.

[Roy 1994] Rajarshi Roy and K. Scott Thornburg, Jr. *Experimental Synchronization of Chaotic Lasers*, Physical Review Letters 72, 13, 2009-2012, 1994.

[Schiff 1994] S. J. Schiff, K. Jerger, D. H. Duong, T. Chang, M. L. Spano and W. L. Ditto, *Controlling chaos in the brain*, Nature, 370, 615-620, 1994.

[Schwartz 1994] I. B. Schwartz and I. Triandaf. *Controlling unstable states in reaction-diffusion systems modeled by time series*, Physical Review E 50, 4, 2548-2552, 1994.

[Shinbrot 1990] T. Shinbrot, C. E. Ott, Grebogi and J. A. Yorke. *Using Chaos to Direct Trajectories to Target*, Physical Review Letters 65, 26, 3215-3218, 1990.

[Shinbrot 1992b] T. Shinbrot, C. Grebogi, E. Ott and J. A. Yorke. *Using chaos to target stationary states of flows*, Physics Letters A 196, 349-354, 1992.

[Shinbrot 1992a] T. Shinbrot, W. Ditto, C. Grebogi, E. Ott, M. Spano, and J. A. Yorke. *Using the Sensitive Dependence of Chaos (the "Butterfly Effect") to Direct Trajectories in an Experimental Chaotic System*, Physical Review Letters 68, 19, 2863-2866, 1992.

[Shinbrot 1993] Troy Shinbrot, Celso Grebogi, Edward Ott and James A. Yorke. *Using small perturbations to control chaos*, NATURE 363, 411-417, 1993.

[Singer 1991] J. Singer, Y-Z. Wang and H. H. Bau. *Controlling a Chaotic System*, Physical Review Letters 66, 9, 1123-1125, 1991.

# CHAPTER VI

## CONTROL EXPERIMENTS

---

### 6.1 Introduction

In this chapter, results of the OGY control method [Ott 1990] on two chaotic systems described in chapter III are presented. The systems controlled were a Hénon [Hénon 1976] like iterated map and the Duffing oscillator [Parlitz 1985]. The first of these systems is a discrete and the other a continuous time system.

The aims of these experiments were to put the OGY theory into practice, to examine how well the method works with noise and inaccurate measurements of parameters required for the control, the sensitivity to use of alternative control parameters and the performance of higher periodic control.

The high period control strategy introduced in section 5.7 was also tested along with the Lai *et al.* method [Lai 1993] by using the iterated map. Unstable orbits of periods up to fifty were located and used as the control points.

### 6.2 Control experiment : A variation of the Hénon Map

The Hénon-like function is defined as

$$\begin{aligned} X_{n+1} &= a + bY_n - X_n^2 \\ Y_{n+1} &= X_n \end{aligned} \tag{VI.1}$$

This map is identical to the Hénon map equations in (III.4) page 39, except for the position of the control parameter  $a$ . The dynamics are also very similar to the Hénon map, but the attractor is not stretched horizontally (as the return map was created by using only the values of the  $X$ -coordinate). This iterated map was chosen as it has been controlled by the OGY method [Ott 1990] and we wished to replicate their result.

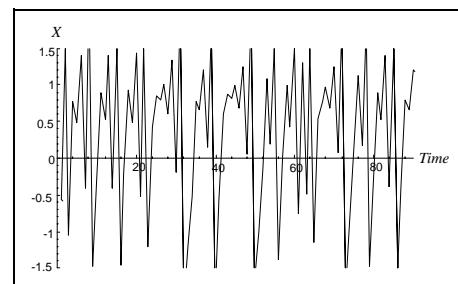


**Figure 6.1** Uncontrolled time series

The map was iterated 10,000 times to obtain a time series, with  $a = 1.4$ ,  $b = 0.3$ ,  $X_0 = 1.4$  and  $Y_0 = 0$ . As this is a discrete time system, we did not need to choose delay and jump times. A part of the time series of the  $X$ -coordinate is illustrated in Figure 6.1.

From the time series, a return map of  $X_n$  versus  $X_{n-1}$  was plotted. A fixed point  $\xi_F$  at (0.883, 0.883) was then located by noting points on the diagonal line in the return map are saddle points. This is illustrated in Figure 6.2. The fixed point was then chosen as the control point.

The local dynamics of the control point as described by the Jacobian matrix can then be directly calculated from the known dynamics. Using (VI.1) and the definition of the Jacobian matrix, the matrix can be written as

$$J = \begin{bmatrix} -2X_F & b \\ 1 & 0 \end{bmatrix} = \begin{bmatrix} -1.766 & 0.300 \\ 1.000 & 0.000 \end{bmatrix} \quad (\text{VI.2})$$

This matrix has eigenvalues of -1.923 and 0.156 and the corresponding eigenvectors are [-0.887, 0.461] and [-0.154, -0.988].

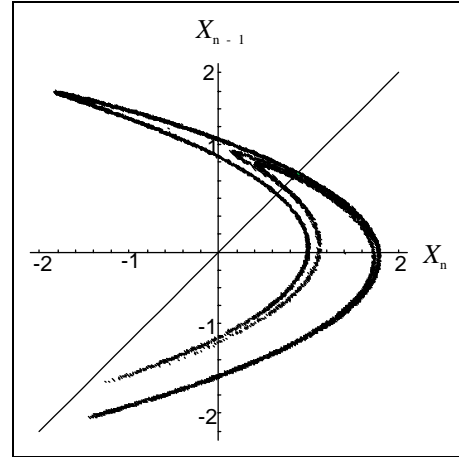


**Figure 6.2** The return map plot with the diagonal line.

Knowing an exact form for the Jacobian matrix we can then examine the efficiency of the least squares fit method, using the time series data. A total of 712 point pairs nearby the control point were collected and used to estimate the matrix. The point pairs were grouped into stable and unstable pairs by noting that a pair with the first data point closer to the control point than the second one must be an unstable pair, otherwise the pair is a stable pair. The number of stable pairs found was 562 and the unstable pairs was 150. The matrix obtained was

$$\begin{bmatrix} -1.633 & 0.277 \\ 1.000 & 0.000 \end{bmatrix} \quad (\text{VI.3})$$

As can be seen, this matrix is a good approximation to the true Jacobian. The unstable/stable manifolds and the associated divergence/convergence rates were calculated from the matrix. They were found to be  $e_u = [-0.873, 0.488]$ ,  $e_s = [-0.153, -0.988]$ ,  $\lambda_u = -1.788$  and  $\lambda_s = 0.155$ .

The sensitivity vector  $u$  was estimated by starting the system sufficiently close to the fixed point and then the control parameter,  $p$ , was changed from  $p_0$  to the maximum allowed value  $p_{MAX}$ , where  $p_0 = 1.4$  and  $p_{MAX} = 1.428$ . The vector was estimated to be the difference between the starting and the next data points

as in (V.11) page 82. Using this method we estimated  $u$  to be [1.011, 0.009]. Using the relation between  $u$  and  $g$  as in (V.19) page 88, we have estimated  $g$  to be [0.411, 0.420]. We recommend the use of the vector  $u$  instead of  $g$  as it is much easier to estimate from the experimental time series.

The OGY control law in (V.10) page 82, was then used to control the system whenever  $p_{\text{MIN}} \leq p_1 \leq p_{\text{MAX}}$ , otherwise  $p_1$  was set to be  $p_0$ .

We decided to perform two sets of experiments. The first set was to replicate the results achieved by OGY [Ott 1990]. The second set was to attempt to control the system with a higher periodic behaviour and switch between different control points.

The aims of the first set of experiments were as follows.

- To stabilise an unstable orbit of period one of a two-dimensional chaotic iterative map using the return map.
- To control the system with added noise.
- To study the effect of using different parameter as the control parameter. In the Hénon map like equations there are two possible parameters,  $a$  and  $b$ . The aim was to control the system by using either  $a$  or  $b$ .

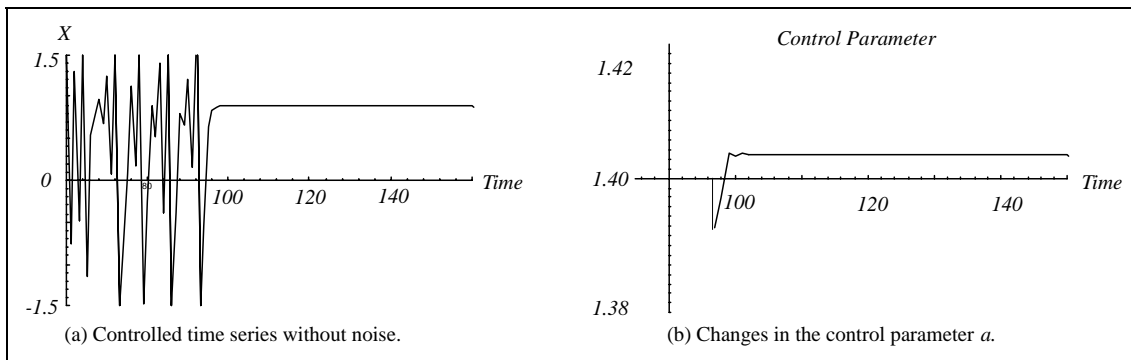


**Figure 6.3** Control of the map using  $a$  as the control parameter (without noise).

First, the chaotic map was controlled without noise. This was performed to study the efficiency of the OGY method using the approximation matrix and to examine any differences which may exist in using alternative parameters for control. We have first chosen to use  $a$  as the control parameter with  $p_{\text{MAX}} = 1.428$ ,  $p_{\text{MIN}} = 1.372$  and  $p_0 = 1.4$ . In Figure 6.3 (a), the time series controlled using  $a$  is illustrated. The changes in  $a$  after the control began are illustrated in Figure 6.3 (b).

In the second experiment, illustrated in Figure 6.4, noise of up to  $|0.013|$  was added to both training and control data. The system was stabilised without any problem, although it took longer for the data point

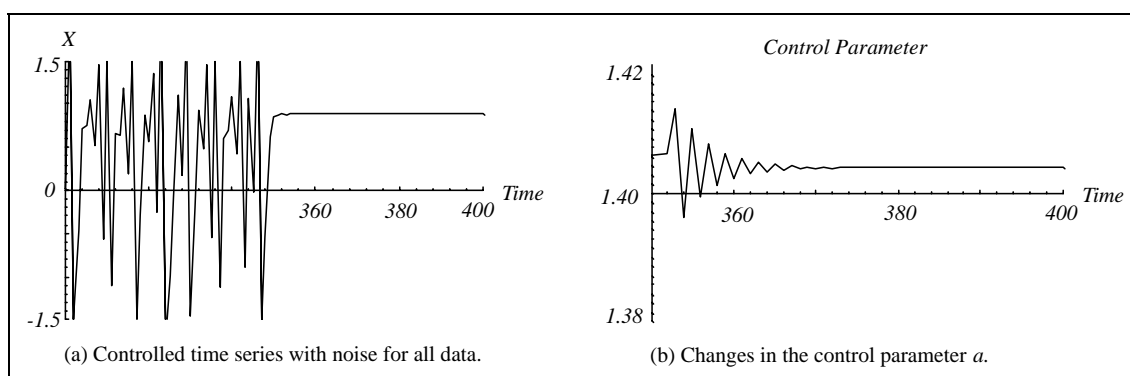


**Figure 6.4** Control of the map using  $a$  as the control parameter (with noise for whole data).

to fall into the region where the control could be achieved. This is not surprising as the dynamics of the learned and controlled systems are the same.

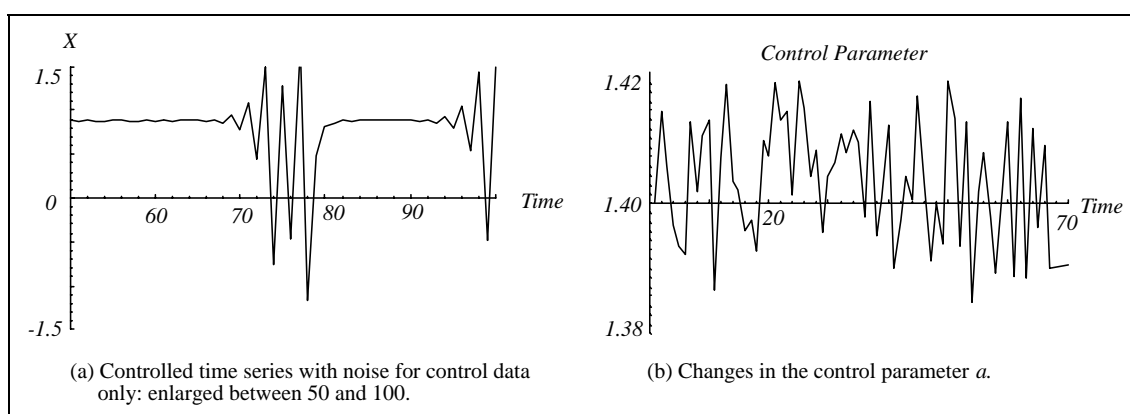


**Figure 6.5** Control of the map using  $a$  as the control parameter (with noise for control data only).

In the third experiment, illustrated in Figure 6.5, the same amount of noise was added to the control data only. Figure 6.5 (a) illustrates in close detail that part of the time series where control was achieved and then lost. The initial conditions were chosen to be the fixed point at  $(0.883, 0.833)$ . The system was initially stabilised but control was lost after some iterations. This was expected as due to the added noise, the learned system was slightly different from the system to be controlled. Many adjustments to the control parameter were required in order to keep the system in the desired region.

Next  $b$  was used as the control parameter, with  $p_{\text{MAX}} = 0.306$ ,  $p_{\text{MIN}} = 0.294$  and  $p_0 = 0.3$ . A new sensitivity vector  $u$  was estimated with respect to small changes in  $b$ .

In Figure 6.5 (a), the time series controlled using  $b$  is illustrated. The changes in  $b$  after the control began are illustrated in (b). It is interesting to note that quicker stabilisation was achieved using  $a$  as the control parameter. Stabilisation was achieved at around  $t = 100$ . Using  $b$  it was not until  $t = 1040$ . Also fewer

parameter adjustments were required when using  $a$ . The initial condition used for all experiments except the third one was  $(1.4, 0)$ .

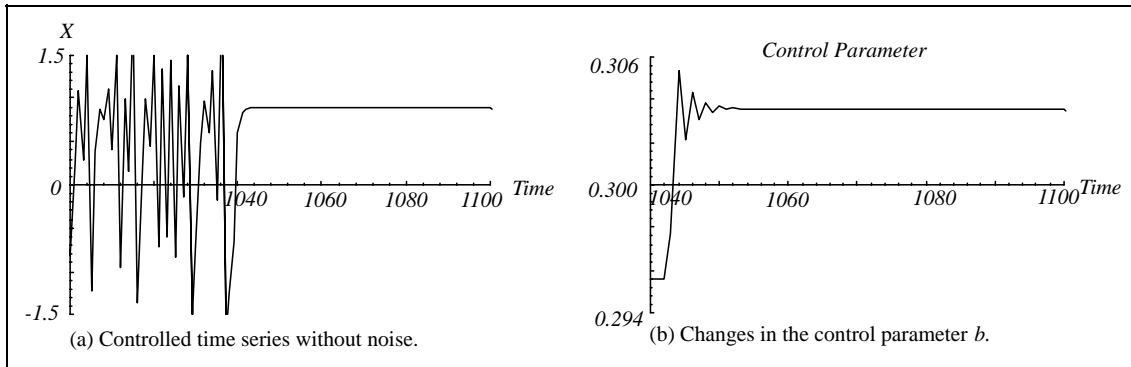


**Figure 6.6** Control of the map using  $b$  as the control parameter (without noise).

In the second set of experiments, the aim was to control unstable orbits of periods more than one. Therefore a number of new unstable periodic points were located from the time series. Using the data set and the techniques described in section 4.7.1, we were able to extract 111 unstable periodic points but only 36 of them were found to be useful. i.e. a reasonable Jacobian matrix could be estimated with stable and unstable manifolds. However, we were successful in controlling the map with only one of the unstable periodic point of period two. The next lowest period which could be located was four. This control point was found to be too difficult for the OGY method.

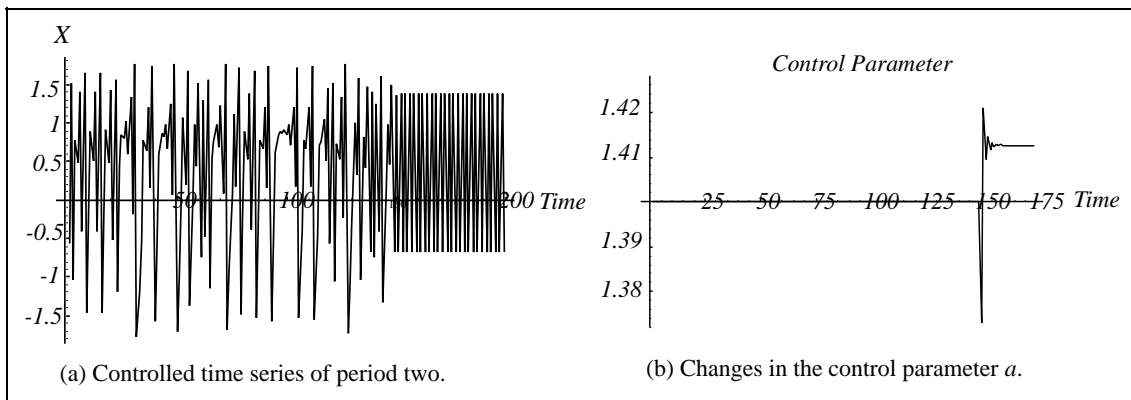


**Figure 6.7** Control of the map for period two and one orbits using  $a$  as the control parameter.

The period two control point was located at  $(-0.662, 1.363)$  and the matrix was approximated by collecting the local pair points which were separated in time by two, as described in section 4.7.2. The number of stable pairs was 290 and there were 198 unstable pairs. The parameters estimated from the matrix were  $\lambda_u = -3.179$ ,  $\lambda_s = -0.043$ ,  $e_u = [-0.931, 0.364]$  and  $e_s = [0.268, -0.963]$ . The sensitivity vector  $u$  was estimated as  $[-2.346, 1.291]$ . The control parameter used was  $a$  as before with  $p_{MAX} = 1.428$ ,  $p_{MIN} = 1.372$  and  $p_0 = 1.4$ . The starting condition was  $(1.4, 0)$ .

The control method was same as before except that the perturbations were applied to the system every two iterations rather than one. The results of two period control are illustrated in Figure 6.7. The Dressler and Nitsche control [Dressler 1992], described in section 5.5, using the two sensitivity vectors  $v$  and  $u$  was used to attempt to control unstable orbits of periods higher than two, but similarly was unsuccessful in effecting control. Again the highest period controlled was two.

Next we attempted to switch between the two control points using the same control parameter. The first control point chosen was the period two point, with the starting condition the same as before.

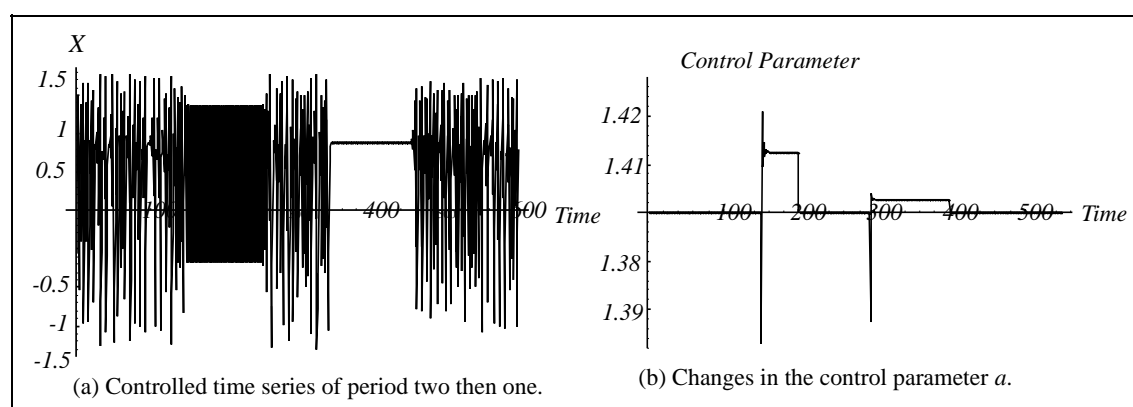


**Figure 6.8** Controlled time series of periods two and one.

Control was achieved at  $t \approx 150$  as before. The control point was then switched to the period one point, i.e. the control point of the first sets of experiments, at  $t = 250$ . The new control was achieved at  $t \approx 345$ , roughly 135 iterations after initiation. Control was released again at  $t = 450$ , and the map behaved chaotically in absence of the control. The results are illustrated in Figure 6.8. The same range of control parameter  $a$  was used to switch between the control points.

Through the experiments, we have seen that the OGY and the Dressler and Nitsche methods could only control unstable orbits of periods up to two. We next tested the high period control strategy presented in section 5.8 to control unstable orbits of periods up to 50.

Before controlling the system, it was necessary to locate unstable periodic orbits of the system. The techniques used were as discussed in section 4.7.1 with the maximum period set to 50. We extracted 237 unstable periodic orbits, excluding cyclic permutations and repetitions of lower orbits, from a time series of the iterated map of length 5,000 with  $r_1 = 0.025$  and  $r_2 = 0.05$ . The number and accuracy of the orbits can be increased by using more data points with smaller  $r_1$  and  $r_2$ . We opted to use only 5,000 data points with relatively large  $r_1$  and  $r_2$  so as to simulate a situation where a rapid achievement of control is required.

Chapter 6 - Experimental results

[Auerbach 1987] reports using 100,000 data points with  $r_1$  of  $10^{-5}$  and  $r_2$  of  $10^{-4}$ , 278 unstable orbits of periods up to ten were located in the map. We have extracted 20 such orbits from the much shorter data set (only 5% in length) with much larger  $r_1$  and  $r_2$ . Both data sets were obtained using  $a = 1.4$  and  $b = 0.3$ . The comparison is presented in Table 6.1.

Period	Number of orbits extracted [Auerbach 1987] 100,000 data points	Number of orbits extracted (Our result) 5,000 data points
1	1	1
2	3	1
3	1	0
4	7	1
5	1	0
6	15	1
7	29	4
8	63	4
9	55	2
10	103	6
Total	278	20

**Table 6.1** Number of unstable periodic orbits of orders up to 10 which were extracted.

For each unstable orbit of period  $k$ , we have estimated a set of  $k$  transformation matrices  $A$  as described in section 5.8. Here 2,500 data points were used to estimate the matrices by the least squares fit method with the maximum distance of 0.25 to collect pairs of data points which fall close to the two successive control points. The sensitivity vectors  $s$  were estimated, using the least squares fit method, as in (V.36) page 93 using a sufficient number of varying  $p$  for  $p_{\text{MAX}} < p < p_{\text{MIN}}$ , where  $p_{\text{MAX}} = 1.428$  and  $p_{\text{MIN}} = 1.372$ .

Sometimes we were unable to estimate the transformation matrices which have both real unstable and stable vectors. These occur due to inaccuracies in the unstable periodic orbits estimated, insufficient amounts of data, or an unsuitable distance used to estimate the matrices. In such cases, we do not attempt control for those intervals. This strategy works well if the control is applied to the orbit again before it diverges.

The high periodic control strategy was applied to each of 237 orbits. Using eigenvectors 205 of the orbits were successfully controlled, using principal axes approach 155 were successfully controlled. The first result represents over 86% of the orbits extracted. Some of the orbits were not controlled due to inaccuracy of the set of control points extracted. The accuracy can be increased by using more data points with smaller  $r_1$  and  $r_2$  (refer to section 4.7.1).

The five tables below summarise the number of unstable periodic orbits extracted grouped by the periodicity and the number of orbits controlled successfully by using principal axes and eigenvectors for the estimations of the stable and unstable directions. Whenever the number of controlled orbits differ from the number of orbits extracted, they are highlighted.

Period	Number of orbits extracted	Number successfully controlled	Number successfully controlled
		Principal axes	Eigenvectors
1	1	1	1
2	1	1	1
3	0	0	0
4	1	1	1
5	0	0	0
6	1	1	1
7	4	4	4
8	4	3	4
9	2	1	1
10	6	5	5
Sub-total	20	17	18

**Table 6.2** Control of unstable orbits of periods between 1 and 10.

Chapter 6 - Experimental results

Period	Number of orbits extracted	Number successfully controlled	Number successfully controlled
		Principal axes	Eigenvectors
11	7	7	7
12	6	<b>4</b>	<b>4</b>
13	7	<b>2</b>	7
14	3	<b>2</b>	<b>1</b>
15	6	<b>4</b>	6
16	6	<b>5</b>	6
17	4	4	4
18	5	<b>4</b>	5
19	7	<b>5</b>	<b>6</b>
20	7	<b>5</b>	<b>6</b>
Sub-total	58	42	52

**Table 6.3** Control of unstable orbits of periods between 11 and 20.

Period	Number of orbits extracted	Number successfully controlled	Number successfully controlled
		Principal axes	Eigenvectors
21	5	5	5
22	1	1	1
23	7	<b>4</b>	7
24	3	<b>2</b>	3
25	6	<b>4</b>	6
26	7	<b>6</b>	7
27	9	<b>8</b>	9
28	5	<b>4</b>	<b>4</b>
29	7	<b>3</b>	<b>4</b>
30	6	<b>4</b>	6
Sub-total	56	41	52

**Table 6.4** Control of unstable orbits of periods between 21 and 30.

Period	Number of orbits extracted	Number successfully controlled	Number successfully controlled
		Principal axes	Eigenvectors
31	6	4	6
32	6	3	6
33	5	3	4
34	5	3	3
35	3	2	2
36	1	0	1
37	5	4	4
38	4	2	3
39	3	2	2
40	6	1	4
Sub-total	44	24	35

**Table 6.5** Control of unstable orbits of periods between 31 and 40.

Period	Number of orbits extracted	Number successfully controlled	Number successfully controlled
		Principal axes	Eigenvectors
41	5	2	5
42	9	7	9
43	4	4	4
44	4	1	4
45	8	3	5
46	6	4	5
47	5	4	5
48	5	1	2
49	5	2	5
50	8	3	4
Sub-total	59	31	48

**Table 6.6** Control of unstable orbits of periods between 41 and 50.

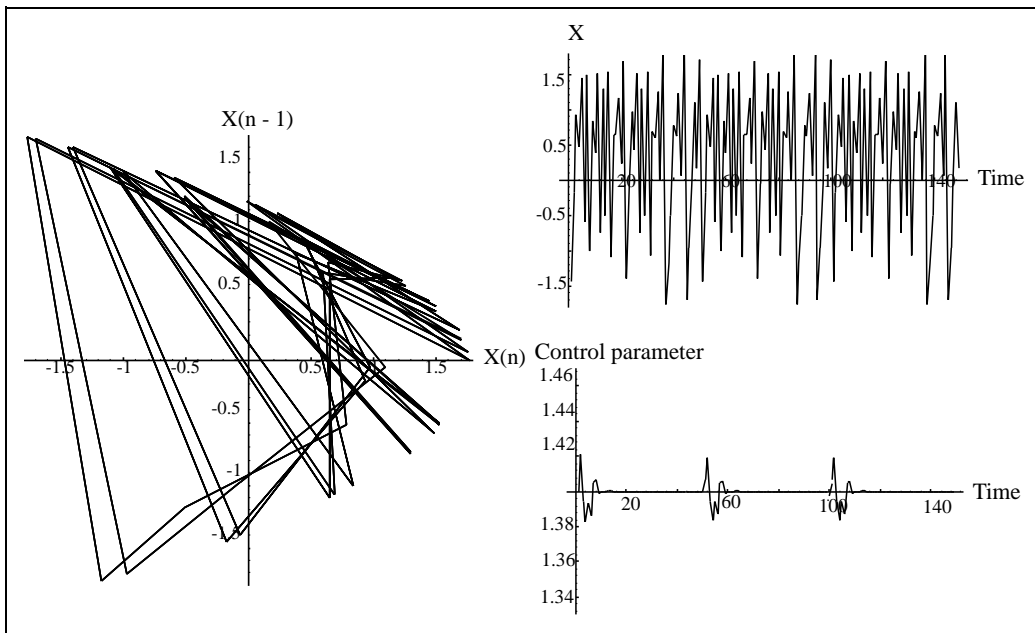


**Figure 6.9** Control of unstable orbit of period 50, orbit 1.

Two of the highest periodic orbits controlled successfully are illustrated in Figure 6.9 and Figure 6.10. The diagrams include the return maps, time series and the changes in the control parameter. Both orbits belong to the class of unstable orbits of period 50 but their behaviour is quite different.

We have observed that a periodic behaviour of period  $k$  emerges in the changes of control parameter whenever successful control of an unstable orbit of period  $k$  is achieved. This fact may hold a significant importance and further experiments were conducted and are discussed in section 6.4.

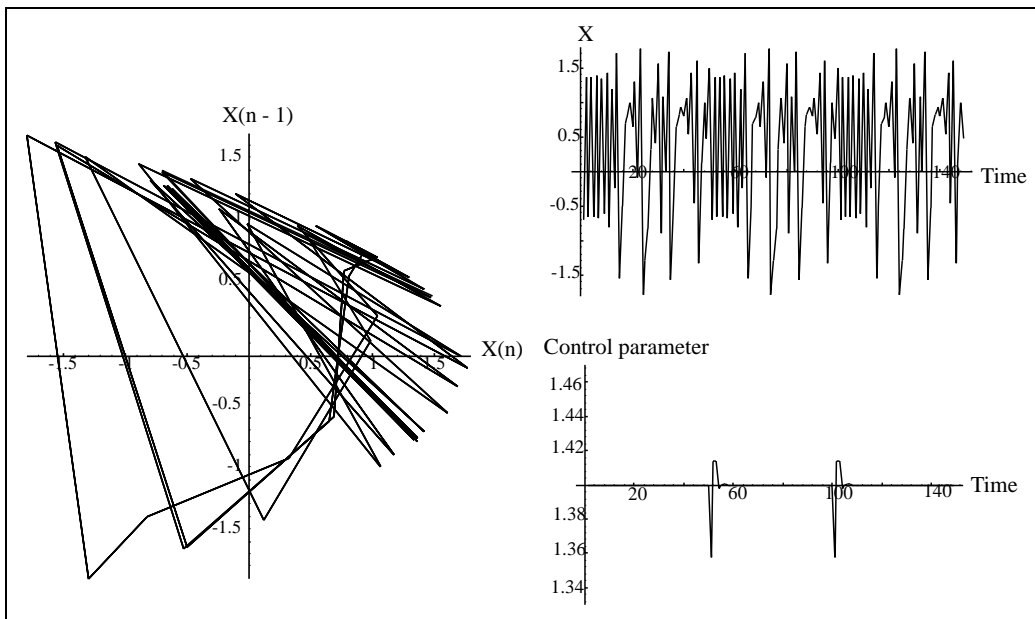


**Figure 6.10** Control of unstable orbit of period 50, orbit 2.

### 6.3 Control experiment : The Duffing's oscillator model

In this experiment, the OGY method was used to control the Duffing oscillator, described in section 3.3.4. As mentioned in the section, the model has a forcing frequency of  $2\pi/\omega$ . This was used to determine the delay and jump times. An embedding dimension  $d_E = 2$  was chosen to create a two-dimensional stroboscopic return map using the  $x$ -coordinate. The return map is illustrated in Figure 6.11. The parameters used were  $d = 0.2$ ,  $\omega = 0.665$  and  $f = 36$ . Plots of the time series of the  $x$ -coordinate sampled at  $2\pi/\omega$  (roughly 9.45 seconds) and 0.1 second are illustrated in Figure 6.13 and Figure 6.12, respectively.

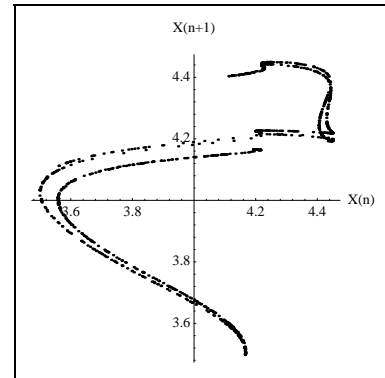


**Figure 6.11** Return map of the oscillator model.

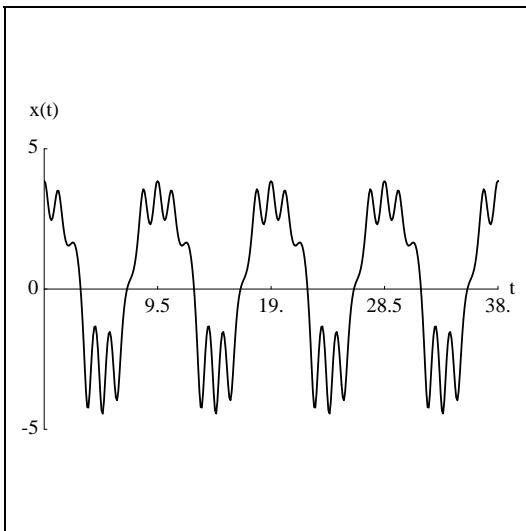


**Figure 6.12** The time series sampled at 0.1 second.

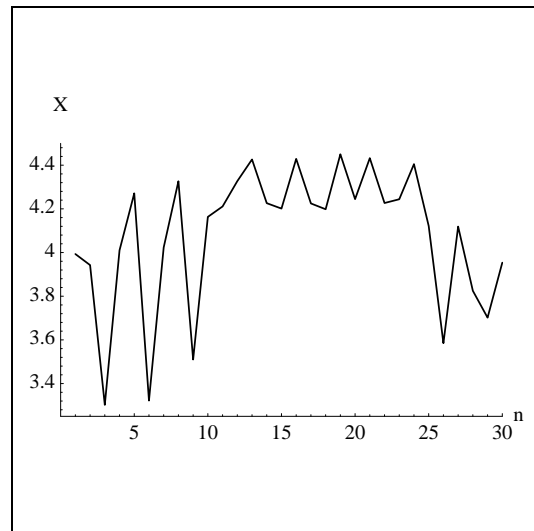


**Figure 6.13** The time series sampled at  $2\pi/\omega$ .

The sensitivity vector  $u$  was estimated to be  $(0.281, 0.002)$  using (V.11) on page 82. The control point was chosen by finding a point  $(3.785, 3.785)$  on the line of identity which is an unstable periodic point of period one, as in the previous section. Using  $f$  as  $p$  with  $p_{MAX} = 34.2$ ,  $p_{MIN} = 37.8$  and  $p_0 = 36.0$ , i.e. the allowed perturbation of  $\pm 5\%$  of the nominal value of 36.0, the model was controlled successfully by the OGY control law in (V.10) page 82. The initial conditions used were  $x_0 = 4.2$ ,  $y_0 = 1.2$  and  $z_0 = \omega/2\pi$ .

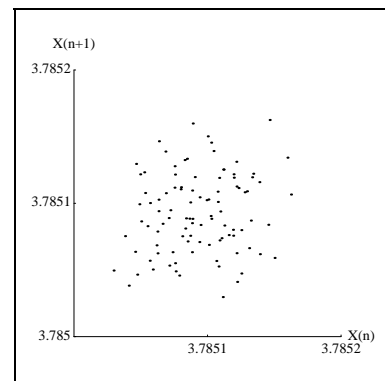


**Figure 6.14** The controlled map.

Iterates of the map near the control point when the control was achieved are shown in Figure 6.14. In the diagram, the points seem to be sparse, but they are actually very close to each other as the global range of the section is roughly between 3.45 and 4.55.

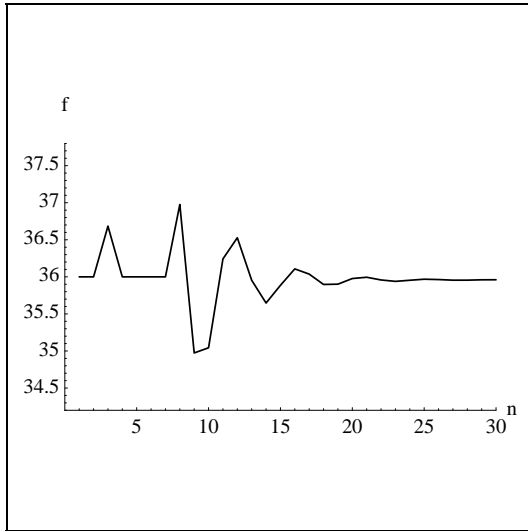


**Figure 6.15** Changes in the control parameter.

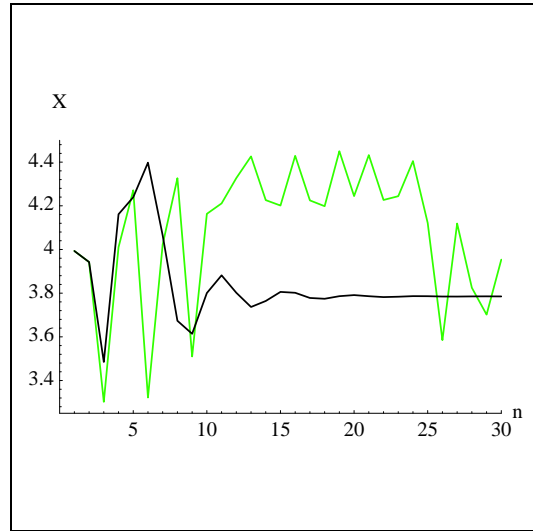


**Figure 6.16** Difference between the controlled and uncontrolled time series sampled at  $2\pi/\omega$ .

The control of the model was achieved within 20 iterations (roughly 190 seconds) of the return map. The changes in  $p$  are in Figure 6.15. The controlled time series (in black) sampled at  $2\pi/\omega$  intervals is superimposed on the uncontrolled one (in grey) in Figure 6.16.

Let us finally look at the controlled time series sampled at 0.1 second. In Figure 6.17, the same oscillation is repeated every  $2\pi/\omega$ . The trend continued until control was stopped. Each oscillation is equivalent to an iterate of the return map.

Although the graphical results are not presented, the model was successfully controlled by using  $d$  with the allowed perturbation of  $\pm 5\%$  of the nominal value of 0.2. However, the number of iterations required before the realisation of control was around 85.

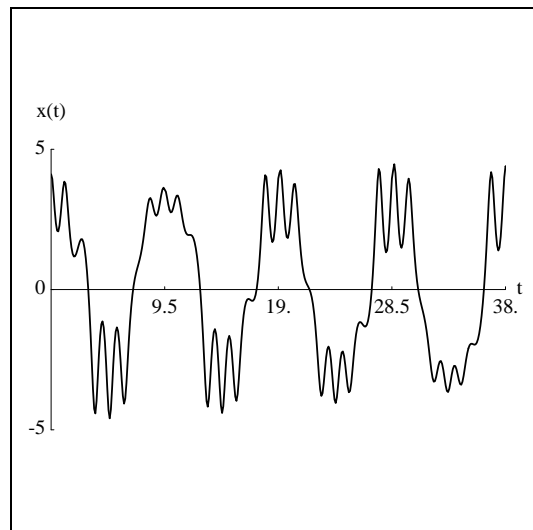


**Figure 6.17** The controlled time series sampled at 0.1 second.

Using  $\omega$  as the control parameter with the allowed perturbation of  $\pm 5\%$  of the nominal value of 0.665,

the model was stabilised at a different point, (0.728, 0.728), in the return map which was *not* visited by the original model. This is because the model is extremely sensitive to small changes in  $\omega$ . As such we could not achieve the desired behaviour by using  $\omega$ . Initial conditions used were the same for all experiments.

The fact that this chaotic oscillator could not be controlled using small variations in the forcing frequency is disappointing in the context of the analogy with neural systems. However, at this stage the analogy is very crude and we note that many other chaotic oscillator *have* been controlled using small variations in the forcing frequency.

#### **6.4 Investigation : Periodic forcing to gain control**

In controlling an unstable orbit of period  $k$ , we have noticed that changes required in the control parameter is also periodic with period  $k$ . When a point in the surface of section comes close to one of the control point the control signal applied to the system forces the next point to be close to the next control point. To control an unstable orbit of period  $k$  requires  $k$  changes in the control signal before the point comes back to near the first control point. This set of changes in the control signal seems to repeat itself, i.e. the subsequent sequence of control signals is very similar. This was an interesting phenomenon from at least two stand points. The Hénon-like iterative map was used again for this set of experiments.

The first question was *'What would happen if we pick and apply a set of  $k$  random values within the permitted range of the changes in the control parameter, in an attempt to produce an orbit of period  $k$ ?'* We generated a number of such sets of various  $k$ ,  $2 \leq k \leq 50$ , then proceeded to apply a set of values to the system. The result was that we could not produce a periodic behaviour for any of the sets generated.

The second question was *'Can we gain control of an unstable orbit of period  $k$  by applying the changes required in the control parameter previously calculated by the high periodic control strategy?'* Surprisingly we could not gain control. Our initial speculation was that if the changes in the control parameter is in a right phase, we might be able to gain control.

In a set of experiments we have taken a number of successfully controlled period  $k$  control signals previously estimated by the high period control strategy. For each set of control signals we have iterated the map for 10,000 iterations before we changed phase. Here, the phase is referred to as a shift in timing of applying each control signal by one. Suppose for a control signal set of period  $k$ ,  $p_1, p_2, \dots, p_k$ , application of signals  $p_1, p_2, \dots, p_k$  to the system is different in phase by one to application of signals  $p_k, p_1, \dots, p_{k-1}$ . The process was repeated for all possible phasing. We could not gain control using any of

the control signal sets.

Our assumption was that the periodic changes in the control signals were same during the whole duration of the control. However, close examinations revealed that the *initial* set of changes in the control parameter were not the same (though similar) as the set of changes later. Once the orbit is completely controlled, the changes in the control signal became same, but until complete control was gained the changes were slightly different from the subsequent sets. It seems that the combination of initial set of control perturbations and subsequent periodic perturbations play a key role in controlling the system. Therefore it may not be possible to control a chaotic system with a simple periodic forcing in one of the accessible control parameters.

## 6.5 Conclusion

In this chapter we have demonstrated the OGY based control method by using two chaotic systems. The first model used for control was a variation of the Hénon map and the second model was the Duffing oscillator.

The first model was easier to control than the second as it is a discrete time system. As such, we did not need to estimate the delay or the jump time usually required by the delay coordinates method. We have also successfully controlled a period one control point using the original control law (V.15) proposed in [Ott 1990] by estimating the  $g$  vector. The result obtained was same as the result presented.

The second model could have been controlled by using all of the three dynamic variable  $x$ ,  $y$  and  $z$  (refer to section 3.3.4 for detail) but we have chosen to use only the  $x$ -coordinate values sampled at every  $2\pi/\omega$  to implement the delay coordinates method. As the model has the periodic oscillation in units of  $2\pi/\omega$ , the delay and the jump times were chosen as  $2\pi/\omega$ . The embedding dimension of 2 was used to construct the return map.

We have tested the method by finding an approximation to the Jacobian matrices using the least squares fit method as described in section 4.7.

The aims of the experiments were as follows.

- To put the OGY theory into practice.
- To examine how well the method works with noise and inaccurate measurements of parameters required for the control.

- To study the effect of using different parameter as the control parameter.
- To study the performance of control in high unstable periodic orbits.

The OGY method works well with chaotic systems with an accessible control parameter which can be modelled by a set of two dimensional vectors. For systems which require higher dimensional vectors, the presented theory does not perform well due to the increased number of the manifolds. The method controlled the two models by using different control parameters. However, it seems that some control parameters are more suited for the control since the time delay before the realisation of control were quite different for exactly the same initial conditions.

Perhaps the major drawback of the OGY method is the inability to control orbits with high periods. This is because the nature of chaotic systems is such that, left alone, two nearby trajectories diverge with time. Since for control points of period  $k$  the method does not apply a control for  $k$  iterations of the surface of section, the butterfly effect becomes more apparent as  $k$  increases. As a result we were unable to control the first model for periods higher than two by either the OGY or the Dressler and Nitsche control methods.

However, the high period control strategy developed in section 5.7 was successful in controlling unstable orbits of periods up to fifty for the first model (the iterative map). Out of 237 such orbits located, 205 of them were controlled using the eigenvectors of the transformation matrices. The use of principal axes instead of the eigenvectors was also examined but its performance was significantly poorer. This indicates that the principal axes method may be more sensitive to the accuracy of the orbits extracted and of the transformation matrices describing the orbits behaviours, alternatively they do not represent the stable and unstable directions as accurately.

The price we pay for the high period control method is that the number of parameters required increases with the period of the orbit. We feel this is a small price to pay, as the ability to achieve a variety of behaviours from the model, within a small range of the control parameter, far exceeds the initial computation required. In our experiments the maximum period was chosen to be fifty but there is no theoretical reason not to choose a higher period. Control of unstable orbits of periods of several thousand should be possible provided that such high unstable periodic orbits exist and can be extracted accurately.

## **Chapter references**

*Chapter 6 - Experimental results*

[Auerbach 1987] Ditza Auerbach, Predrag Cvitanovic, Jean-Pierre Eckmann, Gemunu Gunaratne and Itamar Procaccia. *Exploring Chaotic Motion Through Periodic Orbits*, Physical Review Letters 58, 23, 2387-2389, 1987.

[Dressler 1992] U. Dressler and G. Nitsche. *Controlling chaos using time delay coordinates*. Physics Review letters 68, 1, 1-4, 1992.

[Hénon 1976] M. Hénon. *A Two-dimensional Mapping with a Strange Attractor*, Communications in Mathematical Physics 50, 69-77, 1976.

[Ott 1990] E. Ott, Celso Grebogi and J. A. Yorke. *Controlling chaos*. Physical Review Letters 64, 11, 1196-1199, 1990.

[Parlitz 1985] U. Parlitz and W. Lauterborn. *Superstructure in the bifurcation set of the Duffing equation*, Physics Letters A 107, 8, 351-355, 1985.



## CHAPTER VII

### FUTURE RESEARCH

---

#### 7.1 Introduction

It has been proposed by W. J. Freeman [Freeman 1991] that some functional units of biological brains in mammals are usually in a chaotic mode at rest. He suggests that when a memory is recalled, the activity within the brain orbits a memory-characteristic attractor. More specifically he has observed that in the olfactory bulb of rabbits, an act of perception-recognition consists of an explosive leap from a chaotic to a stable attractor. He postulates that the olfactory bulb and cortex maintain many stable attractors, one for each distinguishable scent. When a new scent is presented an explosive leap still occurs but the state settles down to a new attractor. He also reports that recognition of visual images may derive from a similar mechanism. As a result he has concluded that the control of chaotic states in the brain could be a significant property that makes the brain different from other, more conventional, artificial intelligence paradigms.

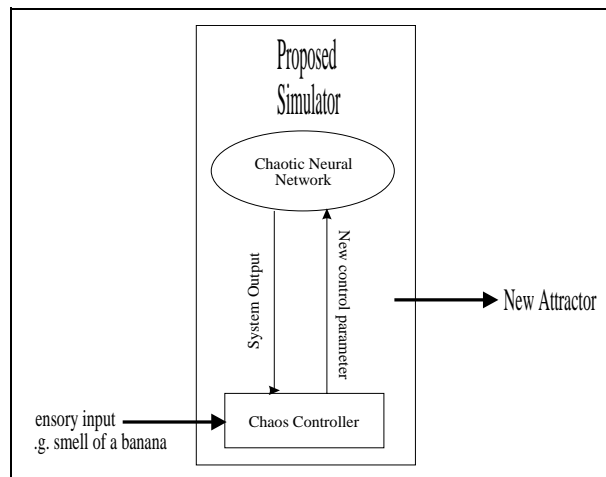


**Figure 7.1** Proposed computer simulator model.

This is an interesting observation, particularly because it raises the questions of the precise mechanism which enables the brain to switch from one unstable mode to another. In [Freeman 1991], Freeman does not propose a mechanism, he merely observes that the brain exhibits such behaviour.

#### 7.2 Alternatives to OGY

Since the original OGY method was developed there have been a number of different alternative methods proposed. It is by no means clear which of these methods might be best suited to applications in neural networks. The general problem of controlling high dimensional systems about unstable high period behaviours will certainly require much further research. However, we have one proposal which we plan

to explore.

*The Otani-Jones control law.*

One of the principal disadvantages of the OGY control law is the requirement to estimate the Jacobian  $J$ . Such estimates can be both time consuming and inaccurate. Inaccuracies in estimating  $J$  are reflected in several facets of the control computation. First the  $d \times d$  Jacobian  $J$  is used to estimate  $\delta\xi_{i+1}$ , i.e. the state of the system at the next iteration if no variation of the control parameter(s) are effected. Second, the estimate of the Jacobian is used to derive the unstable manifold vector  $f_u$  and the associated eigenvector  $\lambda_u$  as both these quantities are required in computing  $\delta p = p - p_0$ . Finally, the effect of iteration without control  $\delta\xi_{i+1} = J\delta\xi_i$  has to be subtracted from the effect *with* control in order to estimate the sensitivity vector(s). Thus the cumulative consequences of errors in  $J$  can have a significant impact on the effectiveness of the OGY control law.

The Otani-Jones control law attempts to overcome some of these shortcomings. In many situations it is possible to create an effective *short term* (fast) predicting function  $\xi_{i+1} = P(\xi_i)$  for the system which is accurate over the whole (or a large part) of the phase space. For example, if we were seeking to control an iterated feedforward neural network there would be very little point in attempting to approximate the Jacobian about a particular fixed point, since the neural network can be iterated without control to give an *exact* prediction of the next system state very rapidly (the network *is its own Jacobian* at every point of state space). For other smooth dynamic systems it has been shown, see for example [Dracopoulos 1993] that a feedforward neural network trained on a single trajectory of the system can form an accurate short term predictor capable of generalising to other trajectories of the system.

In situations where such a short term predictor function  $P$  is available the Otani-Jones method can be employed to effect control and it does not require the computation of either  $f_u$  or  $\lambda_u$ , although it is still necessary to estimate the sensitivity vectors.

The method proceeds as follows. We assume an accurate short term predictor function  $\xi_{i+1} = P(\xi_i)$  is available. Suppose that control parameter(s)  $\mathbf{p} = (p_1, \dots, p_l)$  are available, with nominal value  $\mathbf{p}_0$  and that it is required to control the system about a fixed point  $\xi_F$ . We can describe the situation by the equation

$$\delta\xi_{i+1}(p) = P(\xi_i(p_0)) - \xi_F + \delta p_1 s_1 + \dots + \delta p_l s_l \quad (\text{VII.1})$$

where  $s_1, \dots, s_l$  are the sensitivity vectors with respect to each control parameter.

## Chapter 7 - Future research

We first estimate  $s_1, \dots, s_l$  by collecting statistics from observations of the system state near  $\xi_F$  under small parameter variations. Since  $P$  is known, if sufficient observations are available,  $s_1, \dots, s_l$  can be estimated from (VII.1) using a least squares fit method, or equivalently a fast pseudo-inverse algorithm. We assume that the choice of control parameters is such that  $s_1, \dots, s_l$  are linearly independent, since there would seem to be no advantage in having a linearly dependent set of sensitivity vectors.

Once  $s_1, \dots, s_l$  are known, for any point  $\xi_i$  near  $\xi_F$  the control law then chooses  $\mathbf{p} = (p_1, \dots, p_l)$  so as to minimise the squared Euclidean distance

$$|\xi_{i+1}(p) - \xi_F(p_0)|^2 \quad (\text{VII.2})$$

i.e. we choose  $\mathbf{p}$  so as to minimise

$$|P(\xi_i(p_0)) - \xi_F(p_0) + \delta p_1 s_1 + \dots + \delta p_l s_l|^2 \quad (\text{VII.3})$$

Let  $S$  be the matrix whose column vectors are  $s_1, \dots, s_l$  the the solution to this minimisation problem is given by

$$\delta p = -S^{-1} \left( P(\xi_i(p_0)) - \xi_F(p_0) \right) \quad (\text{VII.4})$$

where  $S^{-1}$  is the inverse matrix of  $S$  if  $l = d$  and the pseudo-inverse otherwise.

The underlying philosophy of the OGY method is rather subtle, the idea is to attempt to nudge the next system iteration back onto the stable manifold. In contrast the Otani-Jones method is brutally direct; it seeks only to minimise the distance of the next iteration from the target unstable fixed point, and therefore we can expect to have to apply the control perturbation at every step.

How practical is the pseudo-inverse calculation in real time at every step? The systems being controlled are likely to have two dimensional embeddings and so computing the pseudo-inverse in customised hardware or on a fast PC is quite feasible, provided the time interval is not exceedingly small. For high dimensional embeddings completing the computation within the available time frame becomes more conjectural. However, for high dimensional embeddings the OGY method is also very likely to fail since there may well be many unstable directions.

Thus in low dimensional embedding space (e.g.  $d = 2$  or  $3$ ) we might expect the OGY method to be more robust than the method proposed here, but in higher dimensional embedding space (e.g.  $d = 6$  or  $7$ ) there

is a possibility that for systems where it is applicable the Otani-Jones method may be more effective.

## 7.2 Future research

Freeman's notion is a plausible one both intuitively and biologically. We hope to pursue the idea one step further by implementing a computer simulation model. The immediate future plan is to make use of a chaotic artificial neural network and to control its behaviour by a strategy based on the OGY method [Ott 1990]. Thereby investigating one possible mechanism by which biological brain may effect such control. It seems unlikely that mechanisms precisely analogous to the OGY method are the means by which biological brains exhibit such behaviour. However, apart from possible practical applications (such as increased memory capacity for certain types of artificial neural circuitry) the ability to control the dynamics of a high dimensional neural circuit is likely to increase our understanding of many similar biological phenomena.

The proposed simulator is illustrated in Figure 7.1. The *chaotic controller* is an implementation of a variation of the OGY method. The *chaotic Neural Network* produces the output as a function of time, and its behaviour is chaotic when running freely. We assume that the network will be of a recurrent type and has at least one system wide control parameter which can be altered readily. The input to the simulator could be a noun such as a 'banana' or an 'orange'. The output is the stable attractor corresponding to the input.

The model should work as follows. Given an input such as a 'banana' the control point corresponding to the attractor, an unstable periodic orbit in this case, is selected and the chaotic controller calculates the perturbations required to force the output of the chaotic neural network to stay in a stable orbit. The output of the model will be the stable attractor corresponding to the input. After a while the controller suspends the control and the output will be the chaotic attractor. If and when another input is presented, say 'orange', the controller forces the output of the chaotic neural network to be in a different stable attractor which corresponds to 'orange', in the same manner as before.

A biological brain has an enormous memory capacity when compared to a computer system and operates with very slow individual components, yet recall time for a *fuzzy piece of memory* is marginally quicker than that of any so called artificial intelligence computer systems. Here, a fuzzy piece of memory means a memory which cannot be described precisely, such as a human face or smell of a perfume. Does chaos play a role in this perception-recognition? If so precisely how is this done?

Freeman's observations imply that the brain has an enormous number of attractors. Do all of them exist

## Chapter 7 - Future research

within a larger chaotic attractor? If so, the memory capacity may depend upon the complexity of the chaotic attractor, rather than just the number of neurons. We seek to create an artificial neural network, made up of a small number of neurons, which produces a complex chaotic attractor in which the number of unstable periodic orbits exceeds the number of patterns which can normally be stored by such a network using more conventional approaches using similar networks, e.g. the Hopfield model [Hopfield 1982].

One possible approach to creating a chaotic neural network is to train a feed-forward neural network on data generated by a chaotic system such as the Lorenz model, described in section 3.3.1. After the training phase, the output of the trained network is fed back to itself as input. Another possible approach is to create a neural network which intrinsically displays chaotic behaviour. For example, a variation of the Hoppensteadt's voltage controlled oscillator neuron model [Hoppensteadt 1989] could be used.

We are hoping to perform the control of chaotic systems via a neural network so that given an input, the neural network calculates the required change in the control parameter to stabilise the system.

The ultimate aim is to implement a simulated neural model with the chaos controller itself consisting of a neural network, so that the whole simulation model is created by a collection of artificial neurons.

### Chapter references

[Ott 1990] E. Ott, Celso Grebogi and J. A. Yorke. *Controlling chaos*. Physical Review Letters 64, 11, 1196-1199, 1990.

[Freeman 1991] W. J. Freeman. *The physiology of perception*, Scientific American, 34-41, February 1991.

[Hopfield 1982] J. Hopfield. *Neural networks and physical systems with emergent collective computational abilities*, Proc. Natl. Acad. Sci. USA, 79, 2554-2558, 1982.

[Hoppensteadt 1989] F. C. Hoppensteadt, *Intermittent Chaos, Self Organisation, and Learning from Synchronous Synaptic Activity in Model Neuron Networks*, Proc. Natl. Acad. Sci Applied Mathematics, 86, 2991-2995, 1989.



## REFERENCES

---

- [Abraham 1982] R. H. Abraham and C. D. Shaw, *Dynamics - The geometry of behavior Part One : Periodic Behavior*, Aerial Press, California, 1982.
- [Abraham 1984] R. H. Abraham and C. D. Shaw, *Dynamics - The geometry of behavior Part Two : Chaotic Behavior*, Aerial Press, California, 1983.
- [Abraham 1985] R. H. Abraham and C. D. Shaw, *Dynamics - The geometry of behavior Part Three : Global Behavior*, Aerial Press, California, 1985.
- [Abraham 1986] N. B. Abraham, A. M. Albano, B. Das, G. De Guzman, S. Yong, R. S. Gioggia, G. P. Puccioni, and J. R. Tredicce. *Calculating the Dimension of Attractors from Small Data Sets*, Physics Letters A 114, 217-221, 1986.
- [Albano 1988] A. M. Albano, J. Muench, C. Schwartz, A. I. Mees and P. E. Rapp. *Singular-Value Decomposition and the Grassberger-Procaccia Algorithm*, Physical Review A 38, 3017-3026, 1988.
- [Albano 1991] A. M. Albano, A. Passamante and M. E. Farrell. *Using higher-order correlation to define an embedding window*, Physica D 54, 85-97, 1991.
- [Atkinson 1978] K. E. Atkinson, *An introduction to numerical analysis*, John Wiley & Sons, Canada, 1978.
- [Auerbach 1987] Ditzia Auerbach, Predrag Cvitanovic, Jean-Pierre Eckmann, Gemunu Gunaratne and Itamar Procaccia. *Exploring Chaotic Motion Through Periodic Orbits*, Physics Review Letters 58, 23, 2387-2389, 1987.
- [Auerbach 1992] D. Auerbach, C. Grebogi, E. Ott and J. A. Yorke. *Controlling Chaos in High Dimensional Systems*, Physical Review Letters 69, 24, 3479-3482, 1992.
- [Azevedo 1991] A. Azevedo and S. M. Rezende. *Controlling Chaos in Spin-Wave Instabilities*, Physical Review Letters 66, 10, 1342-1345, 1991.
- [Babloyantz 1988] A. Babloyantz and A. Destexhe. *Is the normal heart a periodic oscillator?* Biol. Cybern. 58, 203-211, 1988.
- [Belmonte 1988] A. L. Belmonte, M. J. Vision, J. A. Glazier, G. H. Gunaratne and B. G. Kenny. *Trajectory Scaling Functions at the Onset of Chaos: Experimental Results*, Physical Review Letters 61, 5, 539-542, 1988.
- [Breedon 1992] J. L. Breedon and N. H. Packard. *Nonlinear analysis of data sampled nonuniform in time*, Physica D 58, 273-283, 1992.
- [Broomhead 1986] D. S. Broomhead and G. P. King. *Extracting qualitative dynamics from experimental data*, Physica D 20, 217, 1986.
- [Buzung 1992] Th. Buzung and G. Pfister. *Comparison of algorithms calculating optimal embedding parameters for delay time coordinates*, Physica D 58, 127-137, 1992.

- [Carroll 1992] T. L. Carroll, I. Triandaf, I. Schwartz and L. Pecora. *Tracking unstable orbits in an experiment*, Physical Review A 46, 10, 6189-6192, 1992.
- [Carroll 1993] Thomas L. Carroll and Louis M. Pecora. *Using chaos to keep period-multiplied systems in phase*, Physics Review E 48, 4, 2426-2436, 1993.
- [Casdagli 1991] M. Casdagli, S. Eubank, J. D. Farmer and J. Gibson. *State space reconstruction in the presence of noise*, Physica D 51, 52-98, 1991.
- [Chay 1985] T. R. Chay and J. Rinzel. *Bursting, beating, and chaos in an excitable membrane model*, J. Biophysical Society, 47, 357-366, 1985.
- [Choi 1983] M. Y. Choi and B. A. Huberman. *Dynamic behaviour of nonlinear networks*, The American Physical Society, 28, 1204-1206, 1983.
- [Crutchfield 1980] J. Crutchfield, D. Farmer, N. Packard, R. Shaw, G. Jones and R. J. Donnelly. *Power spectral analysis of a dynamical system*, Physics Letters A 76, 1-4, 1980.
- [Crutchfield 1981] J. Crutchfield, M. Nauenberg and J. Rudnick. *Scaling for External Noise at the Onset of Chaos*, Physical Review Letters 46, 933-935, 1981.
- [Cvitanovic 1988] P. Cvitanovic, G. H. Gunaratne and I. Procaccis, *Topological and metric properties of Hénon-type strange attractors*, Physical Review A 38, 1503-1520, 1988.
- [Cvitanovic 1989] P. Cvitanovic. *Universality in Chaos : second edition*, Adam Hilger, Bristol, 1989.
- [Derrick 1993] W. R. Derrick in *Chaos in chemistry and biochemistry*, Ed R. J. Field and L. Györgyi, World Scientific Publishing, 1993.
- [Ding 1993] Mingzhou Ding, Celso Grebogi, Edward Ott, Tim Sauer and James A. Yorke. *Plateau Onset for Correlation Dimension: When Does it Occur?*, Physical Review Letters 70, 25, 3872 -3875, 1993.
- [Ditto 1990] W. L. Ditto, S. N. Rauseo and M. L. Spano. *Experimental Control of Chaos*, Physical Review Letters 65, 26, 3211-3214, 1990.
- [Ditto 1993] W. L. Ditto and L. M. Pecora. *Mastering Chaos*, Scientific American, 62-68, August 1993.
- [Dracopoulos 1993] D. C. Dracopoulos and Antonia J. Jones. *Neuromodels of analytic Dynamic Systems*. Neural Computing & Applications, 1, 4, 268-279, 1993.
- [Dracopoulos 1994] D. C. Dracopoulos and A. J. Jones. *Neuro-Genetic Adaptive Attitude Control*, Neural Computing & Applications, 2, 4, 183-204, 1994.
- [Dressler 1992] U. Dressler and G. Nitsche. *Controlling chaos using time delay coordinates*. Physics Review letters 68, 1, 1-4, 1992.
- [Eckmann 1985] J. P. Eckmann and D. Ruelle. *Ergodic theory of chaos and strange attractors*, Rev. Modern Physics 57, 3, 617-656, 1985.
- [Farmer 1987] J. D. Farmer and J. J. Sidorowich. *Predicting Chaotic Time Series*, Physical Review Letters 59, 8, 845-848, 1987.
- [Field 1993] R. J. Field and L. Györgyi. *Chaos in chemistry and biochemistry*, World Scientific Publishing, 1993.

## Chapter ~~References~~ research

[Fraser 1986] Andrew M. Fraser and Harry L. Swinney, *Independent coordinates for strange attractors from mutual information*, Physical Review A 33, 2, 1134-1140, 1986.

[Freeman 1991] W. J. Freeman. *The physiology of perception*, Scientific American, 34-41, February 1991.

[Garfinkel 1992] A. Garfinkel, M. L. Spano, W. L. Ditto and J. N. Weiss. *Controlling cardiac chaos*, Science 257, 1230-1235, August 1992.

[Geuvara 1981] M. R. Geuvara, L. Glass and A. Shrier. *Phase locking, period-doubling bifurcations, and irregular dynamics in periodically stimulated cardiac cells*, Science 214, 1350-1352, 1981.

[Gills 1992] Z. Gills, C. Iwata, R. Roy, I. B. Schwartz and I. Triandaf. *Tracking Unstable Steady States: Extending the Stability Regime of a Multimode Laser System*, Physical Review Letters 69, 22, 3169-3172, 1992.

[Gleick 1987] J. Gluick. *CHAOS : Making a new science*, Abacus book, London, 1987.

[Goldberg 1984] A. L. Goldberger, L. J. Findley, M. R. Blackburn and A. J. Mandell. *Nonlinear dynamics in heart failure: Implications of long-wavelengths cardiopulmonary oscillations*, Amer. Heart J. 107, 612-615, 1984.

[Grassberger 1983] P. Grassberger and I. Procaccia, *Characterization of Strange Attractors*, Physical Review Letters 50, 5, 346-349, 1983.

[Grebogi 1982] C.Grebogi, E.Ott, J.A.Yorke. *Chaotic Attractors in Crisis*, Physical Review Letters 48, 1507-1510, 1986.

[Grebogi 1986] C. Grebogi, E. Ott, J. A. Yorke. *Critical Exponent of Chaotic Transients in Nonlinear Dynamical Systems*, Physical Review Letters 57, 1284-1287, 1986.

[Grebogi 1987] C. Grebogi, E. Ott, J. A. Yorke. *Critical exponents for crisis-induced intermittency*, Physical Review A 36, 5365-5380, 1987.

[Grebogi 1988] C. Grebogi, E. Ott, J. A. Yorke. *Unstable periodic orbits and the dimensions of multifractal chaotic attractors*, Physical Review A 37, 1711-1723, 1988.

[Greenside 1982] H. S. Greenside, A. Wolf, J. Swift and T. Pignataro. Physical Review A 25, 3453, 1982.

[Gunaratne 1989] G. H. Gunaratne, P. S. Linsay and M. J. Vision. *Chaos beyond Onset: A Comparison of Theory and Experiment*, Physics Review Letters 63, 1, 1-4, 1989.

[Hall 1992] N. Hall. *The new scientist guide to chaos*, Penguin books, London, 1992.

[Hao 1990] B. Hao, *Chaos II*, World Scientific, 1990.

[Hayes 1993] S. Hayes, C. Grebogi and E. Ott. *Communicating with Chaos*, Physical Review Letters 70, 20, 3031-3034, 1993.

[Hénon 1976] M. Hénon. *A Two-dimensional Mapping with a Strange Attractor*, Communications in Mathematical Physics 50, 69-77, 1976.

[Hilborn 1994] R. C. Hilborn. *Chaos and Nonlinear Dynamics : An introduction for scientists and engineers*, Oxford University press, New York, 1994.

- [Holmes 1990] P. Holmes. *Poincaré. celestial mechanics, dynamical-systems theory and "chaos"*, Physics Reports 193, 3, 137-163, 1990.
- [Holzfuss 1986] J. Holzfuss and G. Mayer-Kress. *An approach to error estimation in the application of dimension algorithms*, in Dimensions and Entropies in Chaotic Systems, editor G. Mayer-Kress, Springer-Verlag, New York, 114-122, 1986.
- [Hopfield 1982] J. Hopfield. *Neural networks and physical systems with emergent collective computational abilities*, Proc. Natl. Acad. Sci. USA, 79, 2554-2558, 1982.
- [Hunt 1991] E. R. Hunt. *Stabilizing High-Period Orbits in a Chaotic System: The Diode Resonator*, Physical Review Letters 67, 15, 1953-1955, 1991.
- [Kaplan 1979] J. Kaplan, J. A. Yorke in *Chaotic behavior of multidimensional difference equations*, H. O. Peitgen et al., Eds., "Springer Lecture, Notes in Mathematics", Springer-Verlag, Berlin, Volume 730, 204-227, 1979.
- [Keener 1981] J. P. Keener. *Chaotic cardiac dynamics*, Lectures in Applied Mathematics 19, 299-325, 1981.
- [Kim 1992] J. H. Kim and J. Stringer, Applied Chaos, John Wiley & Sons, Canada, 1992.
- [King 1987] G. P. King, R. Jones, D. S. Broomhead. *Phase portraits from a time series: a singular system approach*, Nuclear Physics B 2, 379, 1987.
- [King 1992] G. P. King and I. Stewart. *Phase space reconstruction for symmetric dynamical systems*, Physica D 58, 216-228, 1992.
- [Lai 1993] Y-C Lai, M. Ding and C. Grebogi. *Controlling Hamiltonian chaos*, Physical Review E 47, 1, 86-92, 1993.
- [Lai 1994] Ying-Cheng Lai and Celso Grebogi. *Synchronization of spatiotemporal chaotic systems by feedback control*, Physics Review E 50, 3, 1894-1899, 1994.
- [Lathrop 1989] Daniel P. Lathrop and Eric J. Kostelich. *Characterization of an experimental strange attractor by periodic orbits*, Physics Review A 40, 7, 4028-4031, 1989.
- [Levin 1993] A. U. Levin. *Recursive Identification Using Feedforward networks*. Department of Computer Science and Engineering, Oregon Graduate Institute, 2000 NW Walker Road. PO Box 91000, Portland, Oregon OR 97291-1000.
- [Lorenz 1963] E. N. Lorenz. *Deterministic Nonperiodic Flow*, J. Atmospheric Sciences 20, 130-141, 1963.
- [Lorenz 1993] E. N. Lorenz, *The essence of chaos*, University of Washington press, 1993.
- [Martinerie 1992] J. M. Martinerie, A. M. Albano, A. I. Mees, P. E. Rapp. *Mutual information, strange attractors, and the optimal estimation of dimension*, Physical Review A 45, 7085, 1992.
- [Moss 1994] Frank Moss. *Chaos under control*, Nature 370, 596-597, 1994.
- [Ogorzalek 1993] M. J. Ogorzalek. *Taming Chaos Part II: Control*, IEEE Transactions on circuits and systems - 1: Fundamental theory and Applications. Volume 40, 10, 700-706, October 1993.
- [Ott 1990] E. Ott, Celso Grebogi and J. A. Yorke. *Controlling chaos*, Physical Review Letters 64, 11, 1196-1199, 1990.

- [Ott 1994] E. Ott, T Sauer and J. A. Yorke, *Coping with Chaos*, John Wiley & Sons, Canada, 1994.
- [Packard 1980] N. H. Packard, J. P. Crutchfield, J. D. Farmer and R. S. Shaw. *Geometry from a time series*, Physics Review Letters 45, 9, 712-16, 1980.
- [Parker 1989] T. S. Parker and L. O. Chua. *Practical Numerical Algorithms for Chaotic Systems*, Springer-Verlag, New York, 1989.
- [Parlitz 1985] U. Parlitz and W. Lauterborn. *Superstructure in the bifurcation set of the Duffing equation*, Physics Letters A 107, 8, 351-355, 1985.
- [Pearson 1986] C. E. Pearson, *Numerical methods in engineering and science*, Van Nostrand Reinhold Company Inc, England, 1986.
- [Peinke 1992] J. Peinke, J. Parisi, O. E. RöSSLer and R. Stoop, *Encounter with Chaos : Self-Organized Hierarchical Complexity in Semiconductor Experiments*, Springer-Verlag, 1992.
- [Petrov 1993] Valery Petrov, Vilmos Gaspar, Jonathan Masere and Kenneth Showalter. *Controlling chaos in the Belousov-Zhabotinsky reaction*, NATURE 361, 240-243, 1993.
- [Pfister 1992] G. Pfister, Th. Buzug and N. Enge. *Characterization of experimental time series from Taylor-Couette flow*, Physica D 58, 441-454, 1992.
- [Pi 1994] H. Pi and C. Peterson. *Finding the embedding dimension and variable dependencies in time series*. Neural Computation 6, 509-520, 1994.
- [Provenzale 1992] A. Provenzale, L. A. Smith, R. Vio and G. Murante. Distinguishing between low-dimensional dynamics and randomness in measured time series, Physica D 58, 31-49, 1992.
- [Pyragas 1993] K. Pyragas and A. Tamasevicius. *Experimental control of chaos by delayed self-controlling feedback*, Physics Letters A 180, 99-102, 1993.
- [Qu 1993] Zhilin Qu, Gang Hu and Benkun Ma. *Controlling chaos via continuous feedback*, Physics Letters A 178, 265-270, 1993.
- [Romeiras 1992] F. J. Romeiras, C. Grebogi, E. Ott and W. P. Dayawansa. *Controlling chaotic dynamical systems*, Physica D 58, 165-192, 1992.
- [Rosenstein 1994] M. T. Rosenstein, J. J. Collins, C. J. De Luca. *Reconstruction expansion as a geometry-based framework for choosing proper delay times*, Physica D 73, 82-98, 1994.
- [Rössler 1976] O. E. RöSSLer. *An Equation for Continuous Chaos*, Physics Letters A 57, 397-398, 1976.
- [Roux 1993] J. -C. Roux. *Dynamical Systems Theory Illustrated: Chaotic Behavior in the Belousov-Zhabotinsky Reaction*, in *Chaos in Chemistry and Biochemistry*, R. J. Field and L. Györgyi eds, 21-46, World Scientific Publishing, 1993.
- [Roy 1992] R. R. Roy, T. W. Murphy, T. D. Maier, Z. Gills and E. R. Hunt. *Dynamical Control of a Chaotic Lazer: Experimental Stabilization of a Globally Coupled System*, Physical Review Letters 68, 9, 1259-1262, 1992.
- [Roy 1994] Rajarshi Roy and K. Scott Thornburg, Jr. *Experimental Synchronization of Chaotic Lasers*, Physical Review Letters 72, 13, 2009-2012, 1994.

- [Ruelle 1980] D. Ruelle. *Strange Attractors*, The Mathematical Intelligence 2, 126-137, 1980.
- [Russell 1980] D. A. Russell, J. D. Hansen, and E. Ott. *Dimensions of Strange Attractors*, Physical Review Letters 45, 1175-1178, 1980.
- [Sano 1985] M. Sano and Y. Sawada. *Measurement of the Lyapunov Spectrum from a Chaotic Time Series*, Physical Review Letters 55, 10, 1082-1085, 1985.
- [Schiff 1992] S. J. Schiff and T. Chang. *Differentiation of linearly correlated noise from chaos in a biologic system using surrogate data*, Biological Cybernetics 67, 387-393, 1992.
- [Schiff 1994] S. J. Schiff, K. Jerger, D. H. Duong, T. Chang, M. L. Spano and W. L. Ditto, *Controlling chaos in the brain*, Nature, 370, 615-620, 1994.
- [Schwartz 1994] I. B. Schwartz and I. Triandaf. *Controlling unstable states in reaction-diffusion systems modeled by time series*, Physical Review E 50, 4, 2548-2552, 1994.
- [Shinbrot 1992a] T. Shinbrot, W. Ditto, C. Grebogi, E. Ott, M. Spano, and J. A. Yorke. *Using the Sensitive Dependence of Chaos (the "Butterfly Effect") to Direct Trajectories in an Experimental Chaotic System*, Physical Review Letters 68, 19, 2863-2866, 1992.
- [Shinbrot 1992b] T. Shinbrot, C. Grebogi, E. Ott and J. A. Yorke. *Using chaos to target stationary states of flows*, Physics Letters A 196, 349-354, 1992.
- [Shinbrot 1993] Troy Shinbrot, Celso Grebogi, Edward Ott and James A. Yorke. *Using small perturbations to control chaos*, Nature 363, 411-417, 1993.
- [Singer 1991] J. Singer, Y-Z. Wang and H. H. Bau. *Controlling a Chaotic System*, Physical Review Letters 66, 9, 1123-1125, 1991.
- [Smith 1986] W. A. Smith, *Elementary Numerical Analysis*, Prentice-Hall, England, 1986.
- [Stefánsson 1995] Aðalbjörn Stefánsson, N. Koncar and Antonia J. Jones, *The Gamma test: a simple estimate for the best possible performance of a continuous or smooth data model*, report, Dept. Comp. Maths, University of Wales, 1995.
- [Stewart 1989] I. Stewart, *Does God Play Dice : The new mathematics of chaos*, Penguin books, England, 1989.
- [Stewart 1996] I. Stewart, *From Here to Infinity : A guide to today's mathematics*, Oxford University Press, England, 1996.
- [Takens 1981] F. Takens. *Dynamical Systems and Turbulence*. Lecture Notes in Mathematics 898, D. A. Rand and L. S. Young, eds, Springer-Verlag, 1981.
- [Thompson 1994] J. M. T. Thompson and S. R. Bishop, *Nonlinearity and Chaos in Engineering Dynamics*, John Wiley & Sons, England, 1994.
- [Zeng 1991] X. Zeng, R. Eykholt and R. A. Pielke. *Estimating the Lyapunov-Exponent Spectrum from Short Time Series of Low Precision*, Physical Review Letters 66, 25, 3229-3232, 1991.

# INDEX

- $\Gamma$ -test 57, 63
- Asymptotically
  - stable 11
  - unstable 11
- Attractor 10
  - chaotic 13
  - strange 13
- Autocorrelation 26, 49, 53, 60
  - time 26
- Automated embedding method 63
- Autonomous 8
- Average displacement 50, 53, 60, 63
- Basin of attraction 10
- Bifurcation 21
  - diagram 21
  - flip 22
  - global 21
  - Hopf 23
  - local 21
  - quasi-periodicity 23
  - value 21
- Box-counting algorithm 19
- Butterfly effect 13
- Capacity dimension 19
- Chaos 7, 12
  - detection of 24
- Chaotic transient 23
- Characteristic multiplier 18
- Conservative system 9, 11, 35
- Conserved quantities 35
- Control 77
- Control method
  - bifurcation diagram approach 78
  - Dressler and Nitsche 87
  - feedback 77
  - high energy 77
  - low energy 77
  - non-feedback 77
  - OGY 78
- Control point 79
- Correlation dimension 20, 55, 64
- Correlation integral 55
- Creep phenomenon 70
- Crisis 23
- Critical point 10
- Degrees of freedom 8
- Delay coordinates 45
- Delay time 47, 63
- Dissipative system 9, 11
- Divergence of nearby trajectories 12
- Duffing's oscillator model 8, 12, 18, 21, 42, 53, 64, 110
- Embedded time series 45
- Embedding dimension 54, 63
- Embedding space vector 47
- Embedding techniques 23
- Entropies 23
- Equilibrium point 10
- Ergodic 17, 78
- Euclidean length 55
- Extrapolating 30
- Fast Fourier transformation 25
- Feigenbaum
  - constant 22
  - scenario 22
- FFT 25
- Fill factor 52
- Fixed point 18
- Floquet multipliers 18
- Fourier spectrum 26
- Fractal dimension 19, 25
- Fractals 23
- Fuzzy delay coordinate reconstruction technique 52
- Hamiltonian chaos 23
- Hamiltonian system 35
- Hausdorff 19
- Hénon map 39
  - variation 99
- Indecomposability 17
- Integration
  - algorithms 28
  - chaotic systems 30
  - error 28
- Integration error
  - round-off 28
  - truncation 28
- Intermittency 23
- Interpolating 30
- Invariant 17
- Invertible map function 39
- Irrelevance 48
  - error 51
- Iterated map 39
- Jacobian matrix 11
- Jump time 53, 63, 70
- Limit cycle 8
- Limit set 8
- Logistic map 22
- Lorenz model 9, 25, 27, 36, 48, 50, 53, 59, 64

- Lyapunov dimension 20, 38, 56
- Lyapunov exponent 14
- Lyapunov spectrum 15
- Manifold
  - stable 10
  - unstable 10
- Mathematica 29, 36
- Max-norm 55
- Mutual information 50
- Node 11
- Noise 27, 46
- Non-autonomous 9
- Non-stable 11
- Numerical integration algorithms 27
  - Adams-Bashforth 28
  - Adams-Moulton 28
  - Backward Euler 28
  - Forward Euler 28
  - Gear's 28
  - k th-order Runge-Kutta 28
  - multi-step 28
  - single-step 28
  - Trapezoidal 28
- OGY method 78
  - advantages 83
  - assumptions 83
  - disadvantages 84
  - experiment 99
  - variations 84
- Parameter
  - control 8
  - system 8
- Period-doubling 22
- Periodic windows 22, 43
- Perturbation 8
- Phase portrait 8
- Phase space 8
- Poincarè map 16
- Poincarè section 16, 22, 24
- Power spectrum 25
- Quantum chaos 23
- Quasi-periodicity 24
- Quasiperiodic 23
- Reconstruction window 49
- Redundance 48
  - error 50
- Repeller 11
- Return map 17, 25
- Rössler model 40, 53, 64
- Routes to chaos 21
- Saddle point 11
- Scaling region 55
- Secondary resonances 42
- Sensitive dependence on initial conditions
  - 12
- Singular point 10
- Spiral
  - node 11
  - repeller 11
  - saddle point 11
- Stability 10, 18
- Stable 11
- State space 8
- Stroboscopic map 17, 25
- Stroboscopic portrait 17
- Surface of section 18, 54, 80
- Synchronisation of chaos 85
- Time delay 45
- Time periodic 9
- Time span 49, 70
- Trajectory 8
- Trajectory hopping 30
- Universality 23
- Unstable 11
- Unstable orbit of period k 64
- Unstable periodic point of period k 64
- Variable
  - dynamic 8
  - static 8
- Variable step size 29